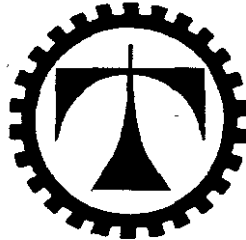


Peninsula Technikon

Faculty of Engineering

Department of Mechanical Engineering



**Prediction of Shrinkage and Warpage in
Injection Moulded Components using
Computational Analysis**

Mornay Riddles

B.Tech (Peninsula Technikon, South Africa)

**Submitted towards the degree of
Master of Technology in Mechanical Engineering**

Under Supervision of

**Nawaz Mahomed, PhD (Warsaw) M.Sc (UCT)
Graeme Oliver, PhD (IFTR Warsaw) M.Sc (UCT)
Oscar Philander, MTECH (Pentech)**

CAPE TOWN, 2003

Acknowledgements

I would like to express my gratitude to Dr. Nawaz Mahomed. Without his guidance and assistance this dissertation would never have materialised.

I would also like to thank Prof. Graeme Oliver, whose advice and assistance enabled me to select the relevant aspects of this project.

Special thanks go to Oscar Philander, who introduced me to the Finite Element Method and Continuum Mechanics, and for his untiring contribution and support to finish this work.

I wish to thank the National Research Foundation (NRF) for funding, the Department of Mechanical Engineering for the use of their computational facilities and the Peninsula Technikon for their financial assistance.

A word of thanks goes to Hellmut Bowles for the Finite Element Stress Analysis, which was performed on the component used for the case study in Chapter 4.

I would also like to acknowledge the assistance and useful insight that I received from my friends and colleagues, especially R Ziegler, P Simelane, E Erfort, W Mitchell and K Jacobs.

Thank you to the lecturers at the Mechanical Engineering Department who never hesitated to assist when they were called upon.

Special acknowledgement goes to Ms. V Van Der Bank for her support during my studies.

Finally I would like to thank my family for their never-ending support and love.

Summary

Injection moulding is a process by which molten polymer is forced into an empty cavity of the desired shape. At its melting point, polymers undergo a volumetric expansion when heated, and volumetric contraction when cooled. This volumetric contraction is called shrinkage. Once the mould cavity is filled, more pressure is applied and additional polymer is packed into the cavity and held to compensate for the anticipated shrinkage as the polymer solidifies. The cooling takes place via the cooling channels where the polymer is cooled until a specific ejection criterion is met. Heat from the polymer is lost to the surrounding mould, a part of this heat reaches the cooling channel surfaces, which in turn exchange heat with the circulating cooling fluid.

Due to the complexity of injection moulded parts and the cooling channel layout, it is difficult to achieve balanced cooling of parts. Asymmetric mould temperature distribution causes contractions of the polymer as it cools from its melting temperature to room temperature. This results in residual stresses, which causes the part to warp after ejection.

Given the understanding of the mathematical model describing the heat transfer process during the cooling stage, the objectives of this study were three fold. Firstly, an alternative numerical model for the heat transfer process was developed. The proposed model was used to investigate the cooling stress build-up during the injection moulding process. The mould region was divided into layers and the cooling stress was identified. Secondly, this cooling stress results was compared with that predicted by the C-MOLD injection moulding simulation software. The last objective was to perform a sensitivity analysis to determine the effect of design and processing parameters on shrinkage.

The above objectives were met using the following methods. The finite element analysis software ABAQUS was used to simulate the heat transfer during cooling, with the aim of identifying the temperature field, while the solution procedure for the cooling stress model was solved using Fortran. The injection moulding simulation software C-MOLD was used to perform the sensitivity analysis. This software program comprises a set of computer programs for plastics moulding simulations. It provides solutions to problems, experienced with plastics moulding processes, in all stages of design and manufacturing.

The results obtained for the ABAQUS simulation revealed a difference between the cooling times predicted by ABAQUS and the cooling times predicted by C-MOLD. Results for the numerical model showed that the final shrinkage for each layer, converges when the cavity thickness is divided into more layers. We expect the solution to become even more accurate if the half cavity is divided into more layers than was selected. As it stands, a significant difference can be noted between the shrinkage predicted by the numerical model and C-MOLD. The assumptions made for the ABAQUS analysis, coupled with the assumptions made for the numerical model was identified as reasons for the differences between shrinkage results.

Based on the above results we can conclude that the solution procedure for the proposed alternative cooling stress model was solved. Some of the trends between the model and the commercial software were reproduced, but an agreement could not be

found, due to both a lack of information regarding parameters, and the approximations of the model. The sensitivity analysis for shrinkage proved sufficient for an academic investigation and we can conclude that changing the process parameters cannot solve excessive shrinkage.

Glossary

- Adiabatic** The term used to describe any process during which heat is prevented from crossing the boundary of the system; hence a system which is thermally insulated from its surroundings.
- Amorphous** Solids that lack a systematic and regular arrangement of atoms over relatively large atomic distances
- Anisotropic** When the measurements of physical properties such as elastic modulus and/or electrical conductivity have different values in different directions
- Clamp Force** It is the force applied by the injection moulding machine's clamping unit to the mould during filling, packing and cooling phases of the moulding cycle, measured in Tons
- Cooling Channels** It is the channels through which coolant flows to remove heat from the mould. The channels should be located thoughtfully in the core and cavity so that the temperature distribution over the mould surface is constant
- Crystalline** Material in which the atoms are situated in a repeating or periodic array over large atomic distances
- Cycle Time** For a sequence of operation that is repeated regularly, the time it takes for one such operation is called the cycle time. For the injection moulding process it is the time required to complete one moulding cycle
- Fibre** Any polymer, metal, or ceramic that has been drawn into a long and thin filament
- Glass Transition Temperature** It is the point at which the molten polymer hardens into a solid
- Injection Rate** It is the flow rate of melt coming out of the nozzle. Melt comes out in the form of a jet and then spreads inside the mould in the shape of the cavity
- Isothermal** At a constant temperature
- Isotropic** Having identical values of a property in all crystallographic directions
- Melt Front** It is the melt at the leading edge of flow while the mould is filling
- Melt Temperature** It is the actual temperature of the molten polymer during processing. The melt temperature is constantly changing. It varies with time and will not be the same at different locations in the mould

- Orientation** It is the change in shape that polymer molecules can undergo when they are made to flow
- Packing** The process of delivering an additional amount of melt to the mould, to compensate for the shrinkage after ejection
- Polymer** A non-metallic compound in which the interatomic bonding is predominantly covalent
- Shear Heating** Heating due to friction caused by the flow of melt through narrow passages in the mould during filling phase
- Shear Rate** A way to describe how quickly the velocity of the melt changes from the mould surface to the center of flow for a given cross section. The size of the shear rate gives an indication of the shape of the velocity profile for a given situation
- Shear Stress** The result of the force that is generated in a melt to overcome its resistance to a particular flow situation. Shear stress is the product of a material and shear rate
- Specific Heat** Temperature is a measure of heat energy level whereas heat is a measure of total internal energy contained in a body. When the same quantity of heat is given to equal masses of different substances, they do not result in the same rise in temperature. The specific heat is defined as the quantity of heat energy, which will rise the temperature of unit mass (1kg) of a substance by 1°C
- Specific Volume** The inverse of density (Volume per unit weight)
- Thermoplastic** A polymeric material that softens and melts when heated, and hardens upon cooling. The process is reversible
- Thermoset** A polymeric material that, once having hardened, will not soften or melt when heated
- Viscoelastic** A type of deformation exhibiting the mechanical characteristics of viscous flow and elastic deformation

Table of Contents

Acknowledgements	ii
Summary	iii
Glossary	v
Table of Contents	vii
Chapter 1: Introduction and Overview	
1.1 Introduction to Shrinkage and Warpage	1
1.2 Objectives of this Investigation	4
1.3 Literature Survey	4
1.4 Available Commercial Systems	7
Chapter 2: The Process of Injection Moulding	
2.1 Introduction to the Injection Moulding Process	10
2.2 Residual Stress	12
2.2.1 Flow-induced Residual Stress	12
2.2.2 Thermal-induced Residual Stress	13
2.3 Causes of Shrinkage	13
2.3.1 Part Thickness	13
2.3.2 Holding Pressure	14
2.3.3 Melt Temperature	14
2.3.4 Injection Rate	14
2.4 Causes of Warpage	15
2.4.1 Uneven Cooling of the Part	15
2.4.2 Part Geometry Asymmetry	16
2.4.3 Variable Packing	16
2.4.4 Molecular or Fiber Orientation due to Flow	17
2.5 Overview of Thermal Transfer	18
2.5.1 Modelling of Heat Transfer in the Mould	18
2.5.2 Modelling of Boundary Conditions	20
2.5.3 Modelling of the Steady Component	21
2.5.4 Modelling of the Time-varying Component	22
Chapter 3: Sensitivity Analysis of Shrinkage	
3.1 The Process Estimator	23
3.2 Varying Thickness	25
3.3 Varying Polymers	26
3.4 Varying Fill Time	30
3.5 Varying Melt Temperature	32
Chapter 4: Injection Moulding Analysis Case Study	
4.1 Background	34
4.2 Filling Process	35
4.3 Process Parameters and Packing	36
4.3.1 Injection Pressure	36
4.3.2 Inlet Melt Temperature	36
4.3.3 Clamping Force	37

4.3.4 Process Cycle Time	37
4.4 Cooling System	38
4.5 Shrinkage and Warpage	39
4.6 Analysis and Discussion of Results	40
4.7 Conclusions	42
Chapter 5: An Alternative Model for the Stress Build-Up during Cooling of Injection Moulded Thermoplastics	
5.1 Introduction	43
5.2 Solidifying Polymer as a Continuum Body	45
5.2.1 Introduction	45
5.2.2 Basic Notations	45
5.2.3 The General Model	47
5.3 Governing Equations	48
5.4 Solution Procedure	51
5.5 Discussion of Results	54
5.6 Conclusions	57
Chapter 6: Conclusions	
6.1 Concluding this Work	58
6.2 Future Work	59
References	60
Appendix A: C-MOLD Report Files	A1
Appendix B: ABAQUS Report	B1
Appendix C: ABAQUS Output Data	C1
Appendix D: FORTRAN Program	D1
Appendix E: FORTRAN Results	E1
Appendix F: C-MOLD Output Data	F1
Appendix G: Melt Front Advancement	G1
Appendix H: Part Performance	H1

Chapter 1

Introduction and Overview

1.1 Introduction to Shrinkage and Warpage

We are all exposed to plastic (polymer) components in our day to day life. Whether it is a fruit bowl, ice-cube tray or laundry basket. These plastic components were manufactured using a process called injection moulding. An injection mould consists of two pieces of tool steel pressed together with a cavity inside. This cavity is then injected with molten plastic, cooled and opened to eject the component that was shaped in the cavity. It should be noted that injection moulding is not the only means of polymer processing. Others are roto moulding, extrusion, transfer moulding etc. This work will focus on injection moulding. All of these processes have one thing in common though: the polymer needs to be heated until molten, before it can be processed.

This brings us to a material property called thermal expansion. At the melting (glass transition) point the polymer undergoes a volumetric expansion when heated, and volumetric contraction when cooled as illustrated by Figure 1.1. When heated, the density of polymers decreases which means an increase in specific volume when measured at ambient temperature and at processing temperature [7].

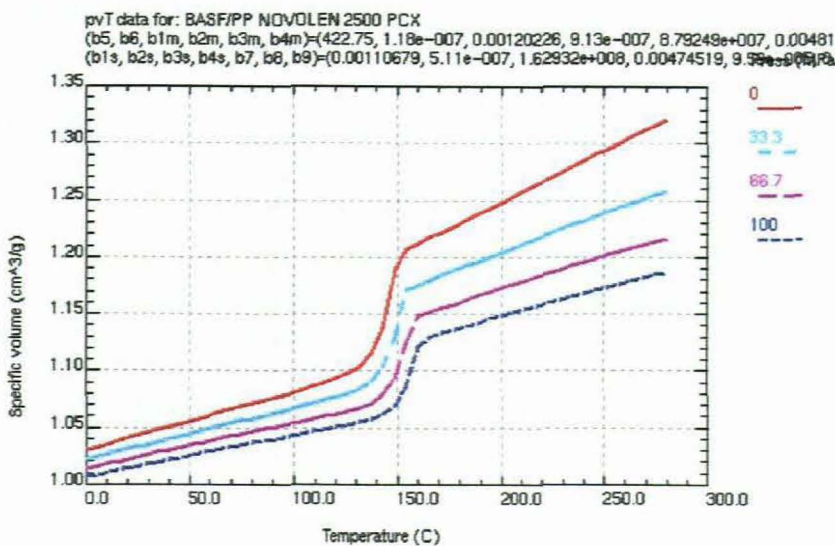


Figure 1.1 Specific volume versus temperature diagram for polymers.
(Diagram obtained from C-MOLD polymer properties database)

When referring to injection moulding, this volumetric contraction during cooling is called shrinkage. Since you need to heat the polymer beyond its glass transition temperature to be able to process it, shrinkage is inherent in the injection moulding process. Polymers have high thermal expansion coefficients, and significant shrinkage occurs during cooling of the plastic in the mould. Some thermoplastics undergo volumetric contractions of up to ten percent [29]. To the mould designer

shrinkage is simply the reduction in linear size that occurs during cooling to room temperature from the moulding temperature [43,46].

Crystalline and semi-crystalline materials are particularly prone to thermal shrinkage with amorphous materials tending to shrink less. When crystalline materials are cooled below their transition temperature, the molecules rearrange in a more orderly fashion, to form crystallites, whereas the microstructure of amorphous materials does not change with the phase change [7,45]. This difference leads to crystalline and semi-crystalline materials having a greater difference in specific volume between their melt and solid phase. Also note that the cooling rate affects the behaviour of crystalline and semi-crystalline materials.

When the molten polymer inside the cavity is cooled, we observe that (if we look at the thickness direction) the cooling starts from the mould surface and penetrates inwards. As long as this shrinkage of the component is even/uniform, that is the shrinkage is the same on both sides of the midplane, the component will just become smaller. If however, there is a variation in the shrinkage through the cross section of a part, this will create internal (residual) stresses. When these stresses start to relax, the component undergoes a distortion where the surfaces of the moulded part do not follow the intended shape of the design. This distortion is called warpage. If the shrinkage throughout the component is uniform, the component will not deform or warp, it simply becomes smaller.

The effects of the aforementioned residual stresses are similar to externally applied stresses (loads). If the residual stresses are high enough to overcome the structural integrity of the part, the part will warp upon ejection from the mould or warp later, when an external service load is applied.

In reality, shrinkage is affected by a number of factors, any of which can alter the amount of contraction experienced by a given polymer. The ones that cause excessive part shrinkage beyond an acceptable level are; low injection pressure or low packing pressure, short packing time, high melt temperature and part thickness.

Warpage can be caused by molecular and fiber orientation, temperature variation within the moulded part, variable packing, or different pressure levels as material solidifies across the part thickness.

To compensate for shrinkage, the dimensions of the mould cavity must be made larger than the specified component dimensions [43,46]. Mould dimensions must also be determined for the particular polymer to be moulded, since the same mould will produce different part sizes for different polymer types. In industry, shrinkage percentages for specific polymers are normally obtained from the polymer supplier prior to making the mould.

One of the problems is that the increase in shrinkage is non-linear. Shrinkage of a specific polymer can change for instance, when the thickness of the component and or the melt temperature at which the polymer is injected change. This makes it very difficult to provide proper dimensional tolerances in mould design. A large number of moulds have thus been produced by trial and error. This practice means the time-to-market-window for producing a working mould takes longer than is necessary.

In order to speed up the production process for injection moulded components, channels are machined into the tool steel halves of the mould. Cooling fluid (generally cold water) is then pumped through these channels, forcing the molten polymer to cool faster, hence increasing production.

The norm for injection mould design seems to require the runner system to be put in first, then the moving cores, followed by the ejectors, and lastly due to a lack of room a few cooling channels are added in a haphazard fashion. This type of design where the cooling is fitted last will probably never run well, because uneven cooling that leads to uneven shrinkage is set up in this fashion [27]. Designs like this normally run slower and produce higher stressed and distorted parts, which will require machine settings to be changed regularly to keep it running. Since cooling channel design is such a deciding factor for ensuring optimum cooling and better parts, this study will focus primarily on mould cooling as a cause of warpage.

It is understood that injection moulding is a business of compromises and most of the time it is not possible to have the optimum location for everything. However, in the design process, that is what should be strived for. When we look at injection moulding, we have to fill the part, so the location of gates and venting are the first priority. Then we have to cool the part so mould cooling channels and temperature control form the second priority. Next the part has to be ejected, this is the third processing priority.

The purpose of this investigation is to predict the shrinkage of an injection moulded component accurately, and to minimise the occurrence of warpage. Dimensional accuracy of the mould cavity needs to be achieved, the first time everytime, in order to reduce cost and time. Part cooling should be discussed and given the same attention as other mould considerations. Computer simulation software that uses finite element analysis should be considered to convince mould manufacturers to do the necessary planning before cutting the steel.

Since the purpose of this study has been defined, the focus now needs to be on the planning required to achieve this goal. Chapter 1 of this work introduces the concept of shrinkage, the concept of warpage, and the relationship between the two concepts. These concepts form the basis of the development of this project. This Chapter also gives a brief overview of the causes of shrinkage and warpage. The objectives of this study are then laid out and at the end of this Chapter, the available commercial software that are used within this project are evaluated in terms of usefulness. Chapter 2 starts with a detailed discussion of the injection moulding process, and also provides an in-depth discussion of the causes of shrinkage and warpage. The fundamentals of residual stresses as they relate to the injection moulding process are defined. Lastly a detailed overview of thermal transfer, pertaining to the injection moulding process is given.

In Chapter 3, a sensitivity analysis is conducted, with the view to laying the foundation for a study aimed at assisting the tooling industry with guidelines to determine shrinkage. In the sensitivity analysis the shrinkage is determined for different polymers, at different thicknesses and with different processing parameters. Chapter 4 is a case study of a commercial component. The aim of this case study is to determine if computer simulation software can accurately predict optimum processing conditions, reduce the turnaround time of producing injection moulds, determine the extent of shrinkage and warpage and achieve balanced cooling.

In Chapter 5 an alternative model for the cooling stress build-up in an injection moulded part is proposed. The role of both pressure history in the molten polymer during cooling, and the interaction between the sample and the mould are identified and numerical calculations of the final cooling stress distribution were performed.

Chapter 6 is a summary of the conclusions of the work that was done in the other chapters. Possible future work and projects are also identified and discussed.

1.2 Objectives of this Investigation

Warpage in polymer components is due to the relaxation of residual stresses caused by non-uniform heat dissipation during the cooling stage of the injection moulding cycle. The first objective of this study would be the understanding of the mathematical model describing the heat transfer process during the cooling stage. Of the three modes of heat transfer, only conduction and convection are considered. Heat transfer within the polymer melt is treated as transient, local, one-dimensional heat conduction with static solidification. Heat transfer within the mould is treated as transient, three-dimensional conduction. Heat exchange between the channel surfaces and the cooling fluid is treated as steady-state and uses convection.

The second objective would be the development of a numerical model and solution algorithm for the cooling/heat transfer process. The proposed model investigates the cooling stress build-up during the injection moulding process, with reference to a rectangular cavity. The mould region gets divided into layers and the relevant equations solved to identify the stress within the solidifying layers during cooling.

The third objective of this work should be the comparison of the abovementioned results with those predicted by the C-MOLD injection moulding simulation software. The last objective is to perform a sensitivity analysis to determine the shrinkage for different component thickness, melt temperatures, etc. and the recommendation of optimisation procedures for the minimisation of warpage.

1.3 Literature survey

Shrinkage and warpage are affected by many factors: the part geometry, properties of moulding material used, moulding process conditions, the injection mould design and manufacturing. Research on the injection moulding process has been around for decades, but initial investigation was limited. In the sixties and seventies, many researchers analysed one-dimensional flow behaviour in rectangular and disk shaped thin cavities. Although these numerical models describing the process were available, it was only in recent years that this benefited from the progress made in computer aided engineering.

The model of Kamal and Kenig [30,31] is some of the earliest work and they proposed an integrated mathematical treatment of the filling, packing and cooling stages of the injection moulding cycle, with reference to the radial filling of a center gated disc model. The packing stage was considered as the non-isothermal flow of a compressible material, while the cooling stage is analysed as a transient cooling problem of a stationary volume of polymer melt. The heat conduction equations were

solved for both the melt and solid with standard boundary conditions. Latent heat effects were also taken into consideration. Numerical results were obtained for the melt front, flow rate, velocity profile and temperature profile throughout the packing and cooling stages. These theoretical prediction was compared with experimental results and yielded significant data at the time, despite the assumptions made.

This next article is a continuation of the previous paper. A simulation of injection moulding was performed by Kamal and Lafleur [32]. The three stages: filling, packing and cooling were analysed with the aim of outlining developments associated with computer simulation of the thermoplastic injection moulding process. This simulation incorporates relationships between resin properties, machine design, moulding conditions, and the development of the microstructure in order to provide information regarding the behavior of the material during moulding. Since there is no fluid motion for the cooling stage, the problem is reduced to the transient heat transfer by conduction of a polymer melt trapped between two cooling plates. In the earlier work, Kamal and Kenig [30,31] solved this problem for a circular cavity using a one-dimensional heat conduction equation with variable polymer properties.

Most of the earlier research regarding the injection moulding process has been focused on the analysis of the filling stage, especially the prediction of injection pressure and melt front advancement, with some consideration to packing and cooling. Researchers later recognised that the properties and quality of the microstructure are determined by the packing pressure and holding time, which regulates the extra mass entering the cavity after filling.

A new model that describes the injection moulding process is proposed by Kamal and Lafleur [34,35]. It claims to be a more realistic simulation that describes pressure drop in the delivery system, melt front advancement, and residual stress characteristics and crystallinity distributions of the final product. The theoretical predictions for the mathematical model were compared with experimental data and were found to be in good agreement.

Darlington et al [13] investigated the pressure loss in the mould during the packing stage of the injection moulding process. Initial experiments were inconclusive due to the polymer solidifying across the transducers. Experiments have been carried out with hot moulds to prolong the packing stage at the expense of cooling, in order to achieve more accurate measurements. This was an important study in terms of predicting pressure losses in the packing stage, and proper control of the injection moulding operation.

Titomanlio et al [48] performed injection moulding tests on a resin. Data of mass entering the mould during the packing-holding stage as a function of flow rate and holding time are presented. The experimental results showed only a small part of the density increase due to crystallisation seems to be compensated for by the packing-holding stage.

More than three-fourths of the cycle time in an injection moulding process is taken by the cooling phase. Improving the cooling design will reduce the cycle time and improve part quality by preventing differential shrinkage, internal stresses and warpage. As with the packing stage, researchers also began to focus their attention on cooling investigations.

A model is proposed by Kamal and Lafleur [33] for the treatment of heat transfer with crystallisation during plastics processing in general, and injection moulding in particular. The model incorporates experimentally determined crystallisation kinetics parameters. It permits the calculation of the distribution of both temperature and crystallinity in the moulding. Theoretical predictions were found to be in good agreement with experimental measurements in both injection moulding and a prototype apparatus.

Titomanlio et al. [47] proposed a model for the cooling stress build-up in the injection moulding process. The role of both pressure history in the melt during sample cooling and the interaction between sample and mould were identified with reference to a rectangular cavity. Numerical calculations of the final cooling stress distribution as affected by different histories of melt pressure were performed with the aim of evaluating the effect of different holding pressures and times. The numerical results favourably compare with experimental indications in other literature.

Himasekhar et al [21] analysed mould cooling with the emphasis on achieving rapid, uniform and balanced cooling. Design parameters for two-dimensional analysis of heat transfer within the mould were found inadequate for complex parts, particularly for the prediction of hot spots and warpage, and a three-dimensional simulation was needed. A computer software package (COOL3D) has been developed for the simulation of heat transfer during the cooling stage of the injection moulding process. A numerical formulation is presented to simulate the cooling stage of the injection moulding process. Simulations of transient non-linear heat conduction within the part melt, three-dimensional heat conduction within the mould and a steady convective heat exchange between the coolant and cooling channels, were simultaneously carried out to model the actual process conditions.

The shrinkage that occurs during solidification of a thermoplastic polymer causes a gap between the part and the mould. The result is a sharp temperature drop across the gap. Yu et al [49] described a method for obtaining the thermal contact resistance (TCR) between an injection moulded component and its mould. TCR for this work was obtained through a combination of experimental and analytical procedures. A remarkable improvement in the accuracy of a computer simulation was noticed when TCR was made an input to a computer program Polycool II.

At this point, relatively little experimental or theoretical work has been carried out with regard to the residual stress setup during the injection moulding process. It also became clear that cooling stress, density distribution and product shrinkage were closely related to packing and holding variables, and that these stages cannot be investigated separately any longer. Researchers began to recognise that an integrated simulation of the entire injection moulding process is necessary to faithfully accommodate the effects on the final moulded component.

With mould cooling programs that can assist in designing the cooling channel system, emphasis is placed on simulating the post-filling stage to address such concerns as shrinkage, warpage and mechanical properties of moulded parts. As part of such an effort, Chiang et al [9,10] present a unified theoretical model to simulate the filling and post-filling stages of the injection moulding process. Implementation of such a model is based on a hybrid finite-element/finite-difference numerical solution of the generalised Hele-Shaw flow of a compressible viscous fluid under non-isothermal conditions. The analysis includes varying specific heat and thermal conductivity as a

function of temperature. It was demonstrated that the unified formulation is well suited to handle complicated moulds where compressibility effects can become important even during the filling stage, as some portions of the cavity undergo packing while other regions are still filling.

Chiang et al [11] performed work that was a continuation of the previous paper. They performed a coupled analysis of the fluid flow and heat transfer in the melted polymer during the filling and post-filling stages of the injection moulding process, and of the mould cooling that occurs during the entire process. The results obtained from this integrated simulation have been compared with experimental data and favourable agreement has been noticed.

Very few studies have included comparison of simulation and experimental results on a relatively complex injection moulded part. Ni and Wang [40] carried out a study on the prediction of shrinkage and warpage using the Injection Moulding Simulation program C-MOLD and then compared it with experimental data from an injection moulded part. The simulation results agree well quantitatively with the experimental data.

The work in this paper is based on the numerical model (to determine cooling stress and part shrinkage) proposed by Titomanlio et al. [47]. Computer simulation software will be used to determine the temperature field through the cavity cross-section, and the results of this model will be compared with results predicted by C-MOLD.

A case study that follows the work of Ni and Wang [40] will be conducted for a commercial plastic component, using the injection moulding simulation software C-MOLD. This investigation will aim to not only determine the extent of shrinkage and warpage of a relatively complex part, but also to accurately predict the optimum process conditions that can be used as guidelines for the manufacturing of both mould and component.

1.4 Available Commercial Systems

The aim of increasing the international competitiveness of the South African manufacturing industry requires applied technological research and development activities, especially in the field of Computer Aided Engineering (CAE). The application of the computer to part and mould design as well as mould manufacturing can be seen as the most remarkable development in the injection moulding process [40]. Although injection moulding, as a process, has been around for decades, the engineer's ability to accurately predict the outcome without computer simulation was limited by the large amount of parameters available [16]. Many were also unaware of the limitations of plastics due to processing which resulted into overdesign, high cost and missed deadlines [16]. This is inadequate in today's increasingly competitive environment when applied to the moulding of larger, more complex, more precise, and costlier parts with new processes and materials.

Substantial progress has been made in CAE technology for both thermoplastics and thermosets, removing most of the guesswork from the design process [8,11]. The engineers designing the component and mould can perform moulding trials on the computer before the part design is completed. Process engineers can systematically predict a process window which guides product, tooling and process design efforts as

well as obtain information about the influence of the process variables on the part performance, cost and appearance. CAE makes it possible to replace traditional trial and error design and decision-making procedures with a concurrent design process.

CAE is integrated with two other widely used computer-aided technologies, Computer-aided design (CAD) and Computer-aided manufacturing (CAM).

CAD is the process of performing design tasks with the aid of computers. This includes the generation and modification of the product geometry using a computer, printing the graphic images as hard copies, and electronically storing, retrieving, and exchanging the design information. In particular, solid models generated by computers aid in visualisation, communication, assembly simulations, interference checking, and fit verification. Geometric models created from the design provide the basis for structural and performance simulations and analysis, and graphical output greatly simplifies interpretation of results.

One of the performance simulations that CAD can provide includes the Injection Moulding Simulation Software program C-MOLD, a widely used polymer-processing operation. This software program comprises a set of computer programs for plastics moulding simulations. It provides solutions to problems, experienced with plastics moulding processes, in all stages of design and manufacturing [3].

C-MOLD employs a simultaneous analysis of the compressible fluid flow and heat transfer in the molten polymer during the filling and packing stages, coupled with a mould cooling simulation during the entire process (mould closed stage). These are then integrated with residual stress calculations and structural analysis [1,5]. The analysis requires accurate input data to generate the best predictions.

To solve the relevant governing equations simultaneously, C-MOLD uses a modified, three-dimensional boundary-element numerical method for the mould region, and a through-thickness one-dimensional heat transfer analysis of the melt region [5]. These two analyses are coupled to match the temperature and heat flux at the mould/melt interface.

The governing equations for coolant flow are solved using the Newton-Raphson iterative method to obtain the flow rate and pressure drop in each element. The heat transfer coefficients for heat exchange between the channel surface and the coolant are calculated using these flow rates.

The C-MOLD simulation software assumes the following:

- The thermal conductivity of the mould material remains constant.
- The analysis starts with heat transfer inside the mould being periodic, assuming that after the first few cycles the initial transients die out.

Stress develops in the plastic part due to the simultaneous application of flow, packing pressure, uneven cooling and non-equilibrium density changes. C-MOLD performs structural analysis and calculates residual stresses while the part is still in the mould and during the period after ejection, in order to predict the shrinkage and warpage.

The structural analysis of the shell structure is based on a faceted approximation, where an assembly of flat triangular elements replaces a curved shell surface [5]. This approach allows analysis of thin-shell structures, including complex parts where sharp

profile changes such as edges or corners restrict lateral motions in the freezing polymers.

The following assumptions are made about the mathematical model of injection moulded parts:

- Injection moulded parts are thin-shell and beam structures.
- Rotations and strains in the structure are small.
- The polymer is a transversely isotropic viscoelastic material.
- The behaviour of the structure is linear and static.
- Lateral deformations in the mould are negligible, but transverse displacements are allowed.
- The application of pressure as the applied stress in the thickness direction is allowed.

As useful as C-MOLD is as an injection moulding simulator, it is a very time consuming program to employ in the modelling of complex geometries. The need arises to find an additional software program that can be used as a drafting tool/pre-processor. The geometry can then be exported from the drafting program and imported into C-MOLD.

The commercially available parametric solid modeller Pro/Engineer® was identified as the software to be used for the creation of the geometry. Pro/Engineer® models are sculpted, rather than drawn from solid volumes of material. A primary and essential difference between Pro/Engineer® and traditional 2D computer aided drafting systems is that Pro/Engineer® models are three-dimensional. In Pro/Engineer®, drawings are produced as views of the model, rather than the other way around.

Solid modelling in Pro/Engineer® is a cumulative process and certain features must, by necessity, precede others. Those that follow must rely on previously defined features for dimensional and geometric references. The relationships between features and those that reference them are termed parent-child relationships. The parent-child relationship is one of the most powerful aspects of Pro/Engineer®, in that it allows quick changes to part geometry [41]. When a parent feature is modified, its children are automatically revised to reflect the changes in the parent feature's geometry.

To prepare the Pro/Engineer® part for export, the part surfaces are paired so that material is sandwiched between selected surfaces. These surfaces are then compressed together to form a single surface having thickness as a property, whereafter it is sent to C-MOLD using the Initial Graphics Exchange Specification (IGES) format. The IGES format transfers graphical and textual information between computer aided design systems. Pro/Engineer® version 20.0 supports IGES version 5.2 and all earlier versions of IGES for export.

Pro/Engineer® also consists of an optional module Pro/Molddesign that provides the tools to simulate the mould design process within Pro/Engineer®. This module allows you to create, modify, and analyse the mould form components, and quickly update them to the changes in the design model.

Chapter 2

The Process of Injection Moulding

The previous Chapter introduced the reader to the concept of shrinkage and warpage of plastic products. This Chapter deals with injection moulding in detail, the causes of shrinkage and warpage, and the mathematical model describing the process.

2.1 Introduction to the Injection Moulding Process

Injection moulding can be described as a cyclic process whereby plastic parts are being formed into a desired shape by forcing the hot polymer melt into a cavity under controlled pressure. Shaping can be achieved by either cooling, in the case of thermoplastics or by a chemical reaction in the case of thermosets [1]. Injection moulding is seen as one of the most common and versatile operations for mass production of complex parts, with excellent dimensional tolerance [1].

Injection moulding is one of the most widely used methods of producing thermoplastic parts, from small components such as pen caps to entire front panels for home entertainment centres [1]. It requires minimal or no finishing and the process can also be extended to other materials such as fibers and ceramics. The reciprocating screw machine, vast new alternative processes and computer aided design and manufacture are seen as major milestones in the field of injection moulding [16].

A typical injection moulding machine consists of an injection-, mould-, hydraulic- and control system; refer to Figure 2.1.

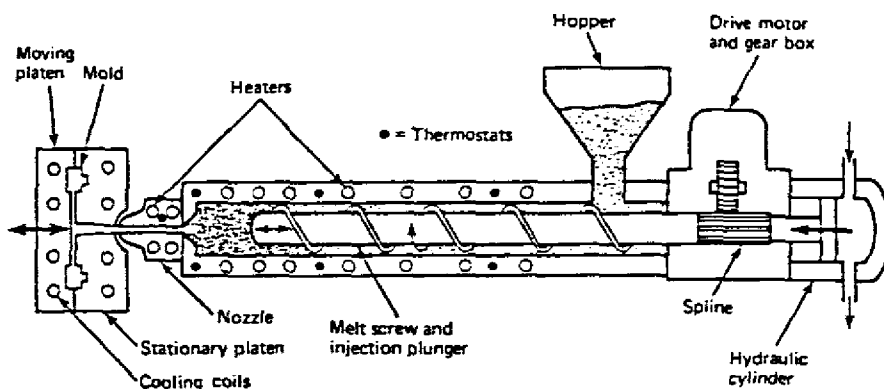


Figure 2.1 Simplified schematic of an injection moulding machine.
(Schematic obtained from Timings, R. L., Manufacturing Technology)

The *injection system* consists of a hopper, reciprocating screw and barrel assembly and an injection nozzle, which melts the plastic pellets, injects the molten polymer into the mould cavity and compresses the melt. The hopper on the machine holds the thermoplastic material which is supplied to injection moulders in the form of small pellets. These pellets are gravity fed from the hopper into the barrel and screw assembly, where it is heated by electric bands [43]. The reciprocating screw consists of three zones: feeding zone, transition zone and metering zone. While the outside

diameter of the screw remains constant, the depth of the flights on the screw decreases from the end of the feed zone to the beginning of the metering zone. These flights compress the material against the inside of the barrel to create viscous (shear) heat, which is mainly responsible for melting the material [1]. The heater bands are not used to melt the pellets (due to the slow heating rate through pure conduction only), but help to maintain the material in its molten state [1]. The resin is pushed along the heated tube by the screw feeder until a sufficient volume of melted plastic is available at the injection nozzle. The nozzle connects the barrel to the sprue bushing of the mould and forms a seal between the barrel and the mould. The screw is then plunged forward to force the plastic into the mould. This is called the filling stage and the fill time is defined as the time needed for the polymer to fill the entire cavity.

The *mould system* is made up of stationary and moving plattens and mould bases, that house the cavity, sprue, runner systems, ejector pins and cooling channels. The mould can be seen as a heat exchanger in which the molten plastic solidifies to the desired shape and dimensional details, defined by the cavity [4].

Once the cavity is filled, the screw is held under pressure, additional polymer is packed into the cavity and hold to compensate for the anticipated shrinkage as the polymer solidifies, hence the packing stage. Cooling channels are passageways located within the body of a mould, through which a cooling medium circulates. Their function is to speed up the cooling process and subsequently reduce the cycle- and production time; refer to Figure 2.2.

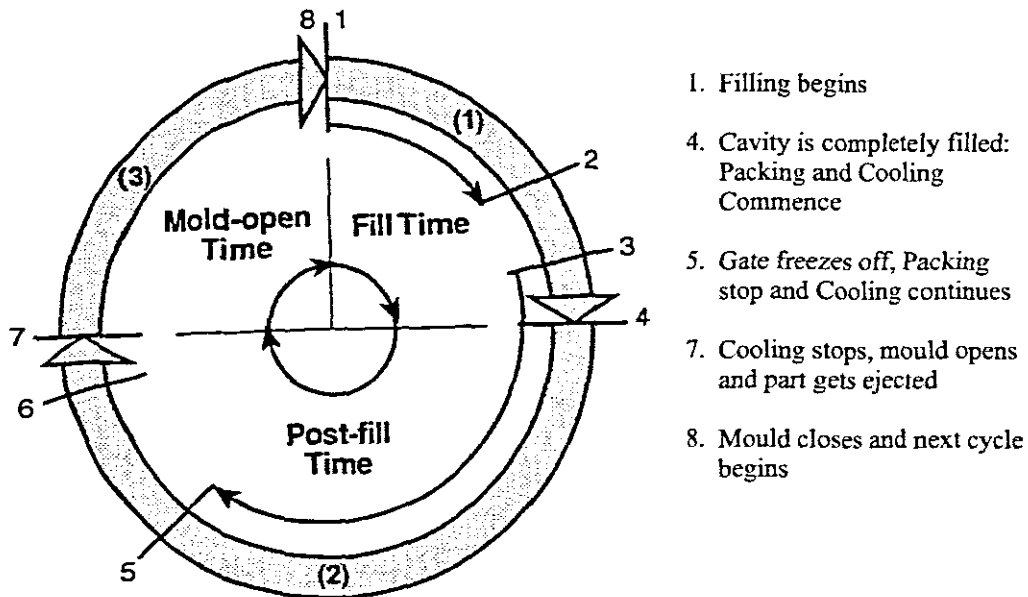


Figure 2.2 The injection moulding cycle.
(Schematic obtained from C-Mold User's Guide Reference Manual)

Heat from the polymer is lost to the surrounding mould, a part of this heat reaches the cooling channel surfaces, which in turn exchange heat with the circulating cooling fluid. The rest of the heat reaches the mould exterior surfaces which lose heat to the ambient air. The cooling stage starts at the same time as the packing stage, and ends when the polymer temperature is sufficiently low and the part is rigid enough to be removed from the cavity without significant deformation. Ejector pins eject the

moulded piece. The post-fill time is defined as the time from the moment when the cavity is completely filled and the instant when the mould opens.

The *hydraulic system* is made up of hydraulic motors, pumps, valves and tubing. It provides the power to open and close the mould, apply the clamp force and drive the screw. After mould opening, the sprue and runners are trimmed off if necessary, usually in a separate trimming press. The mould is then closed again to begin the next cycle. This mould-open stage includes mould-opening and-closing actions as well as component ejection.

The *control system* monitors and controls the processing parameters such as temperature, pressure, injection speed, etc. The process control has a direct impact on the final part quality and modern injection moulding machines have sophisticated microprocessor-based control systems.

2.2 Residual Stress

Consider a scenario where we simply heat polymer pellets in an open container, and allow it to air cool to room temperature. For this scenario, where there is an absence of flow, packing and forced cooling, we would end up with a component that is relatively stress free. With the process of injection moulding however, polymer pellets are heated using viscous shear, then injected into a colder mould under pressure while flowing rapidly. Additional polymer is then pushed into the mould while the molten polymer is forcibly cooled to its ejection temperature. Upon ejection the component core is usually still molten and cooling also occurs at a slower rate than in the mould.

The injection moulding process by its very nature, induces internal stresses [1]. These internal stresses are called residual stresses. Residual stress is a process-induced stress, frozen in a moulded part. It can be either *flow-induced* or *thermal-induced*. Residual stresses affect a part similarly to externally applied stresses. If they are strong enough to overcome the structural integrity of the part, the part will warp upon ejection, or later crack, when external service load is applied. Residual stresses are the main cause of part shrinkage and warpage [1]. The process conditions and design elements that reduce shear stress during cavity filling will help to reduce flow-induced residual stress. Likewise, those process conditions that promote sufficient packing and uniform mould cooling will reduce thermal-induced stress.

2.2.1 Flow-induced Residual Stress

Unstressed, long-chain polymer molecules tend to conform to a random-coil state, when it is above its melt temperature. During injection, the molecules are orientated in the direction of flow, as the polymer is sheared and elongated. If solidification occurs before the polymer molecules are fully relaxed to their state of equilibrium, the orientation of these molecules is locked within the moulded part.

During the injection moulding process the molten polymer molecules at the mould wall are suddenly exposed to a much cooler surface. For this reason the cooling rate is at a maximum at the mould wall, and the orientation of the molecules are locked in. The component generally gets ejected with the core still molten and the outer skin

solidified. Due to the thermal insulating effect of this frozen outer layer, the cooling rate for the hot core is slower and the polymer molecules in the core are able to relax.

This type of stress is called flow-induced residual stress. Because of the stretched molecular orientation in the direction of flow, it introduces anisotropic, non-uniform shrinkage and mechanical properties in the directions parallel and perpendicular to the direction of flow. The correct process conditions will reduce the shear stress in the melt which means the level of flow-induced stress should be reduced.

2.2.2 Thermal-induced Residual Stress

Thermal-induced residual stress arises after the cavity is completely filled when packing and cooling of the component takes place. The moulded part experiences different cooling rates from the mould wall to the midplane. At the same time the density of the polymer changes due to the variation in temperature and packing pressures as the material solidifies.

During the early cooling stages, when the external layers cool and start to shrink, the bulk of the polymer at the hot core is still molten and free to contract. Later on the contraction of the core is constrained by the already-rigid external layers. This results in a stress distribution with tension in the core and compression in the outer layers. Process conditions that lead to sufficient packing and more uniform mould-wall temperatures will reduce the thermal-induced residual stresses.

2.3 Causes of Shrinkage

The previous section described residual stress as a process-induced stress. Although the injection moulding process naturally leads to a certain amount of stress, there are certain bad practices that will aggravate stress. The following are the causes of excessive shrinkage beyond that already inherent in injection moulding.

2.3.1 Part Thickness

Thicker parts show greater shrinkage [1]. Residual stress that arises due to a variation of the part thickness is a thermal-induced stress. A moulded component solidifies from the outside; the polymer in contact with the mould surface forms a skin that grows toward the centre of the part. At some point during solidification, the gate solidifies, isolating the material in the cavity from the runner system and from packing pressure, as illustrated by Figure 2.3.

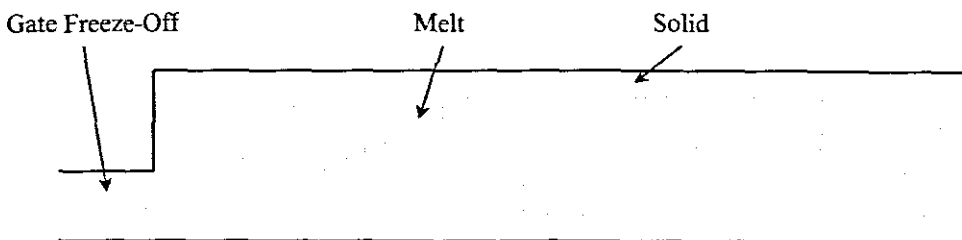


Figure 2.3 Part solidification & gate freeze-off.

When this happens, the molten polymer inside the skin accounts for most of the remaining shrinkage that occurs in the part. A thicker part section, since it contains a higher proportion of molten material, experiences greater shrinkage.

2.3.2 Holding Pressure

Since polymers undergo a volumetric expansion when heated, it makes sense to try and force more molten material into the cavity, so that when it cools and solidifies, the part can shrink to its required dimensions. Provided the dimensions of the cavity have not been increased too much, increasing the holding pressure forces more material into the mould cavity, which then leads to the reduction of shrinkage [24]. Increasing the holding time has a similar effect, assuming the polymer in the gate does not solidify and seal off the cavity. Maintaining pressure forces more material into the cavity while shrinkage is taking place, thereby reducing the shrinkage. Residual stress due to a variation of the holding pressure is a thermal-induced stress.

2.3.3 Melt Temperature

Melt temperature refers to the temperature of the polymer in the cylinder/barrel just before injection. The effect of varying the melt temperature contributes to, both flow- and thermal-induced residual stress. As mentioned before, during filling, the polymer molecules are sheared and elongated, with the maximum shear occurring at the mould wall. An increase in the melt temperature means an increase in the mobility of the polymer molecular chains that will lead to a decrease in shear stress. This decrease in shear stress will reduce shrinkage.

The effect on shrinkage of increasing the melt temperature is however offset by the following. The increase in melt temperature will continue to cause an increase in specific volume, meaning that the difference in volume between processing and room temperature is even greater. The high melt temperature also means an overall lower cooling rate that leads to higher crystallisation levels [5]. Hence the larger volumetric increase more than compensates for the effect on shear stress and viscous heating, and it is found that shrinkage is actually lower at lower moulding temperatures [5].

2.3.4 Injection Rate

The variation of the injection rate affects flow-induced residual stress. Very slow injection rates lead to excessive cooling of the melt front, which subsequently means an increase in shear. It also results in under packing at remote locations away from the gate, and non-uniform crystallising rates of the polymer in the mould [24]. This will result in an increase in shrinkage.

Increasing the injection rate will result in a more uniform polymer and glass fiber distribution, which typically reduce moulded-in stress and shrinkage [24]. A further increase of the injection rate on the other hand will lead to a higher melt velocity, which means the polymer molecules are stretched to a greater degree in the direction of flow. This is illustrated by Figure 2.4. The thickness of the layer of stretched molecules at the part surface is also greater, resulting in increased shrinkage.

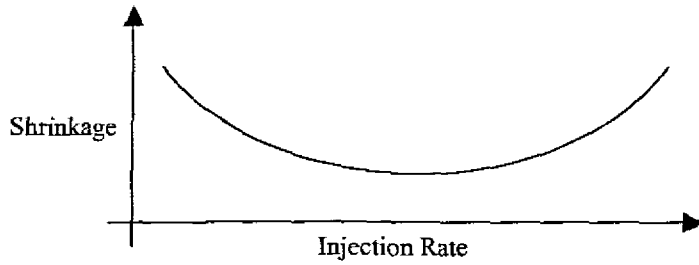


Figure 2.4 Schematic plot of shrinkage versus injection rate.

2.4 Causes of Warpage

As discussed before, warpage is caused by non-uniform shrinkage. If the shrinkage is uniform the part will just become smaller, not deform. There are four mechanisms of warpage, which can individually or together result in the deformation of a component.

2.4.1 Uneven cooling of the part

It can be difficult to achieve uniform and balanced cooling of parts, due to the complexity of part and mould design [5]. Figure 2.5 shows a case that may arise, with a hot upper mould wall and a cold lower mould wall, partly due to uneven cooling channel placement. This type of asymmetric mould wall temperature distribution causes differential thermal contractions of the polymer across the part thickness as it cools from a molten to a solid state. The part warps after it is ejected from the mould due to internal moments that were set up.

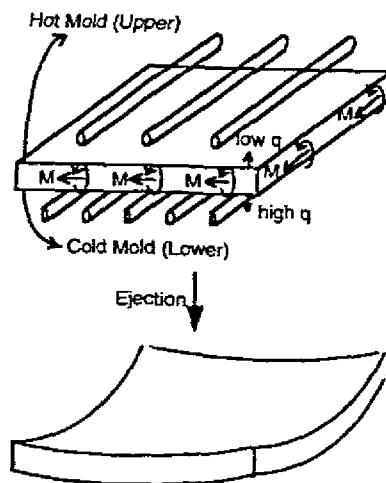


Figure 2.5 Asymmetric thermal shrinkage due to uneven cooling of the part.

M = moment; q = heat flux

(Schematic obtained from C-Mold User's Guide Shrinkage & Warpage)

2.4.2 Part geometry asymmetry

As shown in Figure 2.6, additional differential strain may arise due to the presence of a sharp corner in the moulded part. This type of differential shrinkage is similar to shrinkage generated due to uneven cooling. Owing to poor heat transfer at the inner surface of the corner, it is hotter there than at the outer surface. Consequently, the response of planar regions joined at corners might be different from those that are free.

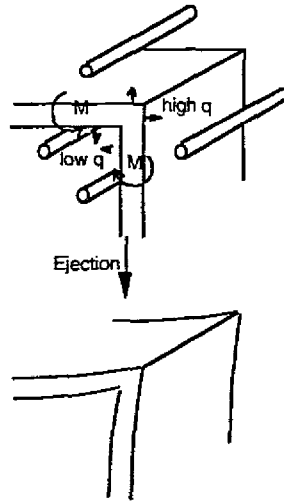


Figure 2.6 Differential thermal strain due to geometry effects.

M = moment; q = heat flux

(Schematic obtained from C-Mold User's Guide Shrinkage & Warpage)

A variation in the thickness of a part will have the same effect, as can be seen from Figure 2.7. Shrinkage increases as the wall thickness increases. Differential shrinkage due to non-uniform wall thickness is a major cause of part warpage in unreinforced thermoplastics [5]. More specifically, different cooling rates and crystallisation levels generally arise within parts with wall sections of varying thicknesses. This causes differential shrinkage, resulting in part warpage.

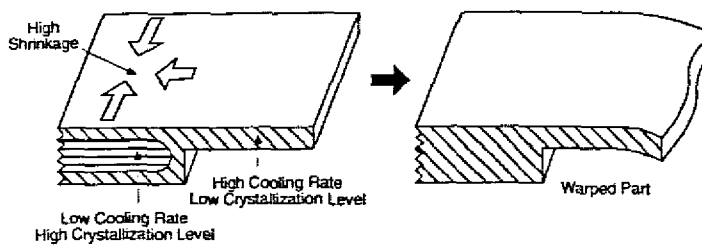


Figure 2.7 Non-uniform wall thickness leads to part warpage.

(Schematic obtained from C-Mold User's Guide Shrinkage & Warpage)

2.4.3 Variable packing

A high processing pressure contributes significantly to the variation of density and thus to the final shrinkage of plastic parts. Also, due to the gate location, the shrinkage within the plastic part is not uniform. Referring to Figure 2.8, the region near the gate has a lower shrinkage as compared to the region far away from the gate [5]. This non-uniform (differential) shrinkage of the part causes warpage.

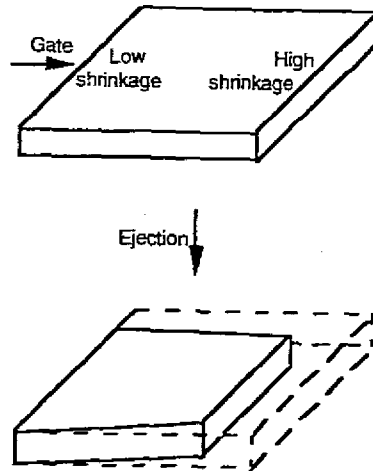


Figure 2.8 Bulk shrinkage and non-uniform planar volumetric shrinkage.
(Schematic obtained from C-Mold User's Guide Shrinkage & Warpage)

2.4.4 Molecular or fiber orientation due to flow

Polymer molecules stretch during the filling stage, which results in some degree of anisotropy in shrinkage or mechanical properties in the longitudinal and transverse directions. Figure 2.9 assists in describing this condition. Material orientation can, in many cases, be related to the direction of the bulk velocity vector during the filling stage. Fiber orientation can significantly alter the linear shrinkage and mechanical properties of the moulded part [5]. The modulus in the direction of fiber orientation is much larger than the moduli in the directions perpendicular to the fiber orientation. This anisotropic behaviour changes the response of the moulded part subjected to the loads generated by other mechanisms.

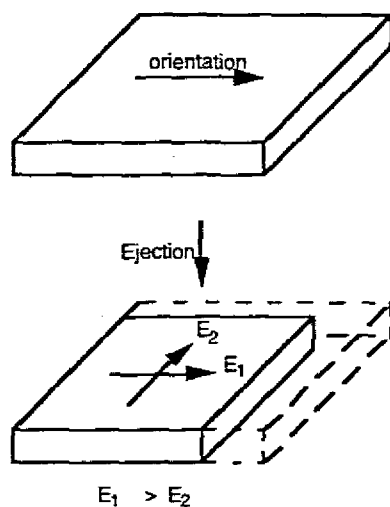


Figure 2.9 Anisotropic material behaviour due to flow orientation.
 E_1 = longitudinal fiber orientation; E_2 = transverse fiber orientation
(Schematic obtained from C-Mold User's Guide Shrinkage & Warpage)

2.5 Overview of thermal transfer

An injection mould is a solid body that transfers heat by conduction, which means that this form of heat transfer will predominate. The source of energy is at the mould-melt interface where the molten polymer gives off heat to the mould which then transfers heat, through conduction towards the cooling channels and the exterior surface. Convection occurs at the cooling channels, where there is a coolant flowing to aid rapid cooling, and at the exterior surface, which is characterised by free convection. The exterior surface is however treated as adiabatic since the ambient temperature does not contribute significantly to the cooling process [5]. Radiation as the third mode of heat transfer is not considered at all.

In order to ease the mathematical manipulation, certain assumptions are made:

- The temperature of molten polymer in the cavity is equal throughout as well as equal to the melt temperature in the barrel; that is, the initial condition is isothermal.
- There is no heat source within the material.
- There is no thermal contact resistance at the interfaces between various parts of the mould; that is, the mould has no inserts or ejector pins.
- The mould material is homogeneous which means thermal conductivity remains constant.
- Heat loss through the exterior of the mould is negligible and will be treated as an adiabatic surface, meaning that the exterior surface will not be modelled.
- The effects of hot and cold runners are negligible and will not be modelled.

2.5.1 Modelling of Heat Transfer in the Mould

Since the mould is assumed to be a solid body, heat flows by conduction according to Fourier's Law of heat conduction [6,22,38], which states that the rate of heat transfer per unit area is proportional to the normal temperature gradient. That is,

$$q_x = -kA \frac{\partial T}{\partial x} \quad (2.1)$$

where q_x = rate of heat transfer in the x direction (W)

k = thermal conductivity (W/m·K)

A = area (m²)

$\frac{\partial T}{\partial x}$ = temperature gradient (K/m)

The minus sign is inserted to show that heat is being lost as depicted by Figure 2.10

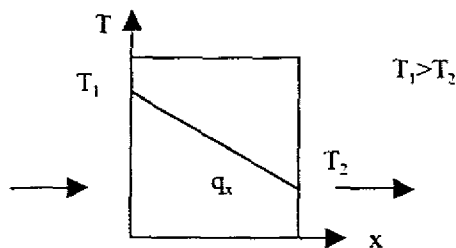


Figure 2.10 Direction of heat flow.

Since we assumed no heat source within the material, the energy balance is:

Energy into the mould = change in energy + energy out of the mould

or

$$q_x = \rho CA \frac{\partial T}{\partial t} + q_{x+dx} \quad (2.2)$$

where ρ = mould density (kg/m^3)

C = specific heat of the mould ($\text{J/kg}\cdot\text{K}$)

t = time (s)

When expressed in the form of a Taylor-series expansion using only the first two terms, we have the governing equation

$$-kA \frac{\partial T}{\partial x} = \rho CA \frac{\partial T}{\partial t} - kA \left[\frac{\partial T}{\partial x} + \frac{\partial}{\partial x} \left(\frac{\partial T}{\partial x} \right) dx \right]$$

So that

$$\frac{\partial}{\partial x} \left(k \frac{\partial T}{\partial x} \right) = \rho C \frac{\partial T}{\partial t} \quad (2.3)$$

Since this is a one-dimensional equation, with the mould being a three-dimensional system, we extend equation (2.3) into a volume equation on a global co-ordinate scale, giving:

$$(\rho C)_m \frac{\partial T_m}{\partial t} = k_m \left[\frac{\partial^2 T_m}{\partial x^2} + \frac{\partial^2 T_m}{\partial y^2} + \frac{\partial^2 T_m}{\partial z^2} \right] \quad \text{for } x \in \Omega \quad (2.4)$$

where Ω is the mould domain and x , y and z are the global cartesian coordinates. The subscript m stands for mould.

This is a periodic heat transfer process in which heat conduction, and thus the temperature, varies with respect to time. To increase the efficiency of the simulation the equation has to be manipulated and simplified to facilitate its application to the injection moulding process.

Consider Figure 2.11 below

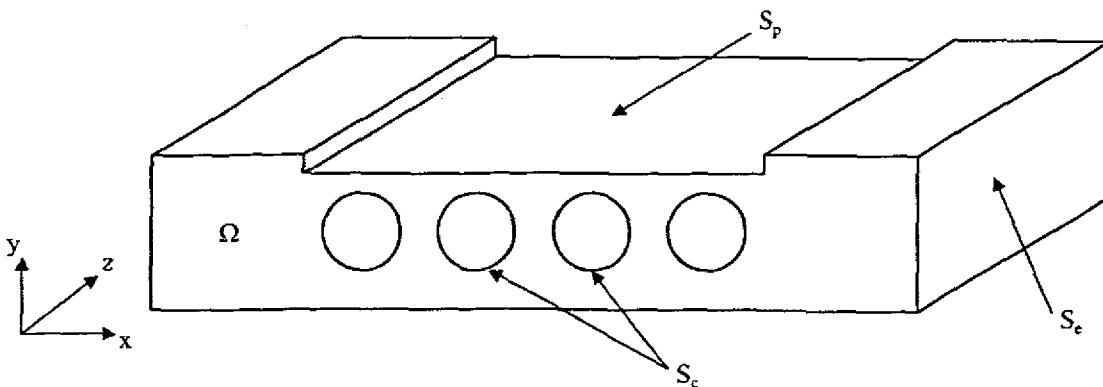


Figure 2.11 Schematic three dimensional mould region.

where Ω = mould region

S_p = part-mould interface

S_c = cooling channels

S_e = exterior surface

In equation (2.4), the mould temperature T_m can be separated into two components:

A steady three-dimensional component $T_{m,s}$

A time-dependent component $T_{m,t}$

Thus

$$T_m(x, y, z, t) = T_{m,s}(x, y, z) + T_{m,t}(x, y, z, t) \quad (2.5)$$

During a typical mould cycle the penetration depth of the thermal pulse due to the time-varying heat flux from the hot polymer melt is limited to within a few millimetres from the cavity surface. This means that the mould temperature at the cooling-channel surface S_c and the exterior surface S_e are not affected by the periodically varying component of the mould temperature at the cavity surface, and we therefore neglect the time variation of temperature at these surfaces and treat them as steady-state conditions. That is,

$$T_{m,t} = 0 \quad \text{and} \quad T_m = T_{m,s}(x, y, z) \quad (2.6)$$

2.5.2 Modelling of Boundary Conditions

Conduction heat transfer takes place at the part-mould interface due to the release of heat from the polymer:

$$-k_m \frac{\partial T_{m,t}}{\partial n} = J \quad (2.7)$$

where n = normal to the surface

J = instantaneous heat flux

J can be obtained by analysing the heat transfer in the polymer melt. During the mould open stage, J is very small and hence neglected

Heat transfer at the mould-cooling channel interface takes the form of forced convection, according to Newton's Law of cooling:

$$q = h_c A(T_m - T_c) \quad (2.8)$$

where q = heat into the coolant (W)

h_c = convection heat-transfer coefficient ($W/m^2 \cdot K$)

T_m = the mould temperature (K)

T_c = cooling channel temperature (K)

A = cooling channel surface area (m^2)

At the mould-cooling channel interface (see Figure 2.12),

$$q_{\text{coolant}} = q_{\text{convection}}$$

which gives:

$$k_m \frac{\partial T_{m,s}}{\partial n} = h_c (T_{m,s} - T_c) \quad (2.9)$$

where h_c = heat transfer coefficient between the mould and the coolant at a bulk temperature T_c .

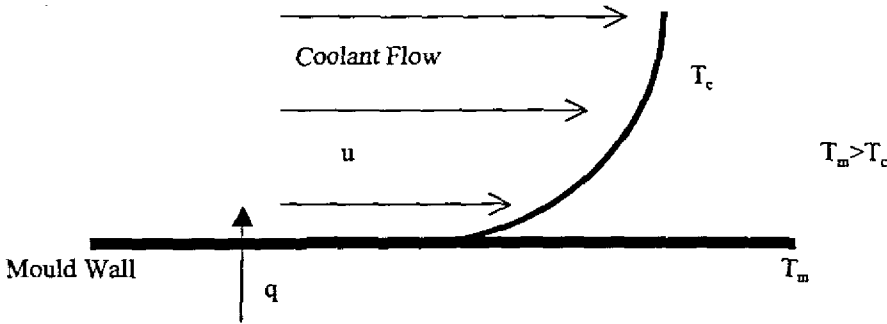


Figure 2.12 Convection heat transfer.

2.5.3 Modelling of the Steady Component ($T_{m,s}$)

The governing equation for the steady component is derived by substituting $T_{m,s}$ (2.6) for T_m (2.4), and since $T_{m,s}$ is not a function of time, we obtain:

$$\frac{\partial^2 T_{m,s}}{\partial x^2} + \frac{\partial^2 T_{m,s}}{\partial y^2} + \frac{\partial^2 T_{m,s}}{\partial z^2} = 0 \quad \text{for } x \in \Omega \quad (2.10)$$

The boundary condition for the above equation is derived by integrating the boundary conditions in (2.7) and (2.9) with respect to time to obtain the following:

$$-k_m \frac{\partial T_{m,s}}{\partial n} = \bar{J} = \frac{1}{t_c} \left[\int_0^{t_c} J(t) dt \right] \quad (2.11)$$

on the part-mould interface,

where $t_c = t_{\text{cycle}} = \text{filling time} + \text{post-filling time} + \text{mould open time}$

and

$$k_m \frac{\partial T_{m,s}}{\partial n} = h_c (T_{m,s} - T_c) \quad (2.12)$$

on the cooling channel surface

The rate of heat transfer between the coolant and the mould is dependent on the temperature gradient, which is in turn dependent on the fluid viscosity, thermal conductivity, specific heat and density.

2.5.4 Modelling of the Time-varying Component ($T_{m,t}$)

The time-varying components at this interface cannot be taken as zero because of the thermal impulse due to the hot polymer. However,

- the thermal pulses in the x- and y- directions travel for less than a few millimetres;
- during one typical cycle time, the distance travelled by this thermal pulse is of the order of the square root of thermal diffusivity times the cycle time;
- this distance is less than the element lengths in a typical mesh;
- the mould temperature gradients in the x- and y- directions are relatively small.

We therefore ignore the effects of the time-varying component from any element lying on the mould cavity upon the surrounding elements in the x- and y- directions, so that:

$$T_{m,t} = T_{m,t}(z,t) \quad (2.13)$$

Thus, the transient one-dimensional equation becomes

$$(\rho C)_m \frac{\partial T_{m,t}}{\partial t} = k_m \left[\frac{\partial^2 T_{m,t}}{\partial z^2} \right] \quad \text{for } x \in \Omega \quad (2.14)$$

This is a boundary condition which occurs at intervals and the time-varying heat flux

$$J_t = J(t) - \bar{J} \quad (2.15)$$

is specified at the mould surface.

Chapter 3

Sensitivity Analysis of Shrinkage

The causes of shrinkage were already discussed in detail in Chapter 2. The objective of this Chapter is to conduct an investigation on the effect of design and processing parameters on shrinkage using the Injection Moulding Simulation program C-MOLD. Shrinkage will be determined and discussed for samples with varying thickness, varying conditions of melt temperature, varying fill times and for 3 different types of polymers while the other parameters are kept constant.

Shrinkage is inherent in plastics, while warpage occurs due to uneven shrinkage. The warpage of a moulded component can be unique to that component, because of a number of parameters such as sharp profile changes in complex parts. The test sample for this exercise will thus be tailored to ensure that little or no warpage takes place.

The geometry of the test part is a rectangle 240 x 120 mm, using a single cavity mould with the location of the gate in the centre. This geometry is selected because it lacks profile changes. Even if the component is not ejected immediately after solidification, it should shrink within the mould, and thereby greatly reduce the possibility of warpage. The location of the gate was chosen to eliminate, as far as possible, variable packing. Cooling is also omitted, which means there are neither cooling channels in the mould, nor any cooling fluid. Heat from the polymer component thus gets transferred evenly through the solid mould body to the exterior surface. Adding cooling will speed up the cycle time, but there is a chance of uneven cooling, that may introduce stresses that will lead to warpage. Lastly, fiber filled polymers are avoided to minimise fiber orientation differences.

Some of the C-MOLD input and output files for this Chapter are illustrated in Appendix A. The rest of the C-MOLD files can be found on the accompanying CD.

3.1 The Process Estimator

The polymer chosen was from the generic family Polypropylene (PP), with an equivalent BASF grade 2500 PCX. Its tensile modulus is 1000 MPa, poisson's ratio 0.38, solid density 0.91 g/cm³, processing temperature 200-280°C and ejection temperature 93°C. Tool Steel of standard DIN 1.2312 with density 7.85 g/cm³, specific heat 460 J/kg·°C, and thermal conductivity 33 W/m·°C was selected. The injection moulding machine is a 182 ton Mannesman Demag horizontal configuration with a maximum clamping force of 165 tons, injection capacity of 304 g or 340 cm³, tie rod clearance of 460 mm, and a maximum machine injection pressure of 133 MPa.

C-MOLD consists of a set of process estimators, which involve computing estimates of key processing conditions based on specified input requirements. One of these estimators is the process window, which displays a plot that outlines the region of acceptable melt-temperature and injection pressure combinations. The required inputs are the selected resin, part thickness and area, range of melt temperatures, mould wall temperature, maximum

machine injection pressure and flow length. The process window computes a recommended fill time and melt temperature, and estimates the injection pressure, which are then indicated on a plot as the optimal process conditions. The outputs from the process window are, however, only estimates. C-MOLD uses these values only to start the analysis. The values for fill time obtained from the analysis will always differ from the estimated fill time because the optimum fill time is computed during the analysis.

The cooling time estimator calculates the estimated amount of time it will take to cool the part. The cool time calculation requires the resin properties, part thickness, melt temperature and maximum machine injection pressure. The estimated outputs are the cycle time and the post fill time.

For the first analysis, samples of thicknesses ranging from 1-5 mm were used. The process estimator was used to estimate the process conditions. The results can be viewed below in Table 3.1. Note that the post-fill time refers to the duration of the post-filling time and not the time at the end of the post-filling stage.

Table 3.1 Varying thickness using the Process Estimator

Thickness	Fill Time	Post-Fill Time	Average Temperature	Minimum Temperature	Maximum Temperature	Shrinkage
(mm)	(seconds)	(seconds)	(°C)	(°C)	(°C)	(%)
1	0.986	3.981	71.00	63.84	78.51	1.54
2	0.930	12.65	71.56	70.05	73.43	1.83
3	0.923	27.30	72.05	71.39	72.87	1.90
4	0.919	47.79	71.92	71.54	72.35	1.94
5	0.960	74.20	72.59	72.34	72.87	1.96

The graph in Figure 3.1 below was generated from Table 3.1. Although the ejection temperature for polypropylene has been specified as 93°C, Figure 3.1 shows part ejection has occurred at an average temperature of +/- 72°C.

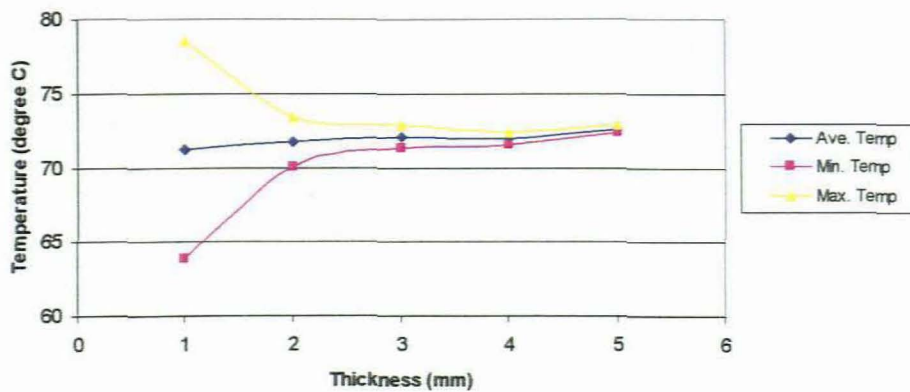


Figure 3.1 Thickness versus ejection temperature.

This is because 72°C is the cooling time estimated by the cooling time estimator, and it overrides the prescribed ejection temperature as the criteria to mark the end of post-filling. The average, minimum and maximum temperature columns in Table 3.1 refer to the component temperature at the end of post-filling, and is across the width-length of the cavity and not across the thickness direction. As the polymer melt front advances, the cooling effect from the mould wall creates frozen layers that progress towards the midplane. For thin components, this phenomenon will result in sections of the component being solidified while the polymer is still flowing elsewhere, leading to temperature differences across the width-length of the cavity.

It was also found that the optimal melt temperature prescribed by the process window was +/- 240 °C. Experience has shown that industry will always attempt to steer clear of using melt temperatures of this magnitude in order to speed up production.

3.2 Varying Thickness

The analysis for varying thickness was repeated using a melt temperature of 220°C to add authenticity to the analysis. The process window is used only to estimate the fill time, and a part temperature of 93°C was used as the criterion to indicate the end of post filling. The results can be viewed in Table 3.2. The sample thickness ranges from 1-12 mm.

Table 3.2 Varying thickness

Thickness	Fill Time	Post-Fill Time	Ejection Temperature	Max. Injection Pressure	Shrinkage
(mm)	(seconds)	(seconds)	(°C)	(MPa)	(%)
1	0.980	3.10	91.15	63.02	1.46
2	0.928	8.64	92.20	17.24	1.79
3	0.922	17.87	92.71	8.57	1.88
4	0.918	30.86	92.75	5.30	1.92
5	0.912	47.09	92.97	3.72	1.94
6	0.930	68.36	92.95	2.76	1.95
8	0.947	126.85	92.95	1.74	1.97
10	1.006	193.52	92.99	1.19	1.98
12	1.188	277.40	92.97	0.81	1.99

The graph in Figure 3.2 below was generated from Table 3.2. Thicker parts show greater shrinkage, as can be seen from Figure 3.2. Injection moulded components solidify from the outside and the polymer that is in contact with the mould surface forms a skin that grows toward the centre of the part. The gate will generally freeze off as the external surface layers cool, leaving the polymer at the core free to contract. The different samples experiences the same packing time, since the gate freezes at the same instant in time. This results in thicker components having a bigger molten core to solid outer skin ratio, leading to a greater percentage of shrinkage for thicker parts. The lack of forced cooling also allows, more than usual, the polymer molecules to relax to their state of equilibrium. The contribution of residual stresses due to flow whilst filling is therefore negligible, especially for the thicker components.

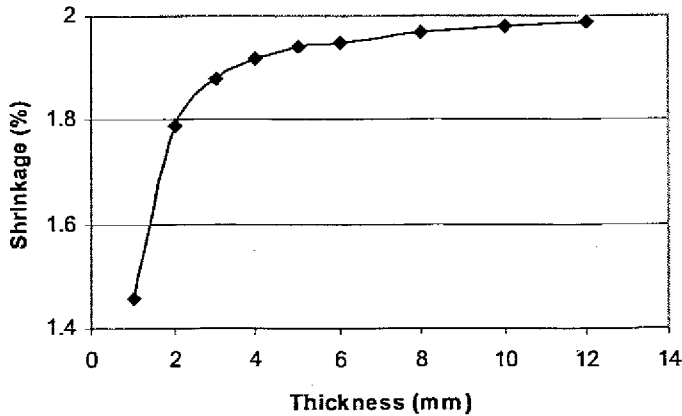


Figure 3.2 Thickness versus shrinkage.

3.3 Varying Polymers

To analyse the differences between three different types of polymers, the same mould and injection moulding machine was used for the analysis between the three polymers. This is the same mould material and machine specifications used for the previous analysis. The thickness of the sample was constant at 3mm, with the injection temperature constant at 220°C. The three polymers are all injected into the cavity in the same filling time. The three most used polymer types in the South African plastics processing industry are Polypropylene, Polyethylene and Polystyrene* with its corresponding BASF equivalent grades being PP Novolen 2500 PCX, PE-LD Lupolen 2410 H and PS Polystyrol 2710. Their properties are given in Table 3.3.

Table 3.3 Comparative Polymer Properties

Generic Type	Polypropylene	Polyethylene	Polystyrene
BASF Equivalent	PP Novolen 2500 PCX	PE-LD Lupolen 2410 H	PS Polystyrol 2710
Transitional Classification	Semi-Crystalline	Semi-Crystalline	Amorphous
Tensile Modulus (MPa)	1000	1500	1500
Poisson's Ratio	0.38	0.4	0.38
Solid Density (g/cm ³)	0.9	0.87	1.05
Melt Density (g/cm ³)	0.765	0.77	0.892
Maximum shear rate (1/s)	24000	40000	40000
Ejection Temperature (°C)	93	80	80
Processing Temperature (°C)	200 – 280	180 - 280	180 – 280
Maximum Shear Stress (MPa)	0.26	0.11	0.24
Transition Temperature (°C)	135	90	100
Applications	Sterilised bottles, packaging film, appliance housings	Squeezable bottles, toys, refrigerated housewares	Wall tile, battery cases, indoor lighting panels

* Information obtained from Sasol Polymers

The results from the comparative analysis between the three polymers, as obtained from C-MOLD can be viewed in Table 3.4.

Table 3.4 Varying Polymers

Polymer Type	Filling Time (sec)	Holding Pressure (MPa)	Maximum Temp. (°C)	Maximum Shear Rate (1/s)	Post-Filling Time (seconds)	Ejection Temp. (°C)	Clamp Force (Ton)	Shrinkage (%)
PP	0.922	8.57	220.16	3042.9	17.873	92.71	22.552	1.88
PE	0.922	9.91	219.87	3107.1	12.544	66.66	22.589	1.32
PS	0.922	13.17	220.41	3062.2	17.257	72.77	33.524	0.63

Considering all three polymers were injected with the same fill time, at the same melt temperature and into the same cavity, the variations in post-fill time, holding pressure and clamp force can be attributed to the polymer properties. Although this chapter is aimed at analysing shrinkage, it would be worthwhile to analyse the aforementioned processing parameters since it adds to the understanding of shrinkage variation.

The polymer properties can be compared, by studying the Cross-WLF viscosity model data plots. This is a plot of viscosity versus shear rate across the processing temperature range. To incorporate the dependence of polymer viscosity on shear rate, temperature, and pressure, the Cross-WLF model is used for simulating the post-filling stages in injection moulding, when the polymer undergoes cooling throughout the cavity.

Viscosity is a material’s resistance to flow, and can be expressed as the ratio of shear stress (force/area) to the shear rate (rate change of shear strain). Shear rate is an important flow parameter since it influences the amount of shear (viscous) heating.

When studying the viscosity versus shear rate diagram, it is important to understand the influence of pressure and temperature on the viscosity and shear rate. As shown in Figure 3.3, the melt viscosity decreases with increasing shear rate and temperature due to the disentanglement and alignment of the molecules and enhanced mobility of polymer molecules, respectively. In addition, the higher the pressure, the more viscous the melt becomes.

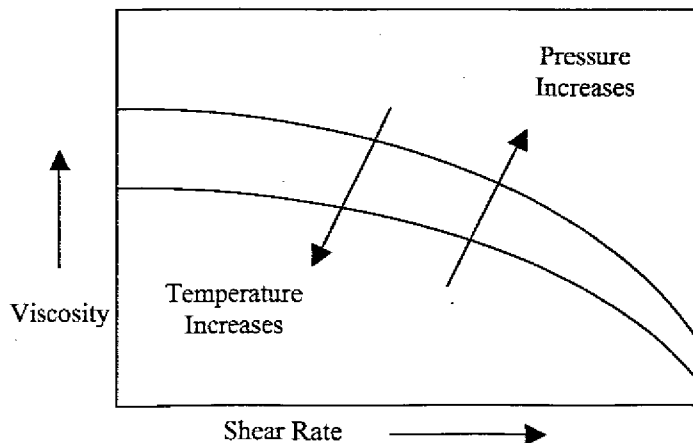


Figure 3.3 Polymer viscosity depends greatly on the shear rate, pressure and temperature.

When looking at the viscosity versus shear rate plots (Figures 3.4 – 3.6), note that the viscosity for polypropylene is slightly less for a given temperature than for polyethylene. This would result in polypropylene experiencing more viscous heating and less pressure during mould filling. This explains the higher values for post-filling time and lower values for holding pressure and clamp force for polypropylene in Table 3.4, compared with polyethylene.

The viscosity versus shear rate plots for polyethylene and polystyrene appears to be fairly similar. When, however, one considers that viscosity is equal to shear stress divided by the shear rate, and noting the higher value of shear stress for polystyrene from Table 3.3, at the same melt temperature, polystyrene generates more viscous heat. This explains why the post-fill time for polystyrene is longer than for polyethylene. Although the increase in temperature means a decrease in pressure, the holding pressure for polystyrene is still more than for polyethylene. This is because Polystyrene undergoes less volumetric increase and is less compressible than Polyethylene and also Polypropylene.

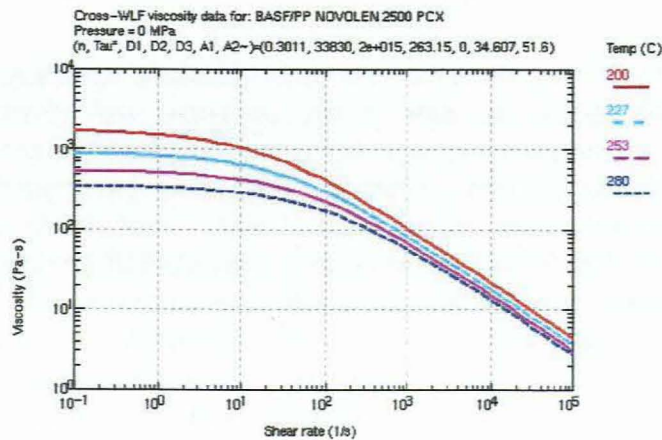


Figure 3.4 Viscosity versus shear rate diagram for polypropylene. (Diagram obtained from C-MOLD polymer properties database)

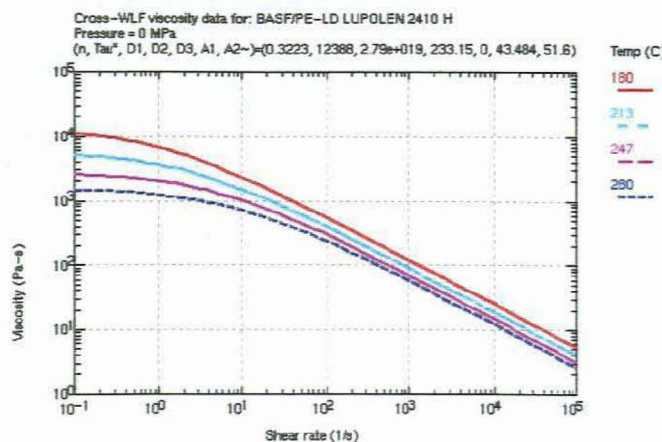


Figure 3.5 Viscosity versus shear rate diagram for polyethylene. (Diagram obtained from C-MOLD polymer properties database)

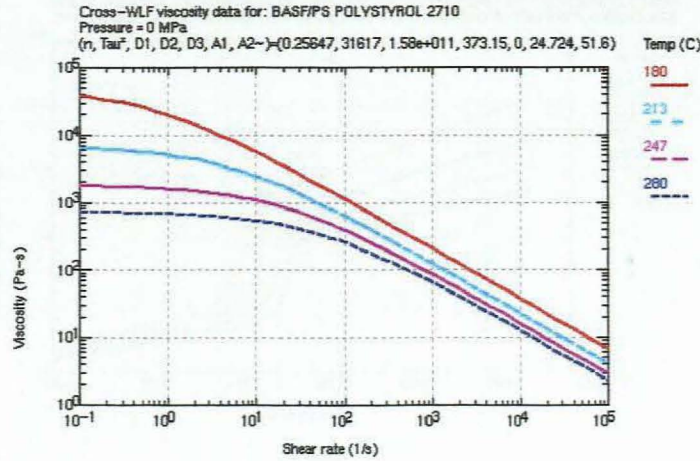


Figure 3.6 Viscosity versus shear rate diagram for polystyrene.
 (Diagram obtained from C-MOLD polymer properties database)

The value of the percentage shrinkage that was obtained from C-MOLD for polystyrene (Table 3.4) is relatively low when compared with the values for polypropylene and polyethylene. This can be attributed to the fact that polystyrene is an amorphous polymer. Semi-crystalline polymers are particularly prone to thermal shrinkage with amorphous materials tending to shrink less. This is because the molecules of crystalline polymers rearrange in a more orderly fashion when cooled below their transition temperature, to form crystallites. The microstructure of amorphous polymers do not change with phase change. This difference leads to crystalline and semi-crystalline materials having a greater difference in specific volume between their melt and solid phases. This phenomenon can also be seen when studying the three specific volume versus temperature diagrams (pvt diagrams: Figures 3.7 – 3.9), and noticing the sudden increase in specific volume at the transition temperatures of polypropylene and polyethylene.

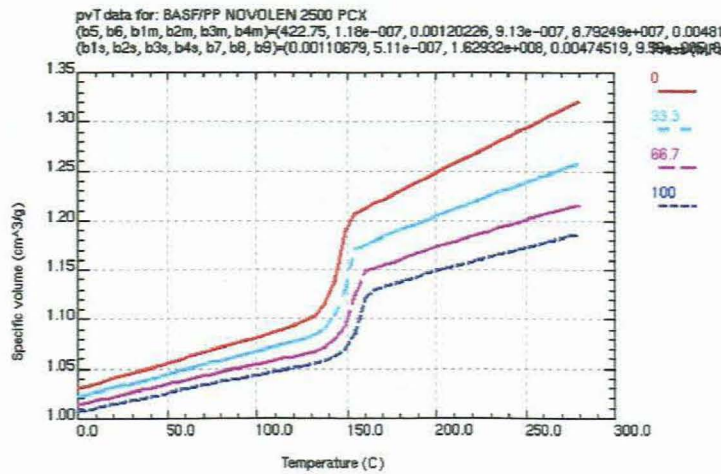


Figure 3.7 Specific volume versus temperature diagram for polypropylene.
 (Diagram obtained from C-MOLD polymer properties database)

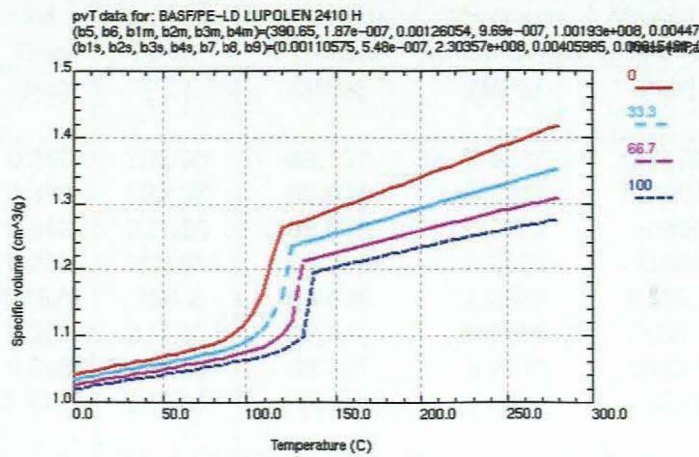


Figure 3.8 Specific volume versus temperature diagram for polyethylene.
 (Diagram obtained from C-MOLD polymer properties database)

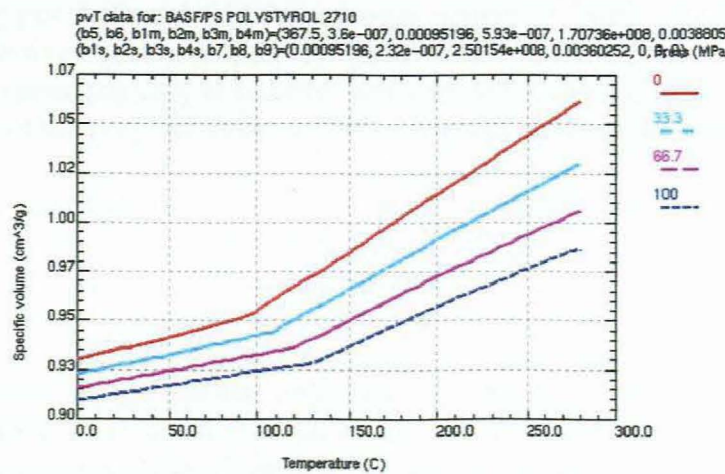


Figure 3.9 Specific volume versus temperature diagram for polystyrene.
 (Diagram obtained from C-MOLD polymer properties database)

3.4 Varying Fill Time

For the analysis on varying fill time, the same polymer, mould material and injection moulding machine was used as for the analysis on varying thickness. Three samples with varying thicknesses ranging from 1-2 mm were analysed. The fill time for each sample was varied, in order to establish the relationship between fill time and shrinkage. The injection temperature was kept constant at 220°C. These results can be viewed in Table 3.5.

Table 3.5 Varying Fill Time

Thickness	Fill Time	Maximum Temp.	Max. Injection Pressure	Maximum Shear Stress	Maximum Shear Rate	Shrinkage
(mm)	(sec)	(°C)	(MPa)	(MPa)	(1/s)	(%)
1	0.269	222.98	59.707	0.3337	33570	1.44
1	0.323	222.37	59.608	0.3217	27967	1.45
1	0.542	221.20	59.828	0.2932	16655	1.46
1	0.762	220.65	61.145	0.2765	11892	1.47
1	0.9829	220.2	63.038	0.2626	9325.3	1.46
1	1.203	219.93	64.844	0.2508	7655.1	1.44
1	1.646	219.60	68.424	0.2515	5622.2	1.43
1	2.2096	219.01	74.65	0.2604	4270	1.52
2	0.526	220.70	18.392	0.2233	8137.2	1.76
2	1.062	220.13	17.063	0.1882	4066.7	1.79
2	1.602	219.92	16.621	0.1721	2712.0	1.81
2	2.141	219.82	16.629	0.1613	2035.6	1.82
2	2.687	219.72	16.792	0.1524	1629.3	1.82
2	3.234	219.63	17.054	0.1449	1358.0	1.82
2	4.322	219.45	17.728	0.1337	1020.0	1.81

The graphs in Figures 3.10 and 3.11 below were generated from table 3.5. Very slow fill times lead to excessive cooling of the melt front, which result in an increase in shear stress. It also results in under packing at remote locations away from the gate, and non-uniform crystallising rates of the polymer in the mould. This will result in an increase in shrinkage.

Increasing the fill time will result in a more uniform polymer and glass fiber distribution, which typically reduces moulded-in stress and shrinkage [24]. A further increase of the injection rate on the other hand will lead to a higher melt velocity, which means the polymer molecules are stretched to a greater degree in the direction of flow. The thickness of the layer of stretched molecules at the part surface is also greater, resulting in increased shrinkage. However, we see that the shrinkage becomes less with a further increase in fill time. This deviation from the norm can be attributed to the fact that there is improved packing caused by the ram effect of the fast moving molecules [25].

Component Shrinkage vs Fill Time

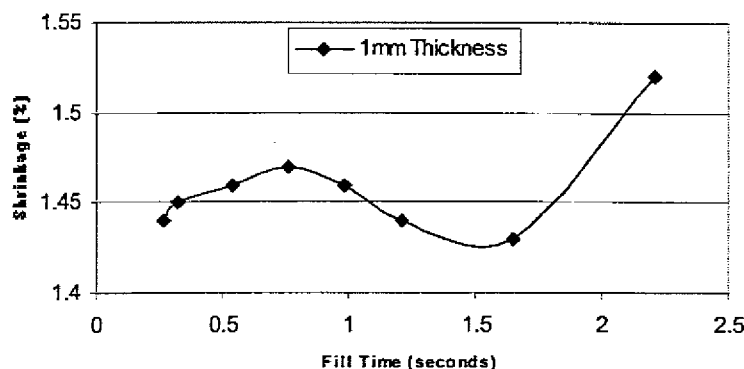


Figure 3.10 Fill time versus shrinkage – 1mm thickness.

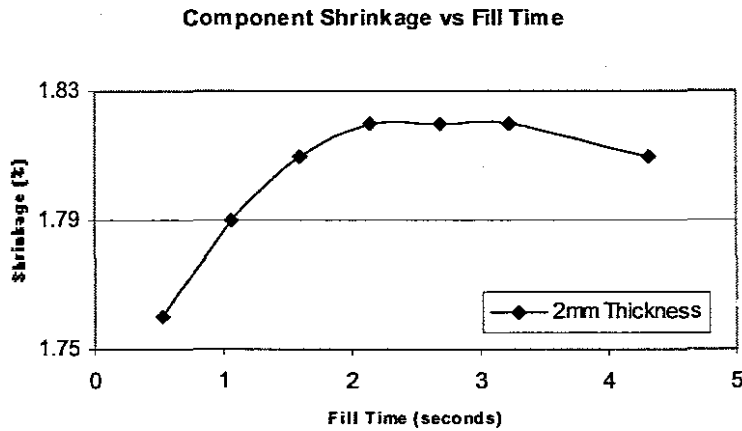


Figure 3.11 Fill time versus shrinkage – 2mm thickness.

3.5 Varying Melt Temperature

In analysing shrinkage with regard to varying the melt temperature, the same polymer, mould material and machine were used as for the varying thickness analysis. Since the specified processing temperature range for polypropylene is 200-280°C, values within this range were selected with 10°C intervals in between. The thickness of the sample that was analysed was kept constant at 4 mm. Mould wall temperatures were also kept constant. The results are shown in Table 3.6 and Figure 3.12.

Table 3.6 Varying Melt Temperatures

Melt Temp. (°C)	Fill Time (sec)	Holding Press (MPa)	Maximum Temp. (°C)	Maximum Shear Rate (1/s)	Post-Fill Time (seconds)	Ejection Temp. (°C)	Shrinkage (%)
200	0.918	6.40	200.33	2262.5	27.359	92.66	1.90
210	0.918	5.82	210.24	2258.8	29.109	92.80	1.91
220	0.918	5.30	220.18	2242.4	30.859	92.75	1.92
230	0.918	4.86	230.12	2248.1	32.610	92.52	1.93
240	0.918	4.45	240.07	2249.9	34.110	92.58	1.94
250	0.918	4.09	250.04	2240.4	35.359	92.93	1.94
260	0.918	3.75	260.02	2234.2	36.870	92.70	1.95
270	0.918	3.46	270.01	2232.8	38.121	92.80	1.95
280	0.918	3.20	280.00	2231.9	39.371	92.79	1.96

During filling, the polymer molecules are sheared and elongated, with the maximum shear occurring at the mould wall. An increase in melt temperature means an increase in the mobility of the polymer molecular chains, leading to a decrease in shear stress. This decrease in shear stress will reduce the shrinkage in the component.

As mentioned before in Chapter 2, the effect on shrinkage of increasing the melt temperature is offset by the following. The increase in melt temperature will continue to

cause an increase in specific volume, meaning that the difference in volume between processing and room temperature is even greater. The high melt temperature also means an overall lower cooling rate that leads to higher crystallisation levels [5]. Hence the larger volumetric increase more than compensates for the effect on shear stress and viscous heating, and it is found that shrinkage is actually lower at lower moulding temperatures [5], as illustrated by Figure 3.12.

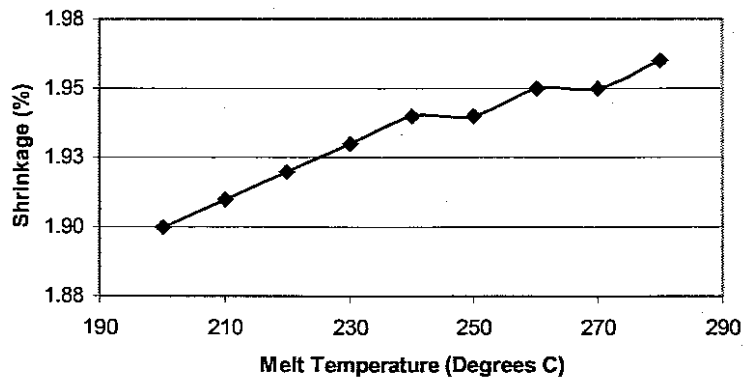


Figure 3.12 Melt temperature versus shrinkage.

Chapter 4

Injection Moulding Analysis Case Study

This Chapter will focus on an injection moulding simulation that was performed for a polymer component using C-MOLD. The C-MOLD simulation is based on a Finite Element Stress Analysis that was performed using ABAQUS. The stress analysis was conducted by an outside contractor, and will subsequently not be discussed in this chapter. The main purpose of the C-MOLD simulation was to establish the necessary parameters and conditions for the subsequent design of the injection mould and for part production. A total number of 9 analyses were performed for the initial designs and a total of 8 analyses for the final design specifications. Characteristic parameters for these runs are discussed in Section 4.6.

4.1 Background

A comprehensive injection moulding analysis is to be performed on a component resembling a polypropylene component (Figure 4.1), under certain particular injection moulding conditions. The injection moulding analysis must be carried out in accordance with the results obtained from the stress analysis, as well as additional design specifications issued by the client.

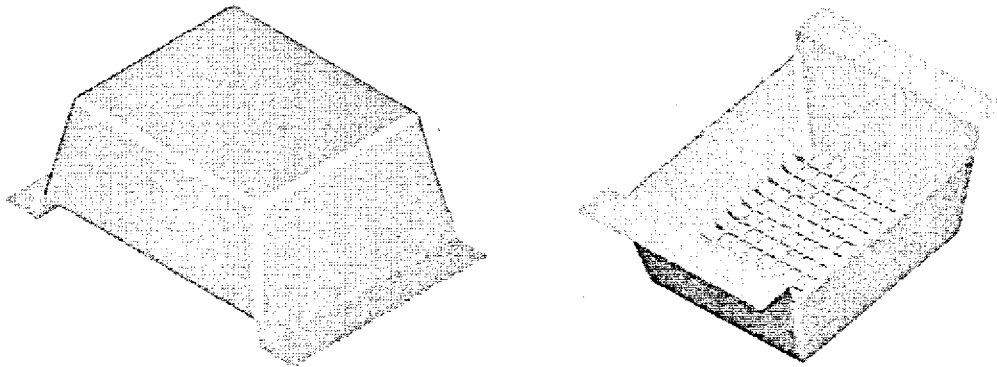


Figure 4.1 Isometric views of the component.

The injection moulding analysis involves the simulation of all the processes, from filling to cooling, as well as an assessment of the shrinkage and warpage of the part. The following specifications and optimum conditions were produced as a result of the analysis:

- gate location
- vent locations
- weld lines in the component
- cooling channel layout and details
- the extent of shrinkage and warpage of the component

The injection moulding analysis consists of the following four facets:

- simulation of the filling process
- simulation of the post-filling (or packing) process
- simulation of the cooling process
- analysis of the shrinkage and warpage of the part

4.2 Filling Process

A single cavity mould was used. It therefore did not require the consideration of runner balancing. However, it was still important to choose the gate locations in such a manner as to produce, as far as possible, balanced flow. Flow balancing involves the minimisation of the variation of the melt front area, and therefore the melt front velocity. Abrupt and sharp changes in the melt front area give rise to surface stresses which cause component warpage (stress relieving through deformation) [2].

An optimum location of the gate will therefore require the melt front sections to reach the outermost cavity boundaries at the same instance. This minimisation of the variation of the melt front area can be coupled to an optimum ram speed profile (variation of the injection rate) to produce, theoretically, a constant melt front velocity [2]. The recommended ram speed profiles were produced by the analysis although it was not certain whether or not the actual machine that would be used would have the necessary capability.

Since the part is bi-symmetrical, the gate was simply located at the intersection of the lines of symmetry (an obvious choice), as shown in Figure 4.2. This position also avoids unwanted jetting of the polymer melt as well as welding of polymer, except at the small inserts near the fringes of the part. A standard pin gate is used. It is envisaged that the injection will be direct (from the melt chamber) into the sprue of the injection mould. Pictures illustrating the melt front advancement can be viewed in Appendix G.

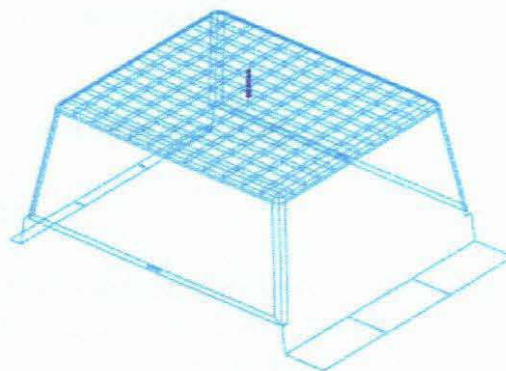


Figure 4.2 Gate location of the component.

An exit sprue diameter of 10-12 mm (depending on the standards available for the chosen sprue length) will suffice. Increasing the gate size would not have improved the packing since the region near the gate freezes off before the actual gate.

The air traps for the part are shown in Figure 4.3. These specify the locations of the air vents in the injection mould. In general, venting is carried out through the mould split as well as the ejector pin holes. However, the mould designer / manufacturer must use this data to ensure proper venting at the outset.

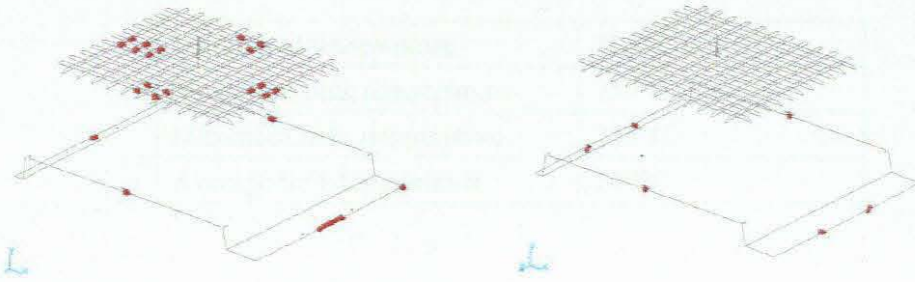


Figure 4.3 Air traps and weld lines.

Weld lines can be observed in the part because of the inserts in the flow region. These weld lines are unavoidable due to the design. The main task is to ensure that the weld lines do not occur in areas of high stresses since they lead to part weakness due to weaker material bonding [1]. According to the stress analyses carried out, the high stress areas (both due to bending and shear) occur around the bends in the part. The weld lines, on the other hand, occur away from these areas, as seen in Figure 4.3. Weaknesses due to polymer welding in higher stress areas are therefore not a cause for concern.

The optimum cavity filling times are chosen so that the injection pressures (at the cavity inlets) are minimal. This condition results in the minimum clamping force necessary. Increasing or decreasing the fill times will increase the injection pressure (due to increased viscosity or increased injection rate respectively), and therefore lead to higher clamping forces necessary [1].

4.3 Process Parameters and Packing

4.3.1 Injection Pressure

The ram pressure at the entrance of the mould steadily increases from zero at the start of the filling stage to a maximum at the end of the filling stage. This maximum pressure is then retained and the mould cavity is allowed to pack under this constant pressure. The maximum injection pressure required to fill the cavity is 53 MPa.

4.3.2 Inlet Melt Temperature

An inlet melt temperature of 255°C has been calculated for optimum performance (with respect to flow length and cavity pressure). Owing to the size of the component, a lower temperature is not recommended for purposes of reducing the cooling (and therefore the cycle) time. This will cause an increase in flow viscosity resulting in higher inlet pressures (and hence requiring higher clamping forces) [2]. Furthermore, lower viscosities will result in inferior part quality, for example, inferior welding of the polymer. The temperature increases due to viscous heating are moderate, and a good average temperature is maintained until the end of the filling process. These values are quantified in Table 4.1 below.

Table 4.1 Melt temperatures at the end of the filling stage

Initial melt temperature	255°C
Maximum bulk temperature	259°C
Minimum bulk temperature	235°C
Average bulk temperature	247°C

4.3.3 Clamping Force

At the end of the filling stage, the inlet pressure is held constant (during the post-filling or packing stage), allowing for the cavity to be compacted. This gives rise to a sudden increase in the clamping force necessary, whereafter it decreases as a result of decreasing pressure in the cavity due to cooling/solidification of the part. The clamping forces required are given in Table 4.2. The maximum value of 925 tons occurs during the post-filling or packing stage. If an 8% factor of safety is used to counter flashing of the part, a 1000 ton capacity machine would be required.

Table 4.2 Clamping forces required

Maximum value at end of filling stage	Maximum value during post-filling (packing) stage	Value using a factor of safety of 1.08
678 Ton	925 Ton	1000 Ton

4.3.4 Process Cycle Time

At the end of the filling time, the mould cavity is packed under pressure. During this compaction stage, the part temperature reduces significantly. After packing, further cooling is required until the ejection temperature of 93°C is reached. The times for the various stages are shown in Table 4.3. A period of 10 seconds has been added to the end of the cooling time to allow for mould opening, part ejection, and mould closing.

Table 4.3 Stage and cycle times

Time at end of Filling Stage	Time at end of Packing Stage	Time at end of Cooling Stage	Cycle Time
6.2 s	22.0 s	30.3 s	40 s

A cycle time of 40 seconds is given in the table above. Note that the cooling time increases exponentially with increasing part thickness. Reducing the part thickness is not recommended since it will lead to other negative effects such as higher viscous resistance (and increased cavity pressure), higher process induced stresses (and increased shrinkage/warping), etc [1].

4.4 Cooling System

Cooling channel layouts are chosen to produce, as far as possible, a uniform heat dissipation (even cooling) from the components. This minimises the thermal stresses, leading to a reduction in the warpage of the part [5]. Equally spaced channels are specified inside both halves of the mould, as shown in Figure 4.4.

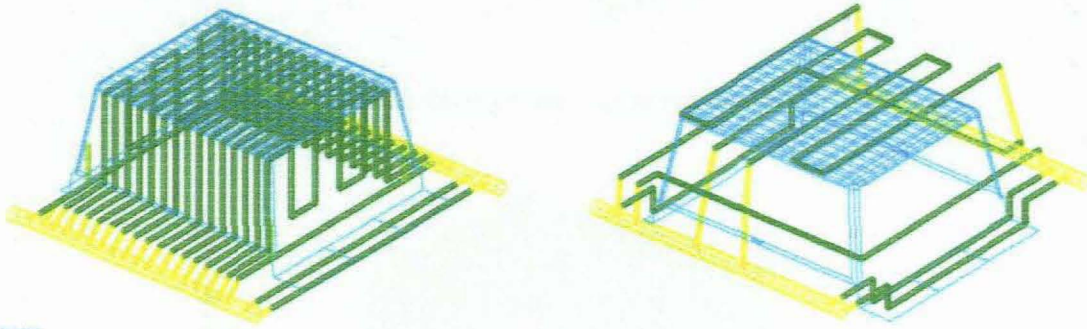


Figure 4.4 Cooling channel layout for core and cavity halves.

The yellow channels represent cooling hoses, temperature controllers and regulators. The green channels represent cooling channels within the mould. The suggested layout also allows for coolant transmission into the core for optimum heat dissipation.

The recommended specifications for the cooling system are given in Table 4.4. It must be noted that a fairly high coolant flowrate has been specified. In the actual injection moulding, this value may have to be compromised (depending on the facilities available), which in turn will compromise the cooling time of the component and hence the cycle time.

Table 4.4 Cooling system specifications

Coolant	Pure Water
Coolant temperature	10°C
Coolant flow rate	420 litres/min
Cooling channel diameter	10 mm

The temperature distribution along the part (bulk averaged) at the end of the cycle time, or at the point of ejection, is given in Figure 4.5. It shows a maximum temperature of 94°C (recommended ejection temperature) and a minimum temperature of 60°C. Figure 4.6 depicts the temperature difference distribution between the cavity and core sides of the part. A maximum value of 18°C is recorded along the corners of the part – due to the difficulties in cooling the part at these locations. Nevertheless, the values are within satisfactory boundaries [4].

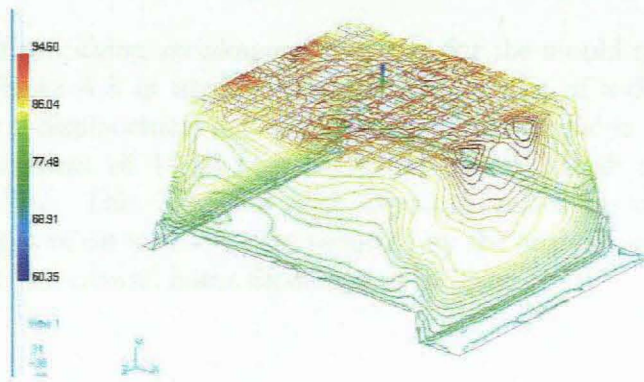


Figure 4.5 Average temperature distribution.

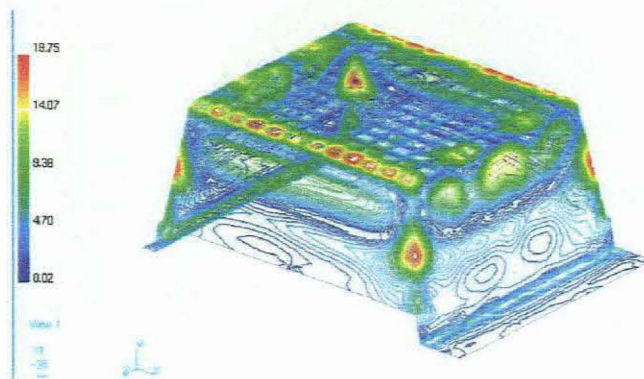


Figure 4.6 Temperature difference.

4.5 Shrinkage and Warpage

Owing to the nature and application of the component, it is important to ensure a high degree of uniform heat dissipation to reduce the degree of warpage [5]. The shrinkage and warpage of the part (that is, the total displacement of the part from the original) is depicted in the two views in Figure 4.7. A visual inspection indicates a degree of shrinkage (which is normal), and the associated warpage of the part. At this stage, the warpage in the centre of the part in the downward y-direction is of concern. But this can easily be reduced in the actual injection moulding, through increased holding pressure.

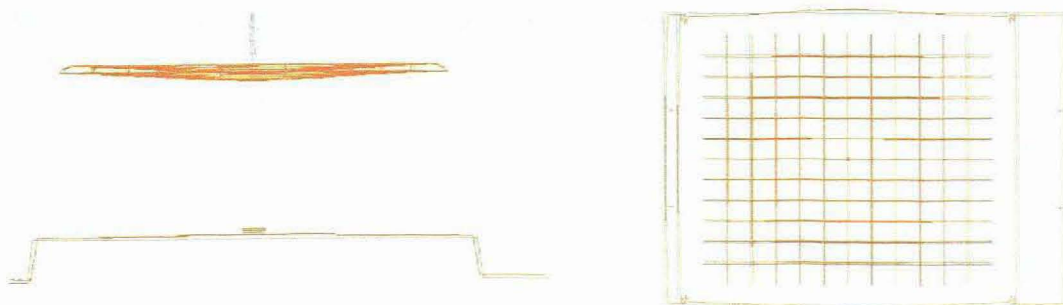


Figure 4.7 Side and top view shrinkage.

For purposes of specifying shrinkage allowances for the mould cavity dimensions, the plot given in Figure 4.8 is used. Although only a plot of x-displacement is given, similar plots for z-displacement and y-displacement are available. Figure 4.8 measures a total x-displacement of 10.84 mm along the overall length of 600 mm, giving a shrinkage of 1.8%. This is in line with expected values for the specified polymer grade. Shrinkages of up to 2.79% are reported by the analysis, but these are localised and do not affect the overall linear shrinkage of the part.

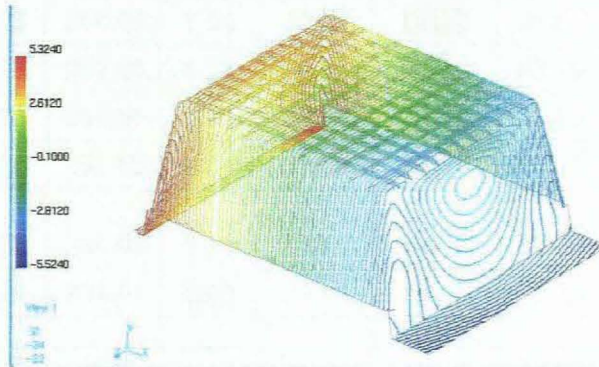


Figure 4.8 X-Displacement plot.

4.6 Analysis and Discussion of Results

The injection moulding analysis started while the finite element stress analysis was still conducted. Even if there are geometric changes, the advantage here is that the basic process parameters and cooling channel layout should be finalised when the component design is done. The finite element stress analysis, necessitated two changes to the component: firstly wall thickness was made uniform, and then the support rib spacing was widened.

In the following Table 4.5, the abbreviations for the headings are as follows:

Wall Thick.	- the wall thickness of the component
Rib Dist.	- distances between the supporting ribs
Melt Temp.	- injection temperature of the polymer
CC Design	- different cooling channel designs
Temp. Difference	- temperature difference between the mould core and cavity
Unbal. Cool. Shrink	- shrinkage due to unbalanced cooling only
Non- Unif. Shrink	- shrinkage due to all other factors except unbalanced cooling
Proc. Shrink	- process induced shrinkage (total of unbalanced cooling & non-uniform)

Table 4.5 Results of injection moulding analyses

C-MOLD Input Data							C-MOLD Output Data			
#	Wall Thick.	Rib Dist.	Melt Temp.	Fill Time	Post-Filling Time	CC Design	Temp. Difference	Proc. Shrink	Non-Unif. Shrink	Unbal. Cool. Shrink
	<i>mm</i>	<i>mm</i>	<i>Deg C</i>	<i>Sec</i>	<i>Sec</i>		<i>Deg C</i>	<i>%</i>	<i>%</i>	<i>%</i>
1.1	2-3	30x28	254.69	6.33	43	No. 1	28.82	12.62	-11.05	0.19
1.2	2-3	30x28	254.69	6.19	28.22	No. 2	34.86	12.98	12.52	0.23
1.3	2-3	30x28	254.69	6.36	30.38	No. 3	30.6	13.98	-10.44	0.52
1.4	2-3	30x28	254.69	6.34	30.36	No. 4	25.67	-8.76	-10.88	0.13
1.5	2-3	30x28	254.69	6.34	30.37	No. 5	25.46	-10.78	7.77	0.16
1.6	2-3	30x28	254.69	6.34	30.36	No. 6	22.55	-9.23	-11.11	0.11
1.7	2-3	30x28	254.69	6.34	30.36	No. 7	20.11	-8.84	-10.61	-0.07
2.1	3	30x28	254.69	6.25	30	No. 7	18.70	-1.77	-1.77	0.07
2.2	3	30x28	254.69	5.12	29.15	No. 7	19.34	-1.75	-2.7	0.08
3.1	3	37x32	250	6.24	30.26	No. 7	18.22	3.32	3.29	0.08
3.2	3	37x32	240	6.24	30.26	No. 7	17.52	3.6	3.57	0.07
3.3 ^o	3	37x32	254.69	6.24	30.26	No. 7	18.75	-2.79	-2.77	0.08
3.4	3	37x32	254.69	6.24	30.26	No. 8	19.60	-2.76	-2.75	0.08
3.5	3	37x32	254.69	6.24	30.26	No. 9	19.65	-2.77	-2.76	0.08
3.6	3	37x32	254.69	7.2	31.21	No. 7	18.30	3.46	3.42	0.07
3.7	3	37x32	254.69	6.64	30.66	No. 7	18.52	3.3	3.26	0.08
3.8 ^o	3	37x32	254.69	6.24	30.27	No. 7	18.73	-2.78	-2.78	0.08



- Colour changes denote input file changes between successive analyses

Φ - Input files between analysis 3.3 & 3.8 are the same, except that a different FEM model was used

The design of the cooling channel layout was completed by the first geometry change of constant wall thickness. The cooling channel spacing was equal to the support rib spacing and yielded relatively good shrinkage results. Once the spacing of the support ribs changed, as with the second geometric change, the spacing of the cooling channels had to change to prevent uneven cooling. Although the shrinkage increased, the finite element stress analysis showed a better designed part.

For analysis 2.2 the fill time was reduced, but this only resulted in an increase in temperature difference and shrinkage. Melt temperature was also reduced for analysis 3.2, but this just increased the shrinkage.

More changes were made, but no significant differences in the results were shown. The parameters and design of analysis 3.3 were finally selected for the manufacture of the injection mould. Appendix H shows the performance of the component on application.

4.7 Conclusions

This study is a case in point that injection moulding is a business of compromises, and most of the time it is not possible to have the optimum position for everything. The cooling channel layout could have been optimised further, but the time delay for additional simulations would not have justified the improvement. The values for shrinkage were already within satisfactory boundaries.

Since the component behaved under moulding and loading as predicted by the simulation analysis, the following conclusions can be drawn

- The elimination of the trial and error process reduced the turnaround time of producing the injection mould.
- Even with the large amount of parameters available, computer simulation improves the engineer's ability to accurately predict the optimum process conditions.
- The extent of shrinkage and warpage was determined.
- Achieving balanced cooling is not difficult when using the appropriate injection moulding simulation software.

Chapter 5

An Alternative Model for the Stress Build-Up during Cooling of Injection Moulded Thermoplastics

5.1 Introduction

The aim of this Chapter is to propose a model for the cooling stress build-up in the injection moulding process, and to compare the shrinkage from the model with the shrinkage determined using commercial software. The pressure history in the molten polymer and the stresses within the solidifying layers during cooling is identified with reference to a rectangular cavity.

When molten polymer is cooled through its solidification temperature, the cooling starts from the mould surface and penetrates inwards. Shrinkage during injection moulding can be demonstrated using free quenching as an example, whereby a component of uniform temperature is suddenly sandwiched by cold mould walls. During the early cooling stages, when the external layers in contact with the mould walls cool and start to shrink, most of the polymer at the core is still molten and free to contract. As the internal core cools, thermal contraction is constrained by the rigid external layers. This means that solidification at the mould surface take place free of constraints, while the internal layers solidify on a rigid shell which already underwent its contraction. This results in a typical state of stress distribution with tension in the core balanced by compression in the outer layers [1], as shown below.

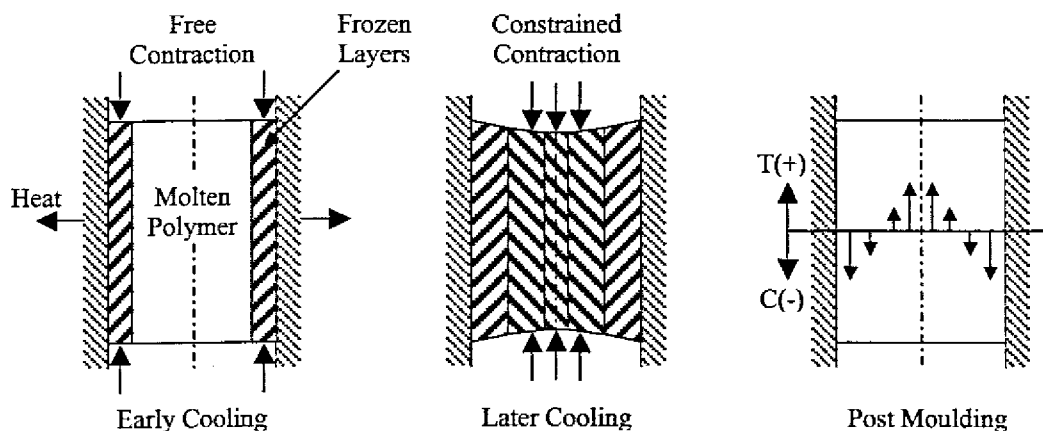


Figure 5.1 Development of cooling stress in a free quenched moulded part.

Models describing the cooling stress build up during free quenching are normally developed based on the above description. However, cooling stress distributions found in articles obtained by injection moulding were very different from articles on free quenching, since injection moulding depends on, for instance, the holding time

[47]. These suggest that features such as interaction of the polymer with the mould and the pressure history in the melt play a very important role.

The pressure profile needs to be traced over the cavity thickness to describe the cooling stress distribution in injection moulded samples. In general, the pressure gradually increases during filling, and continues to increase during packing to reach a maximum in the early packing stage, and then starts to drop due to cooling and gate freezing. Accordingly, the material at the outer layers and centre layers solidify when the pressure level is low, whereas the intermediate layers freeze under high packing pressure [1].

This means that the various layers will shrink differently, according to the specific volume versus temperature curves that govern the shrinkage behaviour of a material. Hypothetically, if each layer was detached from the others next to it as shown in Figure 5.2 below, then the material elements in the left side figure would have shrunk like those in the right side figure. In this case, the intermediate layers tend to shrink less than the others because of the higher frozen-in density. In reality, all the layers are bound together. Therefore, the end result will be a compromised shrinkage distribution with intermediate layers being compressed and outer and centre layers being stretched [1].

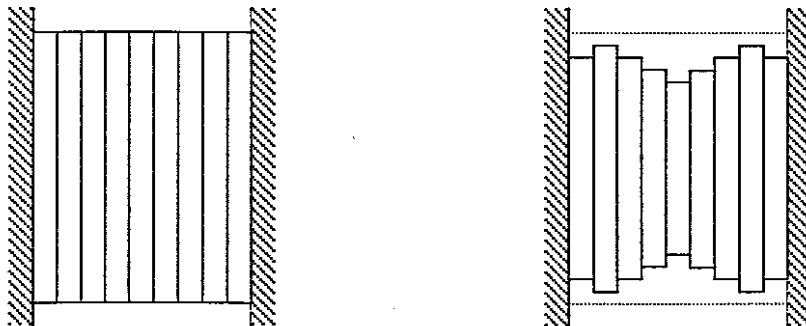


Figure 5.2 Layer deformation as different frozen-in densities interact with each other.

While a component is still constrained in the mould cavity, the internal stress that accumulates during solidification is referred to as **in-cavity** residual stress. This in-cavity residual stress is the force that drives post-ejection part shrinkage and warpage. After part ejection, the constraints from the mold cavity are released, and the part is free to shrink and deform. After it settles to an equilibrium state, the remaining stress inside the part is called **process-induced** residual stress, or simply, residual stress.

The stress profile in the left side figure of Figure 5.3 is the in-cavity residual stress (generally tensile stress), in which the molded part remains constrained within the mould prior to ejection. Once the part is ejected and the constraining force from the mould is released, the part will shrink and warp to release the built-in residual stress and reach an equilibrium state as shown by the right side figure. The equilibrium state means that there is no external force exerted on the part and the tensile and compressive stresses over the part cross-section should balance with each other.

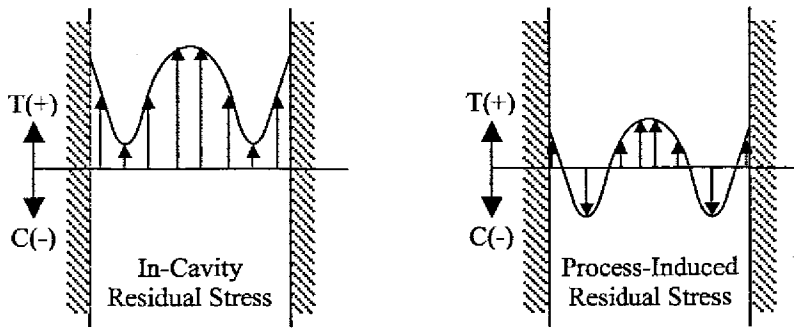


Figure 5.3 In-cavity residual stress profile versus process-induced residual stress profile.

5.2 Solidifying Polymer as a Continuum Body

5.2.1 Introduction

Continuum mechanics considers material bodies in the form of solids, liquids and gasses [39]. The object of mechanics as part of physics is the scientific understanding of the motion of material bodies. Thermodynamics, another field of physics, investigates the transformation and exchange of energy. This includes the concept of heat and temperature and postulates that all processes are irreversible. Using the hypothesis that the spatial distribution of matter is continuous, mechanics and thermodynamics can be described as one unified theory. A material body can therefore be identified with a three-dimensional manifold; the elements of this manifold (or material points) are in one-to-one correspondence with position vectors of their actual places in a Euclidean space on physical observation. Furthermore, the material body is mapped into a reference space, which must be introduced to associate mathematical “names” to the material elements. As a general consequence of those basic assumptions, continuum thermo-mechanics is a field theory in the sense that all physical quantities depend on space and time.

All statements of continuum mechanics and thermodynamics separate into two different categories, namely universal and individual statements. The principles of kinematics and the balance relations of mass, momentum, energy and entropy are universal. These are accepted as general natural laws to be true for all systems, irrespective of their material properties. The individual behaviour of a particular material body is represented by constitutive equations. These are mathematical models rather than natural laws and represent the real behaviour of matter in a certain class of processes and with certain approximations.

5.2.2 Basic Notations

The position vector of a material element in its current and reference configuration is denoted by \mathbf{x} and \mathbf{X} , respectively. According to the choice of reference, \mathbf{x} is related to the Euclidean space of physical observation and denotes the current position of the material element under consideration. The “name” \mathbf{X} of the same material element corresponds to a point in some arbitrary reference space. The deformed position of a material body is given by the function $\mathbf{x} = \varphi_{\mathbf{R}}(\mathbf{X}, t)$, where the index \mathbf{R} , symbolizes the dependence of this function on the choice of reference configuration. In general, the

space of reference is completely independent from the space of physical observation, that is, the reference configuration is not occupied by the body at some instant t_0 . It is however possible to identify the two spaces in special cases. If this is done, the displacement field can be defined as

$$\mathbf{U}(\mathbf{X},t) = \varphi_{\mathbf{R}}(\mathbf{X},t) - \mathbf{X} \quad (\text{Lagrangian Form}) \quad (5.1)$$

$$\mathbf{u}(\mathbf{x},t) = \mathbf{x} - \mathbf{X}(\mathbf{x},t) \quad (\text{Eulerian Form}) \quad (5.2)$$

The two descriptions are related by means of the motion $\mathbf{x} = \varphi_{\mathbf{R}}(\mathbf{X},t)$, namely

$$\mathbf{U}(\mathbf{X},t) = \mathbf{U}[\varphi_{\mathbf{R}}^{-1}(\mathbf{x},t),t] = \mathbf{u}(\mathbf{x},t) \quad (5.3)$$

These considerations are summarized schematically in Figure 5.4. For each fixed time, t the mapping $\varphi_{\mathbf{R}}$ is invertible. Accordingly, any time dependent physical quantity can be represented either by \mathbf{x} or \mathbf{X} as an independent variable. This correspondence is due to the choice of the spatial (Eulerian) or material (Lagrangian) representation, respectively. The different representations lead to different fields for one and the same physical quantity. Although these two fields are completely equivalent, particular quantities may naturally appear in the context of a spatial or material representation.

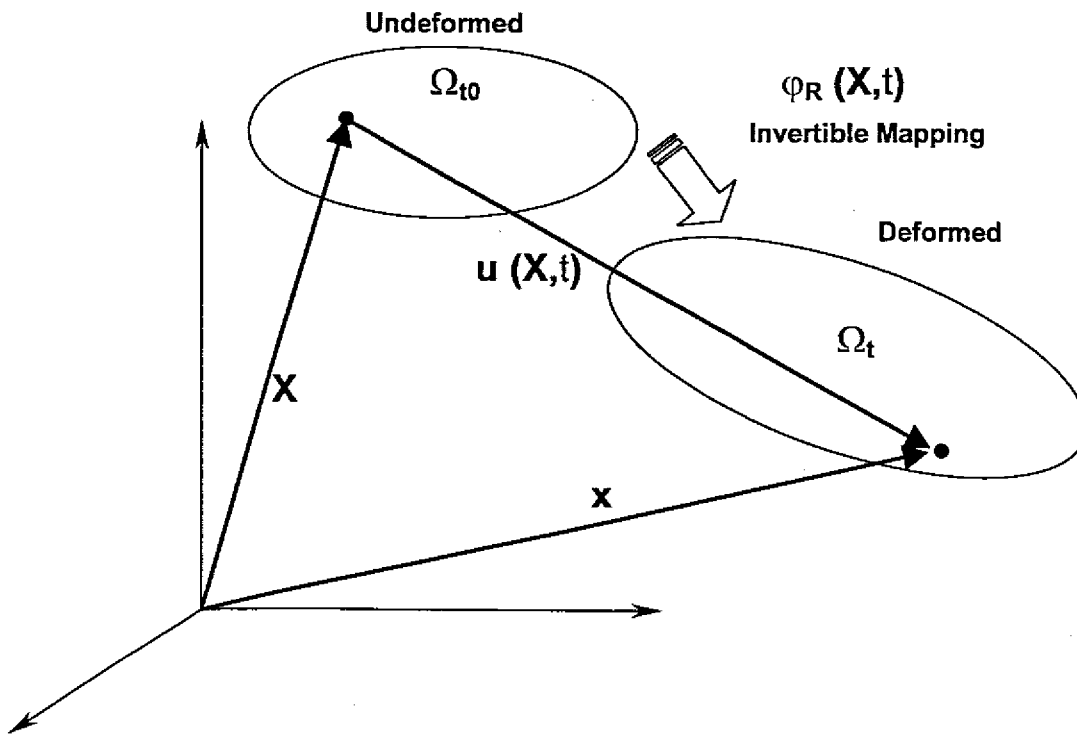


Figure 5.4 Configurations of a material body.

The modelling of flows occur naturally in the context of a spatial (Eulerian) representation. Although this thesis deals with the deformation of a solid (solidified melt), we use the spatial representation so as to be consistent with previous analysis on the flow of the molten polymer. Hence, the deformation of the continuum body will be described using infinitesimal deformation theory and the Eulerian description of body motion will be employed.

5.2.3 The General Model

Consider a rectangular mould having thickness $2b$. The four thin faces of the polymer and mould will be referred to as edges and the remaining two larger faces as walls.

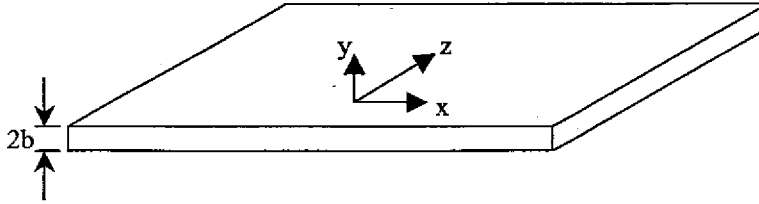


Figure 5.5 Model geometry and axis.

In order to simplify the mathematical manipulation the following assumptions are made:

- Any effect of the distance from the gate is disregarded.
- Directions normal to the thickness are all considered equivalent.
- The temperature distribution of the molten polymer at the end of filling, when packing starts, is taken to be uniform.
- Mould wall temperature changes are neglected.
- Convection at the edges are negligible, so that at each instant, the temperature changes only along the thickness direction.

When packing starts, the first solid layer forms on the mould wall and solidification proceeds inwards towards the midplane with time. While the part is solidifying, the length (x -axis) and width (z -axis) can undergo some deformation. This length and width deformation is non-linear with respect to thickness. The pressure will stretch the part walls against the mould walls during the initial packing stages and shrinkage can only occur once the internal pressure starts to drop.

If both the pressure in the molten polymer and the adhesion of the part to the mould walls are negligible, the part is subjected to free quenching. Under such conditions the part will undergo continuing length shrinkage due to the effect of thermal contraction of the layers, from the solidification temperature to the wall temperature.

If internal pressure is considered, it can be seen from Figure 5.6 that, at the instant when solidification starts, a force proportional to the melt pressure builds up on the sample edges.

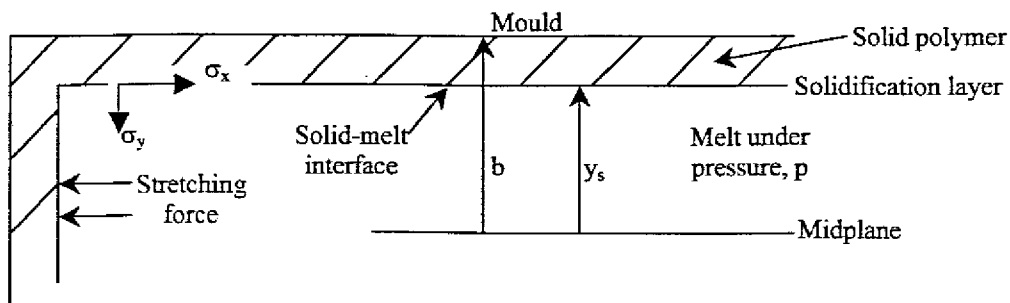


Figure 5.6 Polymer cross section during solidification.

This force stretches the solid polymer laying on the mould walls, but as long as the mould remains closed, neither the length nor width of the sample can increase above its initial values. This pressure build-up also causes densification of the layers at the instant of their solidification. This density increase, counteracts the tendency to shrink that was caused by the temperature decrease. At each instant, the stress distribution in the solid shell laying on the mould walls must be in equilibrium with the external forces acting on it. These forces are related to the melt pressure that squeezes the solid polymer against the mould, and the interaction between the solid polymer and the mould.

5.3 Governing Equations

The generalized Hooke's law will be used here as our constitutive relation. In a three dimensional space [17] the strain along a direction x normal to y and z is represented as follows:

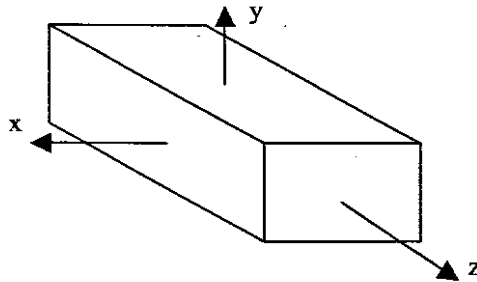


Figure 5.7 Element subjected to tri-axial stresses.

$$\varepsilon_{xx} = \frac{1}{E} (\sigma_{xx} - \nu\sigma_{yy} - \nu\sigma_{zz})$$

where ε = strain
 E = young's modulus
 σ = stress
 ν = poisson ratio

then

$$\varepsilon_{xx} = \frac{1}{E} \{ \sigma_{xx} + \nu\sigma_{xx} - \nu\sigma_{xx} - \nu\sigma_{yy} - \nu\sigma_{zz} \}$$

$$\varepsilon_{xx} = \frac{1}{E} \{ (1 + \nu)\sigma_{xx} - \nu(\sigma_{xx} + \sigma_{yy} + \sigma_{zz}) \} \quad (5.4)$$

The stress tensor for the three-dimensional element is:

$$\bar{\sigma} = \begin{bmatrix} \sigma_{xx} & \sigma_{xy} & \sigma_{xz} \\ \sigma_{yx} & \sigma_{yy} & \sigma_{yz} \\ \sigma_{zx} & \sigma_{zy} & \sigma_{zz} \end{bmatrix}$$

Defining one third of the trace of the stress tensor:

$$\sigma = \frac{1}{3}(\sigma_{xx} + \sigma_{yy} + \sigma_{zz}) \quad (5.5)$$

and substituting equation (5.5) into (5.4) gives:

$$\varepsilon_{xx} = \frac{1}{E} \{(1 + \nu)\sigma_{xx} - 3\nu\sigma\} \quad (5.6)$$

Consider the sample when solidification is taking place at y_s as shown in Figure 5.6. Referring to the solid layer at the solidification temperature T_s , the strain along a direction x normal to y can be written as

$$\varepsilon_x = \frac{1}{E} \{(1 + \nu)\sigma_x - 3\nu\sigma\} + \varepsilon_T \quad (5.7)$$

where ε_T is the linear thermal contraction evaluated from the solidification temperature. For an amorphous polymer, ε_T can be written as

$$\varepsilon_T = \int_{T_s}^T \alpha(T) dT \quad (5.8)$$

where α is the linear thermal expansion coefficient. From Figure 5.6, we consider normal stress along width and length directions to be equal; that is, the normal stress along any direction z normal to both x and y is equal to σ_x :

$$\sigma_x = \sigma_z$$

As long as pressure in the melt remains positive, the solid layer is held against the mould walls. Under these conditions σ_y does not depend on y . Hence:

$$\sigma_y = \sigma_{\text{normal}} - p$$

where p = pressure in the melt, and since we are neglecting normal stress, from equation (5.5):

$$\begin{aligned} \sigma &= \frac{1}{3}(\sigma_x + (-p) + \sigma_x) \\ &= \frac{1}{3}(2\sigma_x - p) \end{aligned} \quad (5.9)$$

Substitute equation (5.9) into (5.7), so the strain at the solidification layer becomes:

$$\varepsilon_x = \frac{1}{E} \{(1 + \nu)\sigma_x - \nu(2\sigma_x - p)\} + \varepsilon_T$$

$$\begin{aligned}\varepsilon_x &= \frac{1}{E} \{ \sigma_x + \nu \sigma_x - 2\nu \sigma_x + \nu p \} + \varepsilon_T \\ \varepsilon_x &= \frac{1}{E} \{ \sigma_x - \nu \sigma_x + \nu p \} + \varepsilon_T \\ \varepsilon_x &= \frac{1}{E} \{ (1-\nu) \sigma_x + \nu p \} + \varepsilon_T\end{aligned}\quad (5.10)$$

At the solid-melt interface, solidification takes place under hydrostatic pressure, so that all three stress components are equal to the hydrostatic pressure ($-p$) at this point.

$$\begin{aligned}\varepsilon_x &= \frac{1}{E} \{ (1-\nu)(-p) + \nu p \} + \varepsilon_T \\ \varepsilon_x &= \frac{1}{E} \{ -p + \nu p + \nu p \} + \varepsilon_T \\ \varepsilon_x &= \frac{1}{E} (2\nu - 1)p + \varepsilon_T\end{aligned}\quad \text{for } y = y_s \quad (5.11)$$

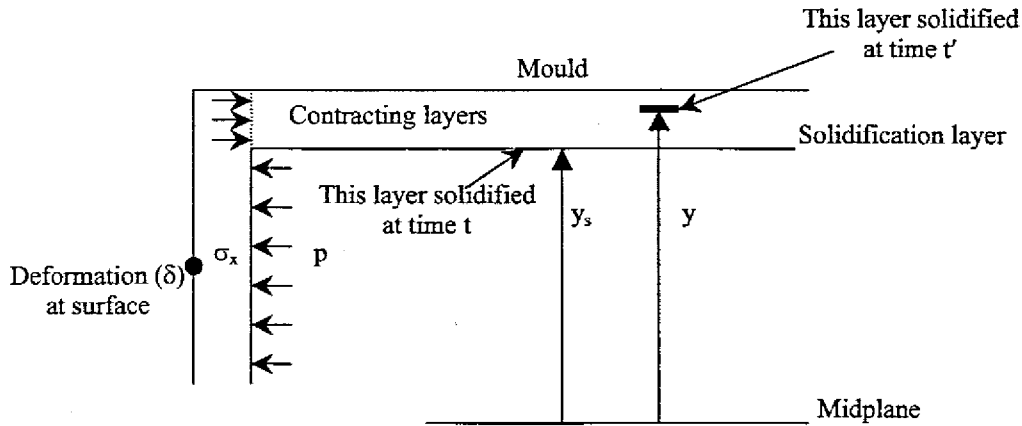


Figure 5.8 Polymer sample undergoes a continuous length shrinkage due to thermal contraction of the layers.

The stress distribution will change with time, and is not dependant on y . This means that the change in deformation of each solid layer between two different instants t and t' does not depend on y . However, the change in strain in the layers is equal to the change in shrinkage at the mould surface, giving:

$$\varepsilon_x(t, y) - \varepsilon_x(t', y) = \delta(t) - \delta(t')$$

where $\delta(t)$ is the shrinkage with respect to the mould, and t' is the instant when solidification takes place at y . Further manipulation gives

$$\begin{aligned}\varepsilon_x(t, y) &= \varepsilon_x(t', y) + \delta(t) - \delta(t') \\ &= \varepsilon_s(y) + \delta(t) - \delta_s(y)\end{aligned}$$

where $\delta_s(y)$ is the shrinkage of the layer y when it solidified, and $\varepsilon_s(y)$ is the strain of that layer at the instant of solidification.

Grouping $\varepsilon_s(y)$ and $\delta_s(y)$ into $\eta(y)$, the above equation becomes

$$\varepsilon_x(t, y) = \eta(y) + \delta(t) \quad (5.12)$$

Substituting equation (5.12) into (5.10) gives

$$\frac{1}{E} \{(1-\nu)\sigma_x + \nu p\} + \varepsilon_T = \eta(y) + \delta(t) \quad (5.13)$$

This equation holds for each layer of y in the solid polymer shell. Since ε_T only becomes applicable once the layer is solidified, at the solid-melt interface

$$\frac{1}{E} \{2\nu - 1\}p = \eta(y) + \delta(t') \quad (5.14)$$

and at the surface layer

$$\frac{1}{E} \{2\nu - 1\}p = \eta(b) \quad \text{at } t=0 \quad (5.15)$$

Although friction between the two solid polymer shells and the mould walls gives rise to a change of the stress distribution along the x and z planes it is neglected. Only the interaction between the solid polymer and mould edges is accounted for, since it prevents the sample from exceeding its initial dimensions. The melt pressure stretches the solid shell through the force acting on the sample edges.

At any solidification layer

$$\begin{aligned} p y + \text{interactions with mould edges} &= \text{internal forces} \\ &= \int_y^b \sigma_x(y) dy \end{aligned} \quad (5.16)$$

$$p y = \int_y^b \sigma_x(y) dy \quad \text{when } \delta(t) < 0 \quad (5.17)$$

5.4 Solution Procedure

The solution to the final stress distribution will now be discussed.

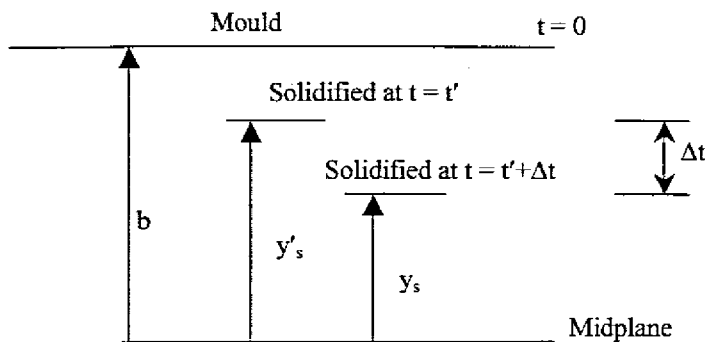


Figure 5.9 Polymer cross section.

Integrating equation (5.13) over the solidified polymer layers

$$\frac{1}{E} \int_{Y_s}^1 (1-\nu)\sigma_x dY + \frac{1}{E} \int_{Y_s}^1 \nu p dY + \int_{Y_s}^1 \varepsilon_T dY = \int_{Y_s}^1 \eta(Y) dY + \int_{Y_s}^1 \delta(t) dY$$

where $1 = \frac{b}{b}$, $Y_s = \frac{y_s}{b}$ and $Y = \frac{y}{b}$

and substituting equation (5.17):

$$\begin{aligned} \frac{1}{E} (1-\nu)pY_s + \frac{1}{E} \nu p(1-Y_s) + \int_{Y_s}^1 \varepsilon_T dY &= \int_{Y_s}^1 \eta(Y) dY + \delta(1-Y_s) \\ \frac{p}{E} [(1-\nu)Y_s + \nu(1-Y_s)] + \int_{Y_s}^1 \varepsilon_T dY &= \int_{Y_s}^1 \eta(Y) dY + \delta(1-Y_s) \\ \frac{p}{E} (Y_s - 2\nu Y_s + \nu) + \int_{Y_s}^1 \varepsilon_T dY &= \int_{Y_s}^1 \eta(Y) dY + \delta(1-Y_s) \end{aligned} \quad (5.18)$$

Assume that the function $\eta(Y)$ is known from Y down to Y'_s , where Y'_s refers to the layer that solidified at time t' . At time $t = t' + \Delta t$, solidification takes place at Y_s . δ can be numerically calculated from equation (5.81) once the actual pressure and temperature fields are known. Within first order numerical approximation, the integral of η can be written as

$$\int_{Y_s}^1 \eta(Y) dY = \int_{Y'_s}^1 \eta(Y) dY + [\eta(Y'_s) - \eta(Y_s)] \frac{Y'_s - Y_s}{2}$$

and substituting equation (5.14):

$$\int_{Y_s}^1 \eta(Y) dY = \int_{Y'_s}^1 \eta(Y) dY + \left[\eta(Y'_s) - \left\{ \frac{1}{E} (2\nu - 1)p - \delta \right\} \right] \frac{Y'_s - Y_s}{2} \quad (5.19)$$

Equation (5.15) is the starting point to the numerical procedure, when solidification takes place on the surface layer. Equation (5.19) is substituted into equation (5.18) in order to determine $\delta(t)$. If the value obtained for δ is positive, the interaction between the sample and the mould cavity keeps it zero. Equation (5.15) is used only to start the procedure at the surface layer. For subsequent layers, the value of $\delta(t)$, provided it is negative, as obtained in equation (5.18) will be used in equation (5.14), to calculate η . Once $\delta(t)$ and η are known, the stress can be calculated from equation (5.13). This procedure is then repeated in order to solve the shrinkage throughout melt solidification.

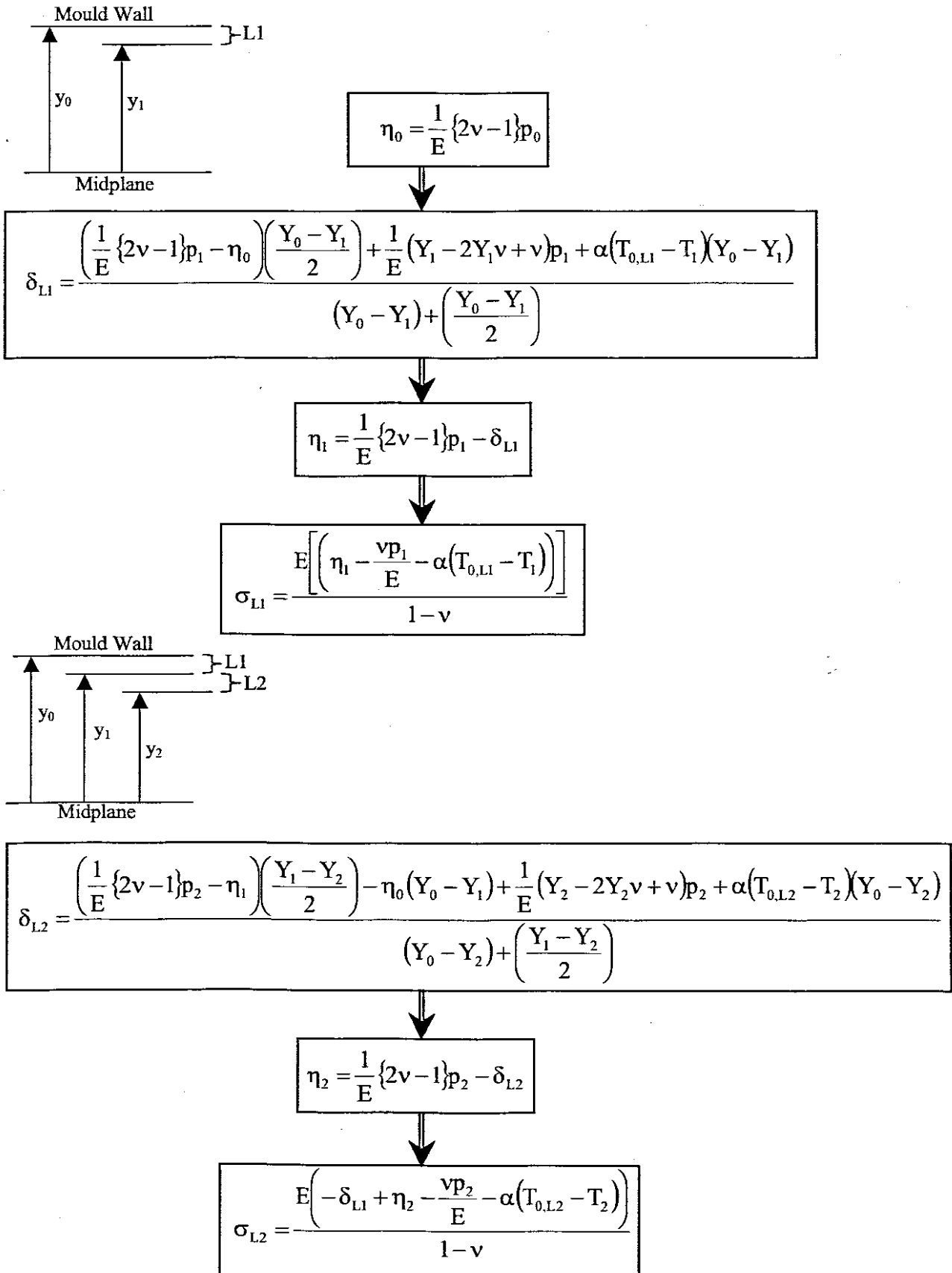


Figure 5.10 Algorithm for the solution of shrinkage during melt solidification.

5.5 Discussion of Results

The calculations for the solution procedure was performed with the aim of determining the cooling stress across the injection mould cavity, and to compare the shrinkage from the proposed model with the shrinkage determined using commercial software.

The polymer that was chosen for the analysis is a polypropylene with the commercial name Borealis. All of the relevant properties were sourced from the database of the commercial software C-MOLD. The tensile modulus is 1700 MPa, poisson's ratio 0.38, linear thermal expansion coefficient $9.44e-5$ $1/^{\circ}\text{C}$ and the ejection temperature 93°C .

Once the complete cooling time for this particular sample was known, this overall time had to be divided into an arbitrary number of equal time intervals. For these layers of equal time intervals, the pressure and temperature fields needed to be identified, in order to solve the shrinkage and stress. The finite element analysis software package ABAQUS was used to determine the temperature field, and also to identify the dimensional instances of y_s across the half-gap b . The ABAQUS input data is discussed in Appendix B, while the output data is illustrated in Appendix C.

The sample chosen for the analysis was 4mm thick, and since we assume cooling to be symmetrical and the stress distribution to be even, only one half of the part is analysed. This half-gap distance is 2mm or since the dimensional instances is relatively small, 2000 microns. The ABAQUS analysis shows the total time to solidification for the specimen to be 34.36 sec. This time is divided into equal time intervals and the closest ABAQUS time interval is selected (see Appendix C). Time intervals of 80 and 60 were chosen with multiples of 40, 30, 20, 10 and 5 generated from it. The distance from the midplane is also identified for each layer.

The commercial software C-MOLD is not programmed to simulate forced cooling until such time that the part is solidified across its entire thickness, but rather programmed to calculate the ejection temperature which is the more relevant criterion for industrial users. This means that a C-MOLD analysis would predict cooling of a part typical of a situation where the core would still be molten polymer, but the outer shell would be rigid enough to counter the pressure in the melt. In this case the ejection time predicted by C-MOLD is 18.687 seconds (Appendix F).

The solution procedure for the cooling stress model was solved using Fortran. The Fortran input data is discussed in Appendix D, while the output data is shown in Appendix E.

In the case of the model, the initial layers show a positive value for shrinkage due to the pressure in the melt. At a distance of 1475 microns from the midplane and a time of 10.31 seconds, shrinkage for all the different layer intervals becomes negative, (Figure 5.11) indicating ejection criteria. Ejection time for the model is 7 seconds faster than in C-MOLD.

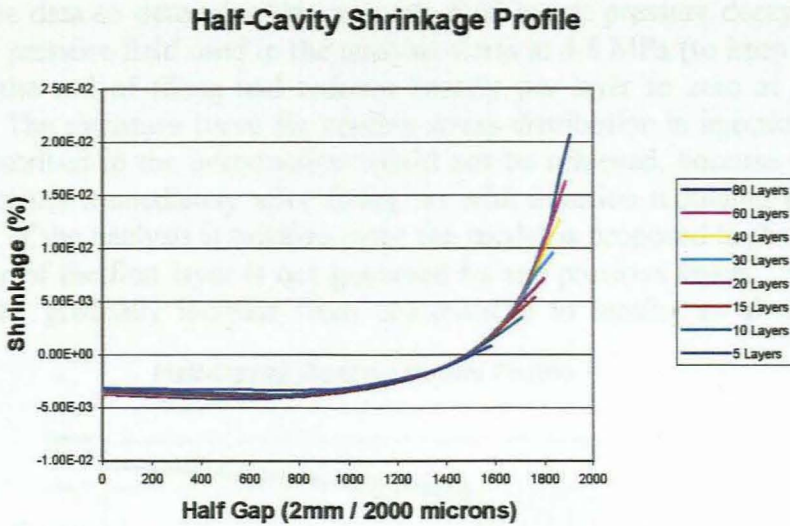


Figure 5.11 Graph illustrating shrinkage versus thickness distance.

The difference in time between C-MOLD and the model can be attributed to the following reasons. The model assumes that cooling starts once the cavity is filled and that the temperature distribution of the molten polymer at the start of the analysis is uniform. Although this should mean a longer ejection time for the model, it is offset by the fact that the mould wall temperature changes for the model was neglected, meaning faster cooling. This is evident from the solidification profile (Figure 5.12), where there is an increase in cooling at the mould wall. This would not be the case for C-MOLD, where the mould temperature would increase due to the thermal pulse. Also, the model does not take into account viscous heating due to flow, which increases the temperature. The increase in cooling close to the midplane is expected since the hot core that served as a source of energy for intermediate layers is removed.

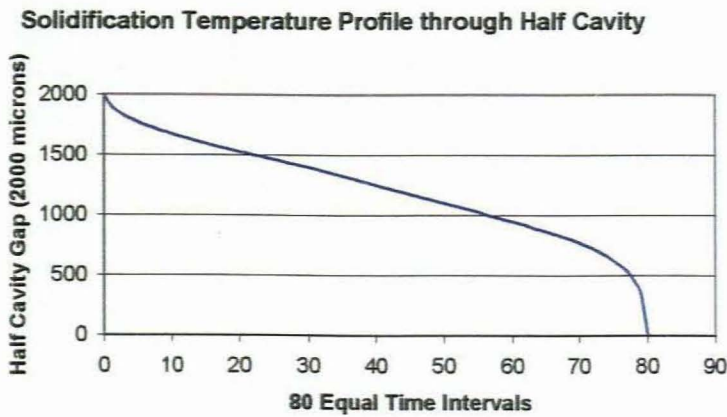


Figure 5.12 Solidification temperature profile.

Although the pressure increases in the early packing stage and then starts to drop, a lack of pressure data to determine this pressure field meant pressure decay had to be assumed. The pressure field used in the analysis starts at 4.8 MPa (to keep inline with C-MOLD) at the end of filling and reduces linearly per layer to zero at the end of solidification. The signature curve for cooling stress distribution in injection moulded samples, as described in the introduction would not be achieved, because there is no increase in pressure immediately after filling, as with injection moulding in practice. The first layer of the analysis is positive since the model is proposed in that way, that is, the behavior of the first layer is not governed by any previous layers. Subsequent layers, however, gradually increase from compressive to tensile, as observed from Figure 5.13.

Half-Cavity Cooling Stress Profile

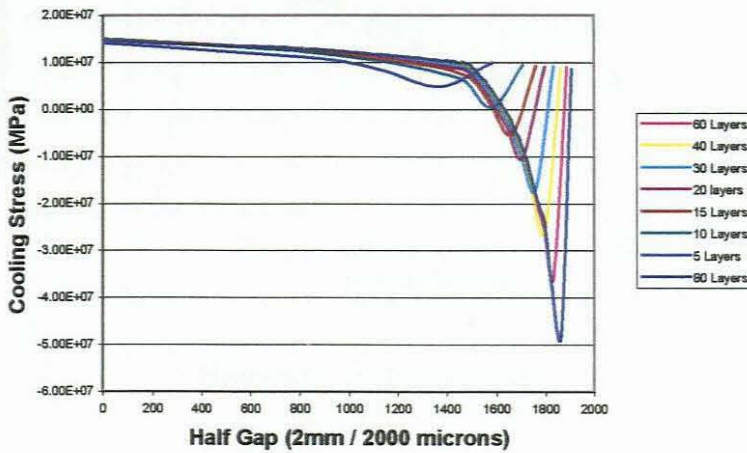


Figure 5.13 Graph illustrating cooling stress versus thickness distance.

Figure 5.14 illustrates the final shrinkage versus the different numbers of layers chosen. When more layers are analysed, these layers become thinner and a more accurate result for shrinkage is obtained. This is simply because the stress that is set up and the resulting shrinkage can be traced more closely. For this reason the shrinkage curve in Figure 5.14 is converging.

Shrinkage Convergence Curve

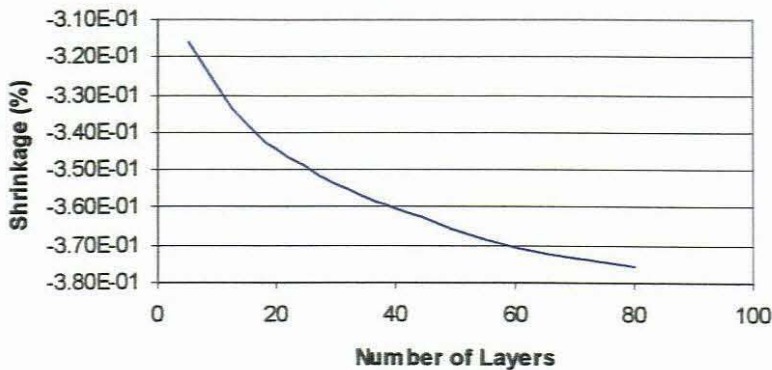


Figure 5.14 Shrinkage convergence curve.

The final shrinkage result obtained for the model (half cavity divided into 80 layers) is 0.376% (Appendix E), and the C-MOLD result is 0.63% (Appendix F). If the half cavity were divided into more layers than 80, we would expect the shrinkage results for the numerical model to approach the result for C-MOLD.

From figure 5.15 we notice that the curve for the final cooling stress per number of layers is converged.

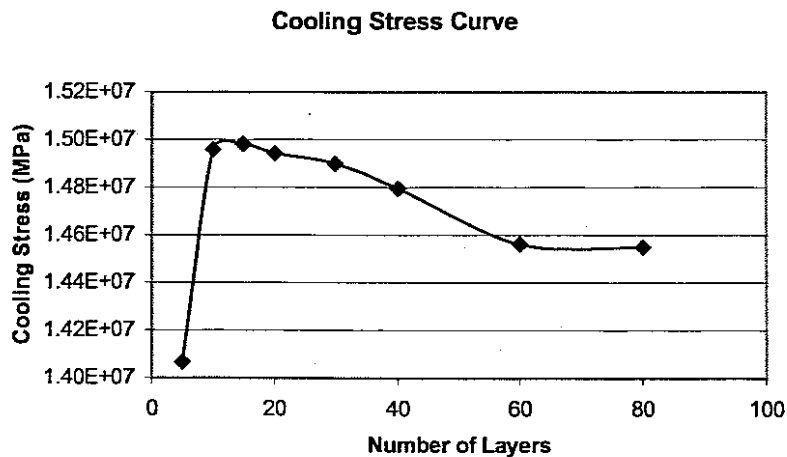


Figure 5.15 Cooling stress curve.

5.6 Conclusions

The proposed model compares fairly well in terms of shrinkage and stress predictions with the commercial software. Inclusion of the effect of a thermal pulse in the ABAQUS analysis to account for the mould wall temperature increase would be required for more accurate computational results. Practical experiments regarding material and process parameters would however allow for better testing of the model, especially the determination of the pressure field. C-MOLD also simulates residual stress induced by both polymer flow and mould cooling. The proposed model only considers stress due to mould cooling.

An agreement between the numerical model and the commercial software could not be found due to both the lack of information regarding parameters and the approximations of the model.

Chapter 6

Conclusions

6.1 Concluding this work

The objectives of this study as presented in Chapter 1 have been achieved. In Chapter 2 the relevant modes of heat transfer, that are applicable to injection moulding cooling, were identified. The objective of understanding the mathematical model describing the heat transfer process during the cooling stage has also been attained.

The sensitivity analysis that was conducted in Chapter 3 proved sufficient for an academic investigation. The variation of the shrinkage for a chosen range is greater when varying polymers (especially between amorphous and crystalline) and wall thickness, than for varying fill time and melt temperatures. We can conclude that changing the process parameters cannot solve excessive shrinkage. Plastic components and moulds need to be designed correctly.

The cooling channel layout for the case study conducted in Chapter 4 could have been optimised further but time constraints prevented this. Additional simulations would not have justified more improvements. Compromises are expected with the process of injection moulding and most of the time it is not possible to have the optimum position for everything. The values for shrinkage were already within satisfactory boundaries.

Since the component behaved under moulding and loading as predicted by the simulation analysis, the following conclusions can be drawn

- The elimination of the trial and error process reduced the turnaround time of producing the injection mould.
- Even with the large amount of parameters available, computer simulation improves the engineer's ability to accurately predict the optimum process conditions.
- The extent of shrinkage and warpage was determined.
- Achieving balanced cooling is not difficult when using the appropriate injection moulding simulation software.

The solution procedure for the alternative cooling stress model that was proposed in Chapter 5 was solved. Some of the trends between the model and the commercial software was reproduced, but an agreement could not be found, due to both a lack of information regarding parameters, and the approximations of the model.

The effect of a thermal pulse in the ABAQUS analysis to account for the mould wall temperature increase, should be included for future analysis. This would make for more accurate computational testing. Practical experiments regarding material and process parameters would also allow for better testing of the model, especially the determination of the pressure field.

6.2 Future Work

Although future projects and improvements have already been mentioned in the above, further investigations into this study will be discussed in this section.

The governing equations that were used in Chapter 5.3 to develop the alternative cooling stress model, are based on the hookean model. More accurate results might be achieved if other constitutive relationships can be used for the governing equations.

Also in Chapter 5.2.3 under The General Model certain assumptions were made. The first assumption was that directions normal to the thickness are all considered equivalent. Secondly, we assumed convection at the edges is negligible so that at each instant, temperature changes only along the thickness direction. These assumptions meant we had to consider normal stress along width and length directions to be equal, and also that both directions are equal to the thickness direction. This means that shrinkage was only considered in one dimension. Future studies should be aimed at considering shrinkage in the other dimensions.

The proposed numerical model of Chapter 5 only considers stress due to mould cooling. However, flow induced stress could also be considered. This could take the form of a coupled analysis that integrates stress build-up due to fluid flow and heat transfer for the entire injection moulding process.

Lastly, the aforementioned proposed model is designed to determine shrinkage due to induced stress, and since uniform shrinkage is assumed the ABAQUS model is only analysed from mould wall to midplane.

A situation with uneven cooling can be simulated, whereby a higher temperature can be assigned to one side of the sample. This should induce component warpage. The full sample will have to be modelled in ABAQUS, with heat flow on both sides. Due to the cooling rate being higher on one side, the last layer that solidifies should not be on the midplane. The full specimen will thus be split into two dimensionally unequal halves. Each halve can be analysed using the cooling stress model, to determine the stress across the thickness. The component region can then be discretised into elements, and the displacement solved. The resulting warpage can be compared with simulation software.

These future studies will hopefully result in more accurate comparisons between the proposed model and experiments.

References

- [1] Advanced CAE Technology, (1994), C-MOLD DESIGN GUIDE A Resource for Plastics Engineers, (3rd ed.), New York.
- [2] Advanced CAE Technology, (1995), C-MOLD USER'S GUIDE FILLING & POST-FILLING, New York.
- [3] Advanced CAE Technology, (1995), C-MOLD USER'S GUIDE REFERENCE MANUAL, New York.
- [4] Advanced CAE Technology, (1996), C-MOLD USER'S GUIDE COOLING, New York.
- [5] Advanced CAE Technology, (1996), C-MOLD USER'S GUIDE SHRINKAGE & WARPAGE, New York.
- [6] Bathe, K. J., (1996), Finite Element Procedures, New Jersey: Prentice Hall.
- [7] Callister, W. D., (1985), Materials Science and Engineering. An Introduction, New York: John Wiley.
- [8] Chen, B. S. and Liu, W. H., (1989), Numerical Simulation and Experimental Investigation of Injection Mold Filling with Melt Solidification, Polymer Engineering and Science, (V. 29), pg. 1039-1050.
- [9] Chiang, H. H., Hieber, C. A. and Wang, K. K., (1991), A Unified Simulation of the Filling and Post-Filling Stages in Injection Molding. Part I: Formulation, Polymer Engineering and Science, (V. 31), pg. 116-124.
- [10] Chiang, H. H., Hieber, C. A. and Wang, K. K., (1991), A Unified Simulation of the Filling and Post-Filling Stages in Injection Molding. Part II: Experimental Verification, Polymer Engineering and Science, (V. 31), pg. 125-139.
- [11] Chiang, H. H., Himasekhar, K., Santhanam, N. and Wang, K. K., (1993), Integrated Simulation of Fluid Flow and Heat Transfer in Injection Molding for the Prediction of Shrinkage and Warpage, Journal of Engineering Materials and Technology, (V. 115), pg. 37-47.
- [12] Chiang, H. H., Himasekhar, K., Santhanam, N., Wang, K. K. and Lautenbach, S., (1991), Assesment of Shrinkage and Warpage using an Integrated Analysis of Molding Dynamics, ANTEC, pg. 242.
- [13] Darlington, M. W., Scott, A. J. and Smith, A. C., (1986), Pressure Losses in the Packing Stage of Injection Molding, Polymer Engineering and Science, (V. 26), pg. 1282-1289.
- [14] Delbarre, P., Pabiot, J., Rietsch, F. and Daurelle, J., (1991), Experimental Study of Processing Conditions on Shrinkage and on Warpage of Injected Parts, ANTEC, pg. 301.

- [15] Discipio, W., Wagle, A. and McCarthy, S. P., (1990), Verification Mold for Flow, Cooling, Shrinkage and Warpage Analysis, ANTEC, pg. 283.
- [16] Groover, M. P., (1996)., Fundamentals of modern Manufacturing: Materials, Processes and Systems, New Jersey: Prentice Hall.
- [17] Hearn, E. J., (1991), Mechanics of Materials: An Introduction to the Mechanics of Elastic and Plastic Deformation of Solids and Structural Components, (V. 1, 2nd Ed.), Oxford: Pergamon Press, pg. 362.
- [18] Hibbitt, Karlsson & Sorensen, (2001), ABAQUS Standard User's Manual, (Volume II), Version 6.2, Section 12.2.4-1.
- [19] Hibbitt, Karlsson & Sorensen, (2001), ABAQUS Theory Manual, Version 6.2, Section 2.11.1.
- [20] Hieber, C. A. and Shen, S. F., (1980)., A Finite-Element/Finite-Difference Simulation of the Injection-Molding Filling Process, Journal of Non-newtonian Fluid Mechanics, (V. 7), pg. 1-32.
- [21] Himasekhar, K., Wang, K. K. and Lottey, J., (1989), Mold-Cooling Simulation in Injection Molding of Three-Dimensional Thin Plastic Parts, National Heat Transfer Conference, (V. 110), pg. 129-136.
- [22] Holman, J. P., (1997), Heat Transfer, (8th Ed.), New York: McGraw-Hill.
- [23] <http://scienceworld.wolfram.com/physics/LatentHeatofFusion.html>
- [24] <http://www.cpchem.com/rytonpps/processingconditions.html>, pg. 1.
- [25] <http://www.honeywell-plastics.com/techinfo/litshop/PDF/08-96-BG2700-1000.pdf>, pg. 44.
- [26] <http://www.plastamid.co.za/>
- [27] <http://www.reps.co.uk/articles/destips.html>, pg. 1-4.
- [28] Jacques, M., (1982), An Analysis of Thermal Warpage in Injection Molded Flat Parts due to Unbalanced Cooling, Polymer Engineering and Science, (V. 22).
- [29] John, V. B., (1990), Engineering Materials, Hampshire: Macmillan.
- [30] Kamal, M. R. and Kenig, S., (1972), The Injection Molding of Thermoplastics Part I: Theoretical Model, Polymer Engineering and Science, (V. 12), pg. 294-301.
- [31] Kamal, M. R. and Kenig, S., (1972), The Injection Molding of Thermoplastics Part II: Experimental Results, Polymer Engineering and Science, (V. 12), pg. 302.

- [32] Kamal, M. R. and Lafleur, P. G., (1982), Computer Simulation of Injection Molding, Polymer Engineering and Science, (V. 22), pg. 1066-1074.
- [33] Kamal, M. R. and Lafleur, P. G., (1984), Heat Transfer in Injection Molding of Crystallizable Polymers, Polymer Engineering and Science, (V. 24), pg. 692-697.
- [34] Kamal, M. R. and Lafleur, P. G., (1986), A Structure-Orientated Computer Simulation of the Injection Molding of Viscoelastic Crystalline Polymers Part I: Model with Fountain Flow, Packing, Solidification, Polymer Engineering and Science, (V. 26), pg. 92-102.
- [35] Kamal, M. R. and Lafleur, P. G., (1986), A Structure-Orientated Computer Simulation of the Injection Molding of Viscoelastic Crystalline Polymers Part II: Model Predictions and Experimental Results, Polymer Engineering and Science, (V. 26), pg. 103-110.
- [36] Lee, C. C., (1990), An Improved Flow Analysis Network(FAN) Method for Irregular Geometries, Polymer Engineering and Science, (V. 30), pg. 1607-1614.
- [37] Matsuoka, T., Takabatake, J., Koikai, A., Inoue, Y., Yamamoto, S. and Takahashi, H., (1990), Integrated Simulation to Predict Warpage of Injection Molded Parts, ANTEC, pg. 369.
- [38] Mills, A. F., (1992), Heat Transfer, Burr Ridge: Irwin.
- [39] Muschik, W., (1993), Non-Equilibrium Thermodynamics with Applications to Solids, Springer – Verlag: Wien – New York.
- [40] Ni, S. J. and Wang, K. K., (1993), An Analitical and Experimental Study of Warpage and Shrinkage of an Injection-Molded Part, ANTEC, pg. 1612-1617.
- [41] Parametric Technology Corporation, (1998), Pro/ENGINEER® Mold Design, (Release 20.0), Waltham, Massachusetts.
- [42] Potsch, G. and Michaeli, W., (1990), The Prediction of Linear Shrinkage and Warpage for Thermoplastic Injection Mouldings, ANTEC, pg. 355.
- [43] Pye, R. G. W., (1989), Injection Mould Design. An Introduction and Design Manual for the Thermoplastics Industry, (4th Ed.), New York: Longman Scientific and Technical.
- [44] Santhanam, N. and Wang, K. K., (1990), A Theoretical and Experimental Investigation of Warpage in Injection Molding, ANTEC, pg. 270.
- [45] Schlenker, B. R., (1974), Introduction to Materials Science, Brisbane: John Wiley.

- [46] Timings, R. L., (1992), Manufacturing Technology, (V. 1, 2nd Ed.), Essex: Longman Scientific & Technical.
- [47] Titomanlio, G., Drucato, V. and Kamal, M. R., (1987), Mechanism of Cooling Stress Build-Up in Injection Molding of Thermoplastic Polymers, Intern. Polymer Processing 1, pg. 55-59.
- [48] Titomanlio, G., Piccarolo, S. and Levati, G., (1988), On the Packing-Holding Flow in the Injection Molding of Thermoplastic Polymers, Journal of Applied Polymer Science, (V. 35), pg. 1483-1495.
- [49] Yu, C. J., Sunderland, J. E. and Poli, C., (1990), Thermal Contact Resistance in Injection Molding, Polymer Engineering and Science, (V. 30), pg. 1599-1606.

Appendix A

C-MOLD Report Files

This Appendix shows the C-MOLD results that were used to compile Chapter 3. The input data can generally be found in the log file. The log file also illustrates the filling and post-filling (packing-cooling) analysis. The output data is found in the reports. Only one run with its unique parameters will be shown and discussed. In this case it is the reports of the 1mm thickness analysis that was run using the estimates of the process estimator (Chapter 3.1). The rest of the runs with its own parameters can be found on the accompanying compact disk.

A.1 Log File

The log file contains all the input data as well as the recorded data of the analysis. The component thickness can be calculated from the Total volume and Total projected area (highlighted) information.

C-MOLD Filling 99.7
C-MOLD Post-filling 99.7
C-MOLD Fiber Orientation 99.7
C-MOLD Residual Stress 99.7
(c)1987-1999 by Advanced CAE Technology, Inc.

Date : MAY02-01
Time : 10:24:55

End of memory allocation for analysis.

Beginning of reading the input data

File name : sample_1

Reading parameters

Performing fiber orientation simulation

Reading material data

** WARNING ** Fiber properties is not specified and fiber orientation simulation is turned off.

Reading process conditions

Reading finite-element mesh

** WARNING ** Cooling channel is not specified. C-MOLD Cooling Simulation will not execute without cooling channel information.

** WARNING ** No coolant temperature is specified in coolant manifold control, ambient temperature will be used as cavity wall temperature.

** WARNING ** Parting plane is not specified; the default parting plane normal along the z-axis of the global coordinates will be used.

Reading C-MOLD Cooling data

** WARNING ** Analysis is continuing without .C2P file

Reading re-start data

** WARNING ** Analysis is continuing without .RSP file

End of reading the input data.

Beginning of re-numbering elements and nodes

End of re-numbering elements and nodes.

Beginning of checking input data

End of checking input data.

Beginning of optimizing memory usage

End of optimizing memory usage.

Beginning of initializing variables

End of initializing variables.

The analysis will be based on :

(1) Parameters :

# of layers across full-gap	(12) =	12
# design outputs in filling	(12) =	12
# detail outputs in filling	(0) =	0
# design outputs in post-filling	(12) =	12
# detail outputs in post-filling	(0) =	0
Melt-temp convergence criterion	(0.2) =	2.0000E-001 K(d)
Mold-melt heat transfer coefficient	(2.5E+04) =	2.5000E+004 W/m^2-K
Max # of melt-temp iterations	(100) =	100
Pressure trace sample frequency	(10) =	10 Hz
Total number of pressure trace nodes	=	1
Pressure trace nodal number	1 =	13
Residual stress analysis (W)	(1) =	1
Option for structural package (W)	(0) =	0
Isolate mechanism for warpage? (W)	(1) =	1
# of modes for stress analysis (W)	(3) =	3

C-MOLD fem format

(2) Material :

Polymer 1 : BASF/PP NOVOLEN 2500 PCX

2-domain mod Tait polymer density

1
RHO = -----
Vo*(1-C*ln(1+p/B)) + Vt
where C = 0.0894
Tt = b5 + b6*p
Vo = b1 + b2*Tbar
B = b3 * EXP(-b4*Tbar)
Vt = 0.0 or b7*EXP(b8*Tbar-b9*p)
Tbar = T - b5
b5 = 4.2275E+002 K
b6 = 1.1800E-007 K/Pa

Liquid phase	Solid phase
-----	-----
b1 = 1.2023E-003	b1 = 1.1068E-003 m ³ /kg
b2 = 9.1300E-007	b2 = 5.1100E-007 m ³ /kg-K
b3 = 8.7925E+007	b3 = 1.6293E+008 Pa
b4 = 4.8174E-003	b4 = 4.7452E-003 1/K
	b7 = 9.5900E-005 m ³ /kg
	b8 = 1.5000E-001 1/K
	b9 = 2.0600E-008 1/Pa

Constant polymer specific heat

Cp = 2.9300E+003 J/kg-K

Constant polymer thermal conductivity

K = 1.1800E-001 W/m-K

Cross-WLF polymer viscosity

ETAo = -----
 1 + (ETAo*GAMMA/TAUS)^(1-n)
 A1*(T-TS)
 where ETAo = D1*EXP(- -----)
 A2+(T-TS)
 TS = D2 + D3*p
 A2 = A2T + D3*p
 n = 3.0110E-001
 TAUS = 3.3830E+004 Pa
 D1 = 2.0000E+015 Pa-s
 D2 = 2.6315E+002 K
 D3 = 0.0000E+000 K/Pa
 A1 = 3.4607E+001
 A2T = 5.1600E+001 K

Transition temperature

Ttrans = 4.0815E+002 K

Transversely-isotropic elastic tensor

E1 = 1.0000E+009 Pa
 E2 = 1.0000E+009 Pa
 v12 = 3.8000E-001
 v23 = 3.8000E-001
 G = 3.6200E+008 Pa

Transversely-iso thermal expansion coef.

a1 = 9.4400E-005 1/K
 a2 = 1.0400E-004 1/K

 (3) Process conditions : Description of TCODE

Machine parameters :

Max machine clamp force	(4.905E+07) = 1.6211E+006 N
Max machine injection volume	(0.02) = 3.3993E-004 m ³
Max machine injection pressure	(1.800E+08) = 1.3303E+008 Pa
Max machine injection rate	(6.667E-03) = 2.8981E-004 m ³ /s
Machine hydraulic response time	(0.2) = 2.0000E-001 s

Process parameters :

Fill time	= 8.9722E-001 s
Post-fill time	= 2.9913E+000 s
F/P switch over by % volume	= 9.9000E+001 %
Timer for hold pressure	= 2.9913E+000 s

Ram speed profile (rel):

% stroke	% speed
-----	-----
0.0000E+000	5.0000E+001
2.0000E+001	5.0000E+001
4.0000E+001	5.0000E+001
6.0000E+001	5.0000E+001
8.0000E+001	5.0000E+001
1.0000E+002	5.0000E+001

Pack/hold pressure profile (rel):

% time	% fill pres
0.0000E+000	1.0000E+002
1.0000E+002	0.0000E+000

Ambient temperature	= 2.9800E+002 K
Inlet melt temperature	= 5.2367E+002 K
Average coolant temperature	= 2.9800E+002 K

C-MOLD Cooling mold wall temp data was not used.

(4) Finite-element mesh : .FEM file for model: sample_2

Total number of nodes	=	596
Total number of polymer entrance nodes	=	1

Polymer entrance nodal numbers are: 13

Total number of elements	=	1100
Total number of part elements	=	1100
Total number of sprue/runner/gate elements	=	0
Total number of channel elements	=	0
Total number of connector elements	=	0

Parting plane normal	(dx) = 0.0000E+000
	(dy) = 0.0000E+000
	(dz) = 1.0000E+000

Average aspect ratio of 2D elements	= 1.0226E+000
Maximum aspect ratio of 2D elements	= 1.6033E+000
2D element number w/ max. aspect ratio	= 69
Minimum aspect ratio of 2D element	= 1.0000E+000
2D element number w/ min. aspect ratio	= 811
Total volume	= 2.8800E-005 m ³
Total volume filled initially	= 0.0000E+000 m ³
Total volume to be filled	= 2.8800E-005 m ³
Part volume to be filled	= 2.8800E-005 m ³
Sprue/runner/gate volume to be filled	= 0.0000E+000 m ³
Total projected area	= 2.8800E-002 m ²

C-MOLD Filling 99.7

C-MOLD Post-filling 99.7

C-MOLD Residual Stress 99.7
analysis is beginning

At time = 8.2702E-002 s, 8.8842E+000 % of volume filled,
entrance pressure = 8.8587E+006 Pa,
total clamp force = 6.0926E+003 N,
filling under ram speed control.

At time = 1.6243E-001 s, 1.7210E+001 % of volume filled,
entrance pressure = 1.2689E+007 Pa,
total clamp force = 1.7872E+004 N,
filling under ram speed control.

At time = 2.3067E-001 s, 2.4378E+001 % of volume filled,
entrance pressure = 1.5300E+007 Pa,
total clamp force = 3.0662E+004 N,
filling under ram speed control.

At time = 3.0137E-001 s, 3.1786E+001 % of volume filled,
entrance pressure = 1.7820E+007 Pa,
total clamp force = 4.7565E+004 N,
filling under ram speed control.

At time = 3.7550E-001 s, 3.9506E+001 % of volume filled,
entrance pressure = 2.0300E+007 Pa,
total clamp force = 6.9077E+004 N,
filling under ram speed control.

At time = 4.5038E-001 s, 4.7139E+001 % of volume filled,
entrance pressure = 2.3728E+007 Pa,
total clamp force = 1.0901E+005 N,
filling under ram speed control.

At time = 5.2523E-001 s, 5.4672E+001 % of volume filled,
entrance pressure = 2.7196E+007 Pa,
total clamp force = 1.5701E+005 N,
filling under ram speed control.

At time = 5.9942E-001 s, 6.2075E+001 % of volume filled,
entrance pressure = 3.0716E+007 Pa,
total clamp force = 2.1210E+005 N,
filling under ram speed control.

At time = 6.7341E-001 s, 6.9430E+001 % of volume filled,
entrance pressure = 3.4545E+007 Pa,
total clamp force = 2.7976E+005 N,
filling under ram speed control.

At time = 7.4888E-001 s, 7.6881E+001 % of volume filled,
entrance pressure = 3.8388E+007 Pa,
total clamp force = 3.5469E+005 N,
filling under ram speed control.

At time = 8.2678E-001 s, 8.4541E+001 % of volume filled,
entrance pressure = 4.2482E+007 Pa,
total clamp force = 4.4205E+005 N,
filling under ram speed control.

At time = 8.9941E-001 s, 9.1632E+001 % of volume filled,
entrance pressure = 4.6645E+007 Pa,
total clamp force = 5.4079E+005 N,
filling under ram speed control.

At time = 9.7282E-001 s, 9.8671E+001 % of volume filled,
entrance pressure = 5.1661E+007 Pa,
total clamp force = 6.7244E+005 N,
filling under ram speed control.

At time = 9.7745E-001 s, 9.9063E+001 % of volume filled,
F/P switch over by volume.

At time = 9.7948E-001 s, 9.9235E+001 % of volume filled,
entrance pressure = 5.2288E+007 Pa,
total clamp force = 7.0501E+005 N,
filling under pack/hold pressure control.

At time = 9.8648E-001 s, cavity is completely filled.
entrance pressure = 5.2288E+007 Pa,
total clamp force = 7.1844E+005 N,

At time = 9.8658E-001 s, 3.3436E-003 % of post-filling time,
entrance pressure = 5.2288E+007 Pa,
total clamp force = 7.2044E+005 N,

At time = 9.9918E-001 s, 4.2457E-001 % of post-filling time,
entrance pressure = 5.2288E+007 Pa,
total clamp force = 9.1565E+005 N,

At time = 1.3960E+000 s, 1.3690E+001 % of post-filling time,
entrance pressure = 5.2288E+007 Pa,
total clamp force = 1.0637E+006 N,

At time = 1.6460E+000 s, 2.2047E+001 % of post-filling time,
entrance pressure = 5.2288E+007 Pa,
total clamp force = 9.7736E+005 N,

At time = 1.8960E+000 s, 3.0405E+001 % of post-filling time,
entrance pressure = 5.2288E+007 Pa,
total clamp force = 8.2836E+005 N,

At time = 2.1460E+000 s, 3.8763E+001 % of post-filling time,
entrance pressure = 5.2288E+007 Pa,
total clamp force = 6.2032E+005 N,

At time = 2.3960E+000 s, 4.7120E+001 % of post-filling time,
entrance pressure = 5.2288E+007 Pa,
total clamp force = 4.1962E+005 N,

At time = 2.6460E+000 s, 5.5478E+001 % of post-filling time,

entrance pressure = 5.2288E+007 Pa,
total clamp force = 3.2894E+005 N,

At time = 2.8960E+000 s, 6.3836E+001 % of post-filling time,
entrance pressure = 5.2288E+007 Pa,
total clamp force = 2.4146E+005 N,

At time = 3.1460E+000 s, 7.2193E+001 % of post-filling time,
entrance pressure = 5.2288E+007 Pa,
total clamp force = 1.4019E+005 N,

At time = 3.3960E+000 s, 8.0551E+001 % of post-filling time,
entrance pressure = 5.2288E+007 Pa,
total clamp force = 7.5562E+004 N,

At time = 3.6460E+000 s, 8.8909E+001 % of post-filling time,
entrance pressure = 5.2288E+007 Pa,
total clamp force = 3.8555E+004 N,

At time = 3.8960E+000 s, 9.7266E+001 % of post-filling time,
entrance pressure = 5.2288E+007 Pa,
total clamp force = 1.8608E+004 N,

At time = 3.9687E+000 s, holding pressure is released.

At time = 3.9813E+000 s, 1.0000E+002 % of post-filling time,
entrance pressure = 4.8994E+007 Pa,
total clamp force = 1.4417E+004 N,

Beginning of preparing the interface data

Preparing PPC file for C-MOLD Cooling

Preparing LSP file for C-MOLD Residual Stress/Shrinkage & Warpage

End of preparing the interface data.

C-MOLD Filling 99.7
C-MOLD Post-filling 99.7
C-MOLD Residual Stress 99.7
is successfully completed.

ENDF

A.2 Filling Report

C-MOLD Filling 99.7 summary report of filling analysis.

Date : MAY02-01
Time : 10:24:55
Name : sample_1

C-MOLD Cooling mold wall temp data was not used.

Summary during filling stage

Max entrance pressure (at 9.7847E-001 s) = 5.2288E+001 MPa

Summary at the end of filling stage

Time at the end of filling = 9.8648E-001 s
Total weight = 2.4375E+001 g
Required clamp force = 7.3238E+001 ton(m)

Recommended ram speed profile (rel):
% stroke % speed

```

-----
0.0000E+000      4.3683E+001
2.0000E+001      9.1267E+001
4.0000E+001      1.0000E+002
6.0000E+001      8.1604E+001
8.0000E+001      7.9473E+001
1.0000E+002      6.3329E+001
Melt front is entirely in the cavity at % fill      = 0.0000E+000 %

Part summary during filling stage

Max bulk temp      (at 8.2702E-002 s)      = 2.5028E+002 C
Min bulk temp      (at 9.7948E-001 s)      = 2.0870E+002 C
Max wall shear stress      (at 8.9941E-001 s)      = 2.1853E-001 MPa
Max shear rate      (at 8.9941E-001 s)      = 9.2786E+003 1/s

Part summary at the end of filling stage

Total part weight      = 2.4375E+001 g
Max bulk temp      = 2.5021E+002 C
Min bulk temp      = 2.0876E+002 C
Avg bulk temp      = 2.3103E+002 C
Max wall shear stress      = 2.0997E-001 MPa
Avg wall shear stress      = 1.3984E-001 MPa
Max frozen layer fraction      = 3.4964E-001
Min frozen layer fraction      = 6.7589E-002
Avg frozen layer fraction      = 2.4127E-001
Max shear rate      = 8.1817E+003 1/s
Avg shear rate      = 7.5251E+002 1/s

```

A.3 Post-Filling Report

C-MOLD Post-filling 99.7 summary report of post-filling analysis.

Date : MAY02-01
Time : 10:24:55
Name : sample_1

C-MOLD Cooling mold wall temp data was not used.

Summary during post-filling stage

```

Min peak pressure      (at 1.3960E+000 s)      = 2.8528E+001 MPa
Max clamp force      (at 1.3960E+000 s) = 1.0844E+002 ton(m)
Max total weight      (at 3.9813E+000 s)      = 2.6405E+001 g

```

Summary at the end of post-filling stage

```

Time at the end of post-filling      = 3.9813E+000 s
Total weight      = 2.6405E+001 g

```

Part summary during post-filling stage

```

Max bulk temp      (at 9.8658E-001 s)      = 2.5021E+002 C
Min bulk temp      (at 3.9813E+000 s)      = 6.3839E+001 C
Max wall shear stress      (at 2.3960E+000 s)      = 2.3674E-001 MPa
Max volumetric shrinkage      (at 9.8658E-001 s)      = 1.6919E+001 %
Min volumetric shrinkage      (at 3.8960E+000 s)      = 1.5435E+000 %
Max total part weight      (at 3.9813E+000 s)      = 2.6405E+001 g

```

Part summary at the end of post-filling stage

```

Total part weight      = 2.6405E+001 g
Max bulk temp      = 7.8511E+001 C
Min bulk temp      = 6.3839E+001 C
Avg bulk temp      = 7.1003E+001 C
Max frozen layer fraction      = 1.0000E+000
Min frozen layer fraction      = 1.0000E+000
Avg frozen layer fraction      = 1.0000E+000
Max volumetric shrinkage      = 8.3499E+000 %
Min volumetric shrinkage      = 1.5566E+000 %
Avg volumetric shrinkage      = 4.3696E+000 %

```

Max sink index = 3.4989E-001 %
Avg sink index = 1.4112E-002 %

A.4 Shrinkage and Warpage Report

=====
C-MOLD Shrinkage and Warpage 99.7 summary report.
Name : sample_1
Date : MAY02-01
Time : 10:27:18

=====
Maximum process-induced shrinkage
=====

Maximum shrinkage is between node 1 and 327

Initial distance = 2.6833E+002 mm

Displaced distance = 2.6420E+002 mm

Change of distance = -4.1293E+000 mm

Percentage of change = -1.54%
=====

A.5 Finite Element Model

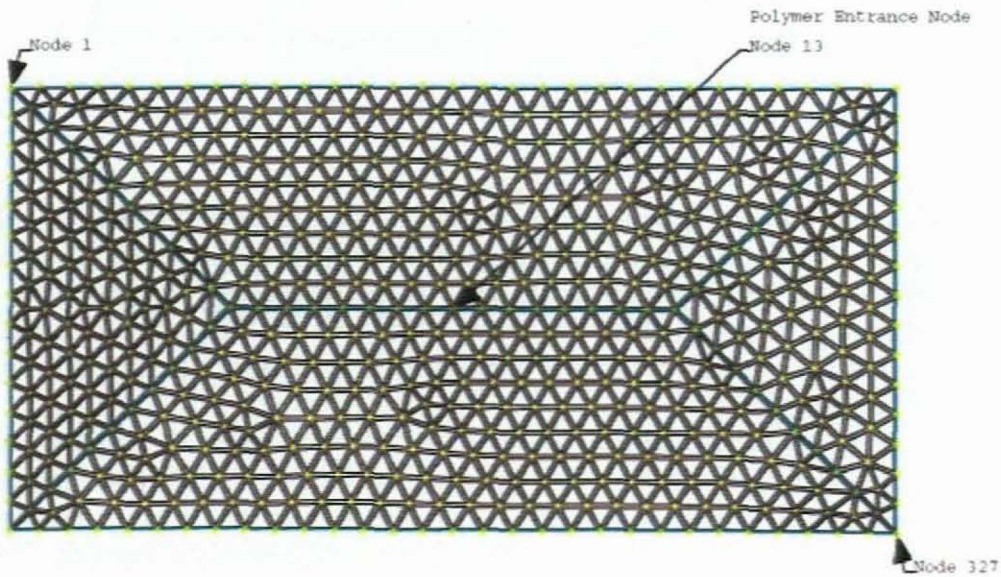


Figure A.1 Finite element model showing elements and nodes.

Nodes 1 and 327 are the points between which maximum shrinkage occurs, and node 13 is the polymer entrance node. See the log file and shrinkage and warpage report.

Appendix B

ABAQUS Report

The solution procedure that is discussed in Chapter 4, will be used to solve the shrinkage of a given sample, and also the cooling stress through the cavity thickness. This Appendix will discuss the input data of the ABAQUS analysis that were completed.

B.1 The Problem Description

An injection mould consists of two pieces of tool steel pressed together with a cavity inside. This cavity is filled with molten polymer, such as polypropylene under pressure. The air that originally filled the cavity are vented through specially designed gaps that only allow the air to escape, leaving the cavity volume filled with polymer (Figure B.1). Once filled, the injection pressure are increased and held. The tool steel is not represented in the finite element model.

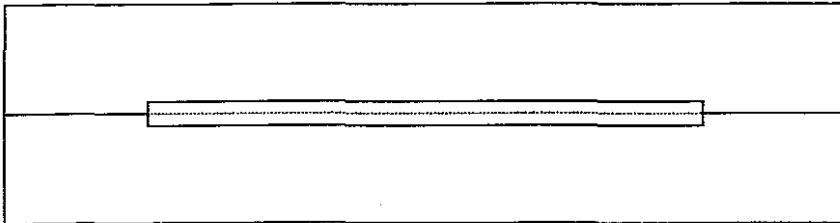


Figure B.1 Injection mould schematic with cavity and midplane.

The mould wall refers to the part of the tool steel that is in contact with the polymer. This mould wall is in a state of preheating, (generally $\pm 40^{\circ}\text{C}$) due to the injection cycle. Since the polymer is at a higher temperature (230°C) than the mould wall, heat is lost to the surrounding tool steel. The mould surface refers to that part of polymer that is in contact with the tool steel. When the molten polymer is cooled, the cooling starts from the mould surface and penetrate inwards towards the midplane.

The analysis is done in two steps. In the initial step a condition of constant temperature (230°C) through the volume of the polymer is set. Step 1 is the second step and it deals with the cooling of the polymer to its solidification temperature of 93°C , through heat loss at the mould wall.

The following assumptions are made:

- the air that originally filled the cavity is vented, and the entire cavity is filled with polymer.
- the cooling stage starts once the cavity is filled.
- the mould wall is preheated due to the injection cycle.
- any mould wall temperature changes will be neglected.
- an initial condition of constant temperature through the polymer exists.
- there is no heat source in the polymer.

B.2 Part Geometry

Consider a rectangular mould having a thickness so much smaller than both its width and length, that width and length can be considered infinite. To determine the heat transfer through a 4mm cavity thickness, consider a 3-Dimensional section ($2000\mu\text{m} \times 50\mu\text{m}$) from the midplane to the mould wall.

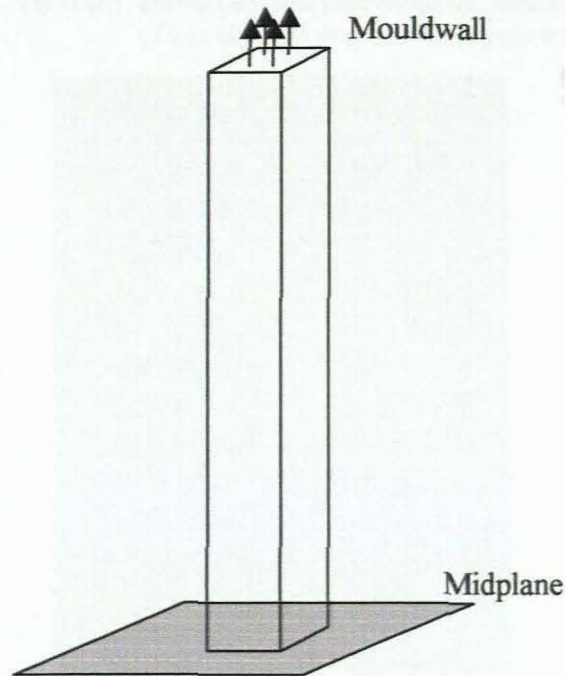


Figure B.2 3-Dimensional polymer section.

B.3 Material Property

All the material properties are sourced from the database of the injection moulding simulation software C-MOLD. The commercial name of the polymer that was used in the analysis is Borealis. Density, which can be classified as a general property, was entered as temperature dependent data. This density values were derived from the specific volume versus temperature graph in Figure B.3.

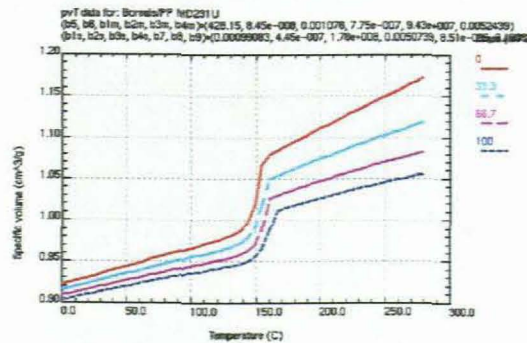


Figure B.3 Borealis specific volume versus temperature.
 (Diagram obtained from C-MOLD polymer properties database)

The mechanical properties for this specimen are Young's modulus of 1700 MPa, and Poisson's ratio of 0.38. Since the main aim of this analysis was the determination of the temperature field, extra care had to be taken with the thermal properties. Temperature dependent data for specific heat and conductivity were used. These data can be seen in tables B.1 and B.2, and is within the injection moulding processing range.

Table B.1 Borealis specific heat versus temperature
(Table obtained from C-MOLD polymer properties database)

Temperature (C)	Specific heat (J/kg-C)
60	1670
70	1750
80	1840
90	1930
100	2060
110	2090
117	13000
120	6690
130	2060
140	2090
150	2120
160	2150
170	2180
180	2210
190	2240
200	2260
210	2290
220	2310
230	2330
240	2340
250	2340

Table B.2 Borealis thermal conductivity versus temperature
(Table obtained from C-MOLD polymer properties database)

Temperature (C)	Thermal cond. (W/m-C)
20	0.301
30	0.299
40	0.297
50	0.295
60	0.293
70	0.292
80	0.291
90	0.290
100	0.289
110	0.288
120	0.287
130	0.286
140	0.285
150	0.284
160	0.283
170	0.282
180	0.281
190	0.280
200	0.279
210	0.278
220	0.277
230	0.276
240	0.275
250	0.274

The last thermal property that was considered is that of latent heat. Latent heat is the heat absorbed as a substance changes phase from liquid to solid [18,23], and in the case of the injection moulding process this is called solidification. When we view the specific heat versus temperature graph (Figure B.4) of Borealis, a definite spike in the specific heat can be seen at the transition temperature. The spike starts at a liquid state of 130°C and ends at a solid state of 100°C. This sudden increase can also be seen for Table B.1 where the spike is at its maximum at 117°C. Latent heat are defined as the area under the spike [18,19] and were calculated to be 92 549.5 J/kg.

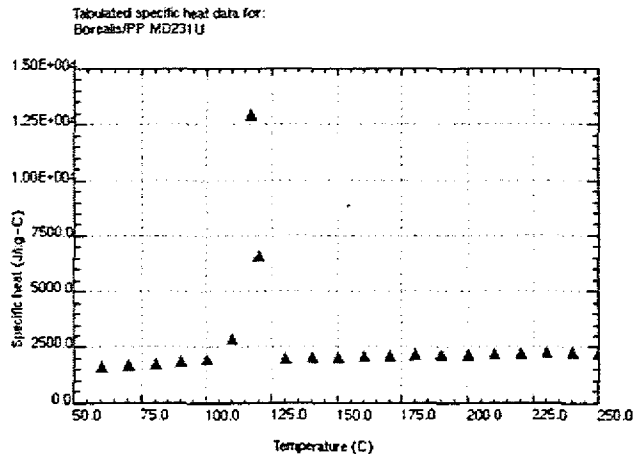


Figure B.4 Borealis specific heat versus temperature
(Diagram obtained from C-MOLD polymer properties database)

B.4 Analysis Step

During the cooldown period, (step 1) and since there is no heat source in the polymer, an uncoupled heat transfer analysis is performed. In this analysis the parameters was set so that automatic time incrementation is used. The increments was an initial size of 0.0005 with the allowed minimum 1e-6 and the maximum 0.05. The end step parameter is set so that the analysis terminates when steady-state conditions are reached. Steady state is defined as the point at which the temperature rate change is less than 0.1°C/s. A total analysis time of 40 seconds was also specified.

B.5 Interaction

A boundary condition is set for the surface at the midplane and along the four surfaces for the length of the section. As mentioned in the problem description, the tool steel is not represented in the finite element model. However, the polymer loose heat at the mould wall/surface to the surrounding tool steel and the thermal conductivity of the tool steel and the heat transfer across the joint need to be considered. A film condition type boundary is set for the polymer surface in contact with the tool steel.

It is assumed that the polymer loose heat through contact-conductance with the mould wall surface. The physical mechanism of contact conductance may be better understood by examining a joint in more detail.

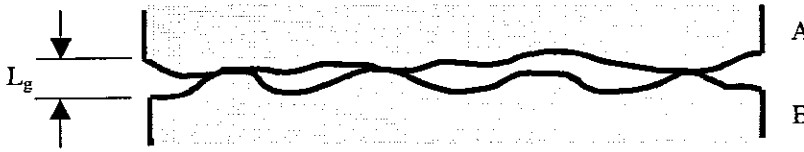


Figure B.5 Roughness model for a joint.

No surface is perfectly smooth, and the surface roughness plays a central role in the transfer of heat. There are two principal contributions to the heat transfer at a joint [22].

- solid to solid conduction at the spots of contact.
- conduction through gases in the voids.

The contact coefficient for heat flow across the joint can be written as

$$h_c = \frac{1}{L_g} \left(\frac{A_c}{A} \frac{2k_A k_B}{k_A + k_B} + \frac{A_v}{A} k_f \right) \quad (\text{B.1})$$

where L_g = thickness of the void space

A_c = contact area

A = total cross-sectional area

A_v = void area

k = thermal conductivity

k_f = thermal conductivity of void fluid

The surface of an injection mould cavity is polished to a very high degree; from 10 μm to as low as 1 μm [26]. L_g were therefore assumed to be 5 μm . Since the assumption is that the air that originally filled the cavity is vented, and the entire cavity is filled with polymer, the void area and thermal conductivity of the void fluid falls away. This results in contact area and total area being equal.

The results obtained for the contact coefficient is entered as the film coefficient in ABAQUS. Since mould wall temperature changes were assumed to be negligible, the mould wall for the tool steel is set at a constant temperature of 40°C.

B.6 Load

The entire volume of the polymer section is firstly defined as a field, and a condition of constant temperature (230 °C) is then set for this field in the initial step.

B.7 Meshing

The model is discretized with 20-node quadratic heat transfer brick elements (element type DCC3D8). Amount of elements over $2000\mu\text{m}$ is 200 elements.

Appendix C

ABAQUS Output Data

The ABAQUS analysis for a sample of 4mm thickness, show the total time to solidification to be 34.36 sec. This time is divided into equal time intervals and the closest ABAQUS time interval is selected. The distance from the midplane is also identified.

Although any arbitrary number of layers can be considered and analysed for a particular sample, only 60 and 80 layers were chosen. From these 40, 30, 20, 15, 10, and 5 layers were generated. For this Appendix only the results for 60 and 80 layers will be illustrated.

Table C.1 ABAQUS results for 80 layers

Layer #	Equal Time Intervals (seconds)	ABAQUS Time Int. (seconds)	Wall Temp. (C°)	Layer Temp (C°)	Distance from Midplane (µm)
0	0	0			2000
1	0.4295	4.05E-01	41.381	92.432	1905
2	0.8590	8.55E-01	40.934	91.855	1860
3	1.2885	1.3052	40.751	93.347	1820
4	1.7180	1.7052	40.655	92.915	1795
5	2.1475	2.1552	40.581	92.626	1770
6	2.5770	2.6052	40.528	92.92	1745
7	3.0065	3.0052	40.491	93.04	1725
8	3.4360	3.4552	40.457	92.987	1705
9	3.8655	3.8552	40.433	92.672	1690
10	4.2950	4.3052	40.409	92.99	1670
11	4.7245	4.7052	40.391	92.951	1655
12	5.1540	5.1552	40.373	92.751	1640
13	5.5835	5.5552	40.36	92.887	1625
14	6.0130	6.0052	40.346	92.855	1610
15	6.4425	6.4552	40.333	92.884	1595
16	6.8720	6.8552	40.323	93.149	1580
17	7.3015	7.3052	40.313	93.246	1565
18	7.7310	7.7052	40.304	92.971	1555
19	8.1605	8.1552	40.295	93.114	1540
20	8.5900	8.6052	40.287	93.263	1525
21	9.0195	9.0052	40.28	93.049	1515
22	9.4490	9.4552	40.272	93.205	1500
23	9.8785	9.8552	40.266	93.007	1490
24	10.3080	10.305	40.259	93.154	1475
25	10.7375	10.755	40.253	92.817	1465
26	11.1670	11.155	40.248	93.087	1450
27	11.5965	11.605	40.242	93.197	1435
28	12.0260	12.005	40.237	92.989	1425
29	12.4555	12.455	40.231	93.072	1410
30	12.8850	12.855	40.227	92.852	1400
31	13.3145	13.305	40.221	92.905	1385
32	13.7440	13.755	40.216	92.938	1370

33	14.1735	14.155	40.212	93.08	1355
34	14.6030	14.605	40.208	93.073	1340
35	15.0325	15.055	40.203	93.05	1325
36	15.4620	15.455	40.199	93.138	1310
37	15.8915	15.905	40.195	93.087	1295
38	16.3210	16.355	40.191	93.026	1280
39	16.7505	16.755	40.187	93.079	1265
40	17.1800	17.155	40.184	93.125	1250
41	17.6095	17.605	40.18	93.05	1235
42	18.0390	18.055	40.176	92.977	1220
43	18.4685	18.455	40.173	93.018	1205
44	18.8980	18.905	40.17	92.951	1190
45	19.3275	19.305	40.167	92.996	1175
46	19.7570	19.755	40.164	92.938	1160
47	20.1865	20.155	40.161	92.986	1145
48	20.6160	20.605	40.159	92.936	1130
49	21.0455	21.055	40.156	92.89	1115
50	21.4750	21.455	40.153	92.942	1100
51	21.9045	21.905	40.151	92.9	1085
52	22.3340	22.305	40.149	92.951	1070
53	22.7635	22.755	40.146	92.909	1055
54	23.1930	23.205	40.144	92.866	1040
55	23.6225	23.605	40.142	92.91	1025
56	24.0520	24.055	40.14	93.106	1005
57	24.4815	24.455	40.138	93.138	990
58	24.9110	24.905	40.136	93.078	975
59	25.3405	25.355	40.134	93.013	960
60	25.7700	25.755	40.132	93.028	945
61	26.1995	26.205	40.13	92.951	930
62	26.6290	26.605	40.128	92.95	915
63	27.0585	27.055	40.127	93.075	895
64	27.4880	27.505	40.125	92.971	880
65	27.9175	27.905	40.123	92.94	865
66	28.3470	28.355	40.121	93.018	845
67	28.7765	28.755	40.12	92.955	830
68	29.2060	29.205	40.118	92.982	810
69	29.6355	29.655	40.117	92.968	790
70	30.0650	30.055	40.115	92.994	770
71	30.4945	30.505	40.113	93.041	745
72	30.9240	30.905	40.112	93.094	720
73	31.3535	31.355	40.11	93.091	690
74	31.7830	31.755	40.108	93.074	660
75	32.2125	32.205	40.107	93.092	620
76	32.6420	32.655	40.105	92.918	580
77	33.0715	33.055	40.103	92.951	530
78	33.5010	33.505	40.101	93	455
79	33.9305	33.905	40.099	92.988	345
80	34.3600	34.355	40.096	92.989	0

Table C.2 ABAQUS results for 60 layers

Layer #	Equal Time Intervals (seconds)	ABAQUS Time Int. (seconds)	Wall Temp. (C°)	Layer Temp (C°)	Distance from Midplane (µm)
0	0	0			2000
1	0.5727	5.55E-01	41.1699	93.4992	1885
2	1.1453	1.1552	40.7993	93.6753	1830
3	1.7180	1.7052	40.6546	92.9148	1795
4	2.2907	2.3052	40.5614	93.0271	1760
5	2.8633	2.8552	40.5036	93.4404	1730
6	3.4360	3.4552	40.4572	92.9872	1705
7	4.0087	4.0052	40.4243	93.2945	1680
8	4.5813	4.6052	40.3954	92.766	1660
9	5.1540	5.1552	40.3735	92.7505	1640
10	5.7267	5.7052	40.3548	92.8684	1620
11	6.2993	6.3052	40.3372	92.8681	1600
12	6.8720	6.8552	40.3231	93.1493	1580
13	7.4447	7.4552	40.3093	93.2834	1560
14	8.0173	8.0052	40.298	93.0652	1545
15	8.5900	8.6052	40.2867	93.2635	1525
16	9.1627	9.1552	40.2772	93.1012	1510
17	9.7353	9.7552	40.2676	92.8057	1495
18	10.3080	10.3052	40.2594	93.1535	1475
19	10.8807	10.8552	40.2516	93.0035	1460
20	11.4533	11.4552	40.2436	93.1624	1440
21	12.0260	12.0052	40.2367	92.9892	1425
22	12.5987	12.6052	40.2294	93.0957	1405
23	13.1713	13.1552	40.2231	92.8895	1390
24	13.7440	13.7552	40.2165	92.9379	1370
25	14.3167	14.3052	40.2106	93.0799	1350
26	14.8893	14.9052	40.2045	93.0599	1330
27	15.4620	15.4552	40.1992	93.1376	1310
28	16.0347	16.0552	40.1935	93.0672	1290
29	16.6073	16.6052	40.1886	93.1027	1270
30	17.1800	17.1552	40.1838	93.1253	1250
31	17.7527	17.7552	40.1788	93.0255	1230
32	18.3253	18.3052	40.1745	93.0416	1210
33	18.8980	18.9052	40.17	92.9512	1190
34	19.4707	19.4552	40.1661	92.9757	1170
35	20.0433	20.0552	40.1621	92.902	1150
36	20.6160	20.6052	40.1586	92.936	1130
37	21.1887	21.2052	40.1549	92.8755	1110
38	21.7613	21.7552	40.1518	92.914	1090
39	22.3340	22.3052	40.1487	92.9507	1070
40	22.9067	22.9052	40.1455	92.8944	1050
41	23.4793	23.4552	40.1427	92.9251	1030
42	24.0520	24.0552	40.1398	93.1063	1005
43	24.6247	24.6052	40.1372	93.1182	985
44	25.1973	25.2052	40.1345	93.0355	965
45	25.7700	25.7552	40.1321	93.0276	945
46	26.3427	26.3552	40.1295	92.9237	925
47	26.9153	26.9052	40.1272	93.108	900
48	27.4880	27.5052	40.1248	92.9713	880
49	28.0607	28.0552	40.1226	92.8991	860

50	28.6333	28.6052	40.1205	93.0058	835
51	29.2060	29.2052	40.1182	92.9816	810
52	29.7787	29.7552	40.1161	92.979	785
53	30.3513	30.3552	40.1139	92.9745	755
54	30.9240	30.9052	40.1118	93.0937	720
55	31.4967	31.5052	40.1095	93.0578	680
56	32.0693	32.0552	40.1072	93.0553	635
57	32.6420	32.6552	40.1046	92.918	580
58	33.2147	33.2052	40.1021	93.0439	505
59	33.7873	33.8052	40.0991	92.9607	380
60	34.3600	34.3552	40.0962	92.9892	0

The graph in Figure C.1 below was generated from the Tables above.

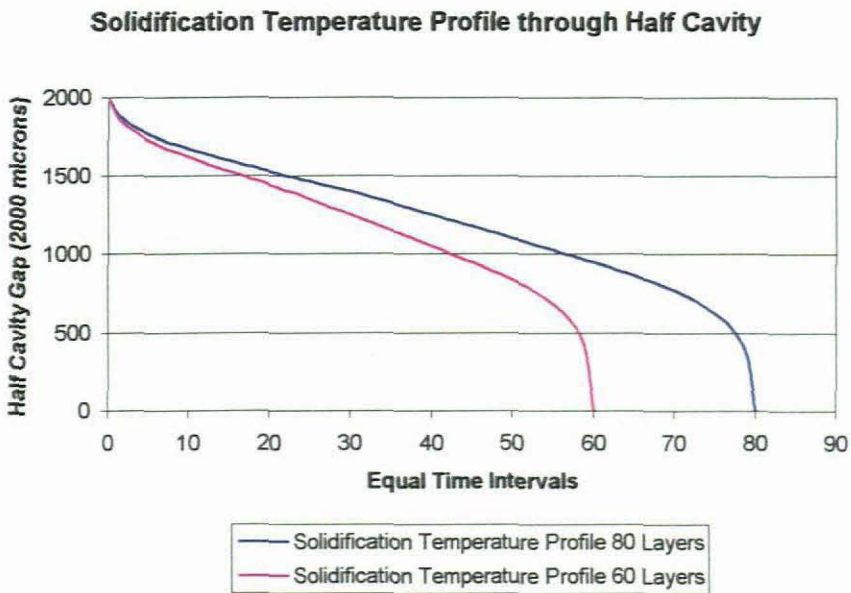


Figure C.1 Solidification temperature profiles.

Appendix D

FORTRAN Program

The solution procedure that was proposed in Chapter 4, will be used to solve the shrinkage and the stress of a given sample. Fortran was identified as the tool to aid in solving the algorithm. This Appendix will illustrate the Fortran program. Although a different number of layers will be considered and analysed for a particular sample, only the program for 10 layers will be illustrated. The rest of the Fortran programs for the other layers can be found on the accompanying compact disk.

```
PROGRAM MORNAY
```

```
REAL ETA0, POI, P0, E, DELTA1, Y0, Y1, P1, DELTA0, ALPHA, TY0Y1S, TY1S, SIG1  
REAL ETA1, Y2, P2, DELTA2, TY1Y2S, TY2S, SIG2
```

```
1 OPEN(UNIT=5, FILE='MORN.txt', STATUS='UNKNOWN')  
1 FORMAT(2X, 2PE10.3, ', ', 5X, 0PE10.3, ', ', 5X, 2PE10.3)
```

```
DELTA0=0  
POI=0.38  
ALPHA=9.44E-5  
E=1.7E9  
Y0=1  
Y1=0.8525  
Y2=0.79  
Y3=0.7375  
Y4=0.685  
Y5=0.625  
Y6=0.565  
Y7=0.5025  
Y8=0.44  
Y9=0.360  
Y10=0.0  
P0 = 4.8E6  
P1 = 4.32E6  
P2 = 3.84E6  
P3 = 3.36E6  
P4 = 2.88E6  
P5 = 2.4E6  
P6 = 1.92E6  
P7 = 1.44E6  
P8 = 0.96E6  
P9 = 0.48E6  
P10 = 0.0  
TY0Y1S=40.4572  
TY1S=92.9872  
TY0Y2S=40.3231  
TY2S=93.1493  
TY0Y3S=40.2594  
TY3S=93.1535  
TY0Y4S=40.2165  
TY4S=92.9379  
TY0Y5S=40.1838  
TY5S=93.1253  
TY0Y11S=40.17
```

```

TY11S=92.9512
  TY0Y6S=40.1586
TY6S=92.936
TY0Y13S=40.1487
TY13S=92.9507
TY0Y7S=40.1398
TY7S=93.1063
TY0Y15S=40.1321
TY15S=93.0276
  TY0Y8S=40.1248
TY8S=92.9713
  TY0Y17S=40.1182
TY17S=92.9816
TY0Y9S=40.1118
TY9S=93.0937
TY0Y19S=40.1046
TY19S=92.918
TY0Y10S=40.0962
TY10S=92.9892

```

```

ETA0 = ((2*POI - 1)*P0) / E
DELTA1 = (((((2*POI - 1)*P1) / E) - ETA0) * ((Y0-Y1) / 2) + (((Y1-
(2*Y1*POI)+POI)*P1) / E) + (ALPHA*(TY0Y1S - TY1S)*(Y0-Y1))) / ((Y0-
Y1) + ((Y0-Y1) / 2))
ETA1 = ((2*POI - 1)*P1) / E
SIG1 = (ETA1 - ((POI*P1) / E) - ALPHA*(TY0Y1S - TY1S)) * (E / (1-
POI))

```

```

WRITE(5,1) DELTA1,Y1,SIG1
PRINT*, DELTA1,Y1,SIG1

```

```

DELTA2 = (((((2*POI - 1)*P2) / E) - ETA1) * ((Y1-Y2) / 2) -
(ETA0*(Y0-Y1)) + (((Y2-(2*Y2*POI)+POI)*P2) / E) + (ALPHA*(TY0Y2S -
TY2S)*(Y0-Y2))) / ((Y0-Y2) + ((Y1-Y2) / 2))
ETA2 = ((2*POI - 1)*P2) / E
SIG2 = (-DELTA1 + ETA2 - ((POI*P2) / E) - ALPHA*(TY0Y2S - TY2S)) * (E
/ (1-POI))

```

```

WRITE(5,1) DELTA2,Y2,SIG2
PRINT*, DELTA2,Y2,SIG2

```

```

DELTA3 = (((((2*POI - 1)*P3) / E) - ETA2) * ((Y2-Y3) / 2) -
(ETA0*(Y0-Y2)) + (((Y3-(2*Y3*POI)+POI)*P3) / E) + (ALPHA*(TY0Y3S -
TY3S)*(Y0-Y3))) / ((Y0-Y3) + ((Y2-Y3) / 2))
ETA3 = (((2*POI - 1)*P3) / E) + DELTA3
SIG3 = (-DELTA2 + ETA3 - ((POI*P3) / E) - ALPHA*(TY0Y3S - TY3S)) * (E
/ (1-POI))

```

```

WRITE(5,1) DELTA3,Y3,SIG3
PRINT*, DELTA3,Y3,SIG3

```

```

DELTA4 = (((((2*POI - 1)*P4) / E) - ETA3) * ((Y3-Y4) / 2) -
(ETA0*(Y0-Y3)) + (((Y4-(2*Y4*POI)+POI)*P4) / E) + (ALPHA*(TY0Y4S -
TY4S)*(Y0-Y4))) / ((Y0-Y4) + ((Y3-Y4) / 2))
ETA4 = (((2*POI - 1)*P4) / E) + DELTA4
SIG4 = (-DELTA3 + ETA4 - ((POI*P4) / E) - ALPHA*(TY0Y4S - TY4S)) * (E
/ (1-POI))

```

```

WRITE(5,1) DELTA4,Y4,SIG4
PRINT*, DELTA4,Y4,SIG4

```

```

DELTA5 = (((((2*POI - 1)*P5) / E) - ETA4) * ((Y4-Y5) / 2) -
(ETA0*(Y0-Y4)) + (((Y5-(2*Y5*POI)+POI)*P5) / E) + (ALPHA*(TY0Y5S -
TY5S)*(Y0-Y5))) / ((Y0-Y5) + ((Y4-Y5) / 2))
ETA5 = (((2*POI - 1)*P5) / E) + DELTA5
SIG5 = (-DELTA4 + ETA5 - ((POI*P5) / E) - ALPHA*(TY0Y5S - TY5S)) * (E
/ (1-POI))

```

```

WRITE(5,1) DELTA5,Y5,SIG5
PRINT*, DELTA5,Y5,SIG5

```

```

DELTA6 = (((((2*POI - 1)*P6) / E) - ETA5) * ((Y5-Y6) / 2) -
(ETA0*(Y0-Y5)) + (((Y6-(2*Y6*POI)+POI)*P6) / E) + (ALPHA*(TY0Y6S -
TY6S)*(Y0-Y6))) / ((Y0-Y6) + ((Y5-Y6) / 2))
ETA6 = (((2*POI - 1)*P6) / E) + DELTA6
SIG6 = (-DELTA5 + ETA6 - ((POI*P6) / E) - ALPHA*(TY0Y6S - TY6S)) * (E
/ (1-POI))

```

```

WRITE(5,1) DELTA6,Y6,SIG6
PRINT*, DELTA6,Y6,SIG6

```

```

DELTA7 = (((((2*POI - 1)*P7) / E) - ETA6) * ((Y6-Y7) / 2) -
(ETA0*(Y0-Y6)) + (((Y7-(2*Y7*POI)+POI)*P7) / E) + (ALPHA*(TY0Y7S -
TY7S)*(Y0-Y7))) / ((Y0-Y7) + ((Y6-Y7) / 2))
ETA7 = (((2*POI - 1)*P7) / E) + DELTA7
SIG7 = (-DELTA6 + ETA7 - ((POI*P7) / E) - ALPHA*(TY0Y7S - TY7S)) * (E
/ (1-POI))

```

```

WRITE(5,1) DELTA7,Y7,SIG7
PRINT*, DELTA7,Y7,SIG7

```

```

DELTA8 = (((((2*POI - 1)*P8) / E) - ETA7) * ((Y7-Y8) / 2) -
(ETA0*(Y0-Y7)) + (((Y8-(2*Y8*POI)+POI)*P8) / E) + (ALPHA*(TY0Y8S -
TY8S)*(Y0-Y8))) / ((Y0-Y8) + ((Y7-Y8) / 2))
ETA8 = (((2*POI - 1)*P8) / E) + DELTA8
SIG8 = (-DELTA7 + ETA8 - ((POI*P8) / E) - ALPHA*(TY0Y8S - TY8S)) * (E
/ (1-POI))

```

```

WRITE(5,1) DELTA8,Y8,SIG8
PRINT*, DELTA8,Y8,SIG8

```

```

DELTA9 = (((((2*POI - 1)*P9) / E) - ETA8) * ((Y8-Y9) / 2) -
(ETA0*(Y0-Y8)) + (((Y9-(2*Y9*POI)+POI)*P9) / E) + (ALPHA*(TY0Y9S -
TY9S)*(Y0-Y9))) / ((Y0-Y9) + ((Y8-Y9) / 2))
ETA9 = (((2*POI - 1)*P9) / E) + DELTA9
SIG9 = (-DELTA8 + ETA9 - ((POI*P9) / E) - ALPHA*(TY0Y9S - TY9S)) * (E
/ (1-POI))

```

```

WRITE(5,1) DELTA9,Y9,SIG9
PRINT*, DELTA9,Y9,SIG9

```

```

DELTA10 = (((((2*POI - 1)*P10) / E) - ETA9) * ((Y9-Y10) / 2) -
(ETA0*(Y0-Y9)) + (((Y10-(2*Y10*POI)+POI)*P10) / E) + (ALPHA*(TY0Y10S
- TY10S)*(Y0-Y10))) / ((Y0-Y10) + ((Y9-Y10) / 2))
ETA10 = (((2*POI - 1)*P10) / E) + DELTA10
SIG10 = (-DELTA9 + ETA10 - ((POI*P10) / E) - ALPHA*(TY0Y10S - TY10S))
* (E / (1-POI))

```

```

WRITE(5,1) DELTA10,Y10,SIG10
PRINT*, DELTA10,Y10,SIG10

```

```

END PROGRAM MORNAY

```

Appendix E

FORTTRAN Results

The results for the shrinkage and cooling stress from the Fortran program for the different layers are shown in this Appendix.

60 Layers

Layer (#)	Shrinkage (%)	Stress (Mpa)
0		
1	1.62E-02	8.82E+06
2	1.27E-02	-3.54E+07
3	1.03E-02	-2.58E+07
4	8.02E-03	-1.92E+07
5	6.51E-03	-1.27E+07
6	5.50E-03	-8.57E+06
7	4.52E-03	-5.64E+06
8	3.92E-03	-3.01E+06
9	3.30E-03	-1.26E+06
10	2.73E-03	5.58E+05
11	2.22E-03	2.20E+06
12	1.74E-03	3.73E+06
13	1.32E-03	5.17E+06
14	1.04E-03	6.36E+06
15	6.55E-04	7.27E+06
16	4.07E-04	8.36E+06
17	1.78E-04	9.04E+06
18	-1.45E-04	9.45E+06
19	-3.47E-04	9.82E+06
20	-6.09E-04	9.78E+06
21	-7.84E-04	1.01E+07
22	-1.01E-03	1.00E+07
23	-1.16E-03	1.02E+07
24	-1.35E-03	1.02E+07
25	-1.54E-03	1.04E+07
26	-1.71E-03	1.05E+07
27	-1.87E-03	1.06E+07
28	-2.01E-03	1.07E+07
29	-2.15E-03	1.08E+07
30	-2.28E-03	1.09E+07
31	-2.40E-03	1.10E+07
32	-2.52E-03	1.11E+07
33	-2.62E-03	1.12E+07
34	-2.73E-03	1.13E+07
35	-2.82E-03	1.14E+07
36	-2.92E-03	1.15E+07
37	-3.00E-03	1.16E+07
38	-3.09E-03	1.17E+07
39	-3.17E-03	1.18E+07
40	-3.25E-03	1.19E+07
41	-3.32E-03	1.19E+07
42	-3.40E-03	1.21E+07
43	-3.48E-03	1.21E+07
44	-3.54E-03	1.23E+07
45	-3.60E-03	1.23E+07
46	-3.65E-03	1.24E+07
47	-3.71E-03	1.25E+07
48	-3.77E-03	1.26E+07
49	-3.81E-03	1.27E+07
50	-3.86E-03	1.28E+07
51	-3.91E-03	1.28E+07
52	-3.95E-03	1.29E+07
53	-3.98E-03	1.30E+07
54	-4.03E-03	1.31E+07
55	-4.05E-03	1.32E+07
56	-4.08E-03	1.33E+07
57	-4.09E-03	1.34E+07
58	-4.09E-03	1.35E+07
59	-4.03E-03	1.38E+07
60	-3.71E-03	1.46E+07

80 Layers

Layer (#)	Shrinkage (%)	Stress (Mpa)
0		
1	2.06E-02	8.47E+06
2	1.67E-02	-4.80E+07
3	1.23E-02	-3.68E+07
4	1.06E-02	-2.47E+07
5	8.84E-03	-2.01E+07
6	7.38E-03	-1.51E+07
7	6.43E-03	-1.10E+07
8	5.56E-03	-8.36E+06
9	5.01E-03	-5.97E+06
10	4.24E-03	-4.34E+06
11	3.77E-03	-2.15E+06
12	3.33E-03	-8.69E+05
13	2.89E-03	4.55E+05
14	2.49E-03	1.72E+06
15	2.13E-03	2.86E+06
16	1.76E-03	4.00E+06
17	1.44E-03	5.09E+06
18	1.25E-03	5.97E+06
19	9.41E-04	6.59E+06
20	6.65E-04	7.53E+06
21	5.01E-04	8.30E+06
22	2.42E-04	8.85E+06
23	9.33E-05	9.57E+06
24	-1.39E-04	9.69E+06
25	-2.60E-04	9.97E+06
26	-4.79E-04	9.84E+06
27	-6.68E-04	1.00E+07
28	-7.84E-04	1.02E+07
29	-9.55E-04	1.01E+07
30	-1.06E-03	1.03E+07
31	-1.21E-03	1.03E+07
32	-1.36E-03	1.04E+07
33	-1.50E-03	1.05E+07
34	-1.63E-03	1.06E+07
35	-1.75E-03	1.06E+07
36	-1.88E-03	1.07E+07
37	-1.98E-03	1.08E+07
38	-2.08E-03	1.09E+07
39	-2.19E-03	1.09E+07
40	-2.29E-03	1.10E+07
41	-2.38E-03	1.11E+07
42	-2.47E-03	1.12E+07
43	-2.55E-03	1.12E+07
44	-2.63E-03	1.13E+07
45	-2.71E-03	1.13E+07
46	-2.78E-03	1.14E+07
47	-2.86E-03	1.15E+07
48	-2.93E-03	1.16E+07
49	-2.99E-03	1.16E+07
50	-3.06E-03	1.17E+07
51	-3.12E-03	1.18E+07
52	-3.19E-03	1.18E+07
53	-3.24E-03	1.19E+07
54	-3.29E-03	1.19E+07
55	-3.35E-03	1.20E+07
56	-3.42E-03	1.21E+07
57	-3.48E-03	1.22E+07
58	-3.53E-03	1.23E+07
59	-3.57E-03	1.23E+07
60	-3.61E-03	1.24E+07
61	-3.65E-03	1.24E+07
62	-3.69E-03	1.25E+07
63	-3.74E-03	1.26E+07
64	-3.78E-03	1.26E+07
65	-3.82E-03	1.27E+07
66	-3.85E-03	1.28E+07
67	-3.89E-03	1.28E+07
68	-3.92E-03	1.29E+07
69	-3.95E-03	1.29E+07
70	-3.99E-03	1.30E+07
71	-4.01E-03	1.31E+07
72	-4.05E-03	1.31E+07
73	-4.07E-03	1.32E+07
74	-4.10E-03	1.33E+07
75	-4.11E-03	1.34E+07
76	-4.12E-03	1.34E+07
77	-4.13E-03	1.35E+07
78	-4.11E-03	1.36E+07
79	-4.07E-03	1.37E+07
80	-3.76E-03	1.46E+07

80 Layers

Layer (#)	Shrinkage (%)	Stress (Mpa)
0		
1	2.06E-02	8.47E+06
2	1.67E-02	-4.80E+07
3	1.23E-02	-3.68E+07
4	1.06E-02	-2.47E+07
5	8.84E-03	-2.01E+07
6	7.38E-03	-1.51E+07
7	6.43E-03	-1.10E+07
8	5.56E-03	-8.36E+06
9	5.01E-03	-5.97E+06
10	4.24E-03	-4.34E+06
11	3.77E-03	-2.15E+06
12	3.33E-03	-8.69E+05
13	2.89E-03	4.55E+05
14	2.49E-03	1.72E+06
15	2.13E-03	2.86E+06
16	1.76E-03	4.00E+06
17	1.44E-03	5.09E+06
18	1.25E-03	5.97E+06
19	9.41E-04	6.59E+06
20	6.65E-04	7.53E+06
21	5.01E-04	8.30E+06
22	2.42E-04	8.85E+06
23	9.33E-05	9.57E+06
24	-1.39E-04	9.69E+06
25	-2.60E-04	9.97E+06
26	-4.79E-04	9.84E+06
27	-6.68E-04	1.00E+07
28	-7.84E-04	1.02E+07
29	-9.55E-04	1.01E+07
30	-1.06E-03	1.03E+07
31	-1.21E-03	1.03E+07
32	-1.36E-03	1.04E+07
33	-1.50E-03	1.05E+07
34	-1.63E-03	1.06E+07
35	-1.75E-03	1.06E+07
36	-1.88E-03	1.07E+07
37	-1.98E-03	1.08E+07
38	-2.08E-03	1.09E+07
39	-2.19E-03	1.09E+07
40	-2.29E-03	1.10E+07
41	-2.38E-03	1.11E+07
42	-2.47E-03	1.12E+07
43	-2.55E-03	1.12E+07
44	-2.63E-03	1.13E+07
45	-2.71E-03	1.13E+07
46	-2.78E-03	1.14E+07
47	-2.86E-03	1.15E+07
48	-2.93E-03	1.16E+07
49	-2.99E-03	1.16E+07
50	-3.06E-03	1.17E+07
51	-3.12E-03	1.18E+07
52	-3.19E-03	1.18E+07
53	-3.24E-03	1.19E+07
54	-3.29E-03	1.19E+07
55	-3.35E-03	1.20E+07
56	-3.42E-03	1.21E+07
57	-3.48E-03	1.22E+07
58	-3.53E-03	1.23E+07
59	-3.57E-03	1.23E+07
60	-3.61E-03	1.24E+07
61	-3.65E-03	1.24E+07
62	-3.69E-03	1.25E+07
63	-3.74E-03	1.26E+07
64	-3.78E-03	1.26E+07
65	-3.82E-03	1.27E+07
66	-3.85E-03	1.28E+07
67	-3.89E-03	1.28E+07
68	-3.92E-03	1.29E+07
69	-3.95E-03	1.29E+07
70	-3.99E-03	1.30E+07
71	-4.01E-03	1.31E+07
72	-4.05E-03	1.31E+07
73	-4.07E-03	1.32E+07
74	-4.10E-03	1.33E+07
75	-4.11E-03	1.34E+07
76	-4.12E-03	1.34E+07
77	-4.13E-03	1.35E+07
78	-4.11E-03	1.36E+07
79	-4.07E-03	1.37E+07
80	-3.76E-03	1.46E+07

40 Layers

Layer (#)	Shrinkage (%)	Stress (Mpa)			
0			19	-2.06E-03	1.06E+07
1	1.26E-02	8.50E+06	20	-2.27E-03	1.07E+07
2	9.59E-03	-2.56E+07	21	-2.43E-03	1.09E+07
3	6.99E-03	-1.72E+07	22	-2.60E-03	1.11E+07
4	5.34E-03	-9886488	23	-2.75E-03	1.12E+07
5	4.12E-03	-5.23E+06	24	-2.89E-03	1.14E+07
6	3.23E-03	-1806617	25	-3.02E-03	1.15E+07
7	2.42E-03	7.65E+05	26	-3.15E-03	1.16E+07
8	1.71E-03	3188682	27	-3.26E-03	1.18E+07
9	1.21E-03	5.23E+06	28	-3.38E-03	1.19E+07
10	6.34E-04	6803567	29	-3.49E-03	1.21E+07
11	2.27E-04	8.48E+06	30	-3.57E-03	1.23E+07
12	-1.50E-04	9297285	31	-3.65E-03	1.24E+07
13	-4.87E-04	9.51E+06	32	-3.73E-03	1.25E+07
14	-7.86E-04	9713409	33	-3.81E-03	1.26E+07
15	-1.06E-03	9.88E+06	34	-3.88E-03	1.28E+07
16	-1.35E-03	9971356	35	-3.94E-03	1.29E+07
17	-1.62E-03	1.02E+07	36	-3.99E-03	1.31E+07
18	-1.86E-03	1.04E+07	37	-4.03E-03	1.32E+07
			38	-4.03E-03	1.34E+07
			39	-4.01E-03	1.36E+07
			40	-3.60E-03	1.48E+07

30 Layers

Layer (#)	Shrinkage (%)	Stress (Mpa)			
0			14	-1.98E-03	1.03E+07
1	9.52E-03	9.05E+06	15	-2.25E-03	1.06E+07
2	7.43E-03	-1.70E+07	16	-2.48E-03	1.08E+07
3	5.18E-03	-1.11E+07	17	-2.68E-03	1.10E+07
4	3.74E-03	-4816149	18	-2.87E-03	1.12E+07
5	2.63E-03	-6.51E+05	19	-3.04E-03	1.14E+07
6	1.67E-03	2634904	20	-3.20E-03	1.16E+07
7	9.87E-04	5.39E+06	21	-3.35E-03	1.18E+07
8	3.73E-04	7446362	22	-3.49E-03	1.20E+07
9	-1.61E-04	8.87E+06	23	-3.60E-03	1.22E+07
10	-6.19E-04	9241272	24	-3.70E-03	1.24E+07
11	-1.01E-03	9.58E+06	25	-3.81E-03	1.26E+07
12	-1.34E-03	9844002	26	-3.89E-03	1.28E+07
13	-1.68E-03	1.00E+07	27	-3.95E-03	1.31E+07
			28	-3.99E-03	1.33E+07
			29	-3.98E-03	1.36E+07
			30	-3.54E-03	1.49E+07

20 Layers

Layer (#)	Shrinkage (%)	Stress (Mpa)
0		
1	7.11E-03	8.97E+06
2	4.85E-03	-1.02E+07
3	3.03E-03	-3819024
4	1.61E-03	1522663
5	5.86E-04	5.70E+06
6	-1.76E-04	8240740
7	-8.00E-04	8824470
8	-1.34E-03	9296607

9	-1.82E-03	9.73E+06
10	-2.22E-03	1.02E+07
11	-2.54E-03	1.06E+07
12	-2.83E-03	1.09E+07
13	-3.08E-03	1.13E+07
14	-3.30E-03	1.16E+07
15	-3.50E-03	1.20E+07
16	-3.65E-03	1.23E+07
17	-3.79E-03	1.26E+07
18	-3.89E-03	1.30E+07
19	-3.90E-03	1.34E+07
20	-3.44E-03	1.49E+07

15 Layers

Layer (#)	Shrinkage (%)	Stress (Mpa)
0		
1	5.37E-03	9100153
2	3.38E-03	-5325076
3	1.55E-03	562347.9
4	3.18E-04	5914780
5	-6.43E-04	7.86E+06
6	-1.33E-03	8871542

7	-1.93E-03	9479545
8	-2.41E-03	1.01E+07
9	-2.79E-03	1.07E+07
10	-3.11E-03	1.12E+07
11	-3.38E-03	1.17E+07
12	-3.61E-03	1.21E+07
13	-3.78E-03	1.26E+07
14	-3.85E-03	1.32E+07
15	-3.38E-03	1.50E+07

10 Layers

Layer (#)	Shrinkage (%)	Stress (Mpa)
0		
1	3.43E-03	9276797
2	1.42E-03	425472.8
3	-2.28E-04	5825820

4	-1.35E-03	7.70E+06
5	-2.15E-03	9107916
6	-2.72E-03	1.02E+07
7	-3.18E-03	1.10E+07
8	-3.52E-03	1.18E+07
9	-3.74E-03	1.26E+07
10	-3.28E-03	1.50E+07

5 Layers

Layer (#)	Shrinkage (%)	Stress (Mpa)
0		
1	8.05E-04	9833465

2	-1.35E-03	4857737
3	-2.59E-03	8338410
4	-3.30E-03	1.08E+07
5	-3.16E-03	1.41E+07

Appendix F

C-MOLD Output Data

Comparisons are drawn between the cooling times and shrinkage for C-MOLD and the cooling times and shrinkage for the numerical model proposed in Chapter 5. The input and output data for the C-MOLD analysis can be found in this Appendix.

F.1 Log File

C-MOLD Filling 99.7
C-MOLD Post-filling 99.7
C-MOLD Fiber Orientation 99.7
C-MOLD Residual Stress 99.7
(c)1987-1999 by Advanced CAE Technology, Inc.

Date : MAY29-03
Time : 10:23:37

End of memory allocation for analysis.

Beginning of reading the input data

File name : sample_4

Reading parameters

Performing fiber orientation simulation

Reading material data

** WARNING ** Fiber properties is not specified and fiber orientation simulation is turned off.

Reading process conditions

Reading finite-element mesh

** WARNING ** Cooling channel is not specified. C-MOLD Cooling Simulation will not execute without cooling channel information.

** WARNING ** Parting plane is not specified; the default parting plane normal along the z-axis of the global coordinates will be

used.

Reading C-MOLD Cooling data

** WARNING ** Analysis is continuing without .C2P file

Reading re-start data

** WARNING ** Analysis is continuing without .RSP file

End of reading the input data.

Beginning of re-numbering elements and nodes

End of re-numbering elements and nodes.

Beginning of checking input data

End of checking input data.

Beginning of optimizing memory usage

End of optimizing memory usage.

Beginning of initializing variables

End of initializing variables.

The analysis will be based on :

(1) Parameters :

# of layers across full-gap	(12) =	12
# design outputs in filling	(12) =	12
# detail outputs in filling	(0) =	0
# design outputs in post-filling	(12) =	12
# detail outputs in post-filling	(0) =	0
Melt-temp convergence criterion	(0.2) =	2.0000E-001
K(d)		
Mold-melt heat transfer coefficient	(2.5E+04) =	2.5000E+004
W/m ² -K		
Max # of melt-temp iterations	(100) =	100
Pressure trace sample frequency	(10) =	10
Hz		
Total number of pressure trace nodes	=	1

```

      Pressure trace nodal number      1 =      128
Residual stress analysis (W)          (1) =      1
Option for structural package (W)     (0) =      0
Isolate mechanism for warpage? (W)   (1) =      1
# of modes for stress analysis (W)   (3) =      3

```

C-MOLD fem format

(2) Material :

Polymer 1 : Borealis/PP MD231U

2-domain mod Tait polymer density

1

RHO = -----
 $Vo*(1-C*\ln(1+p/B)) + Vt$

where C = 0.0894

Tt = b5 + b6*p

Vo = b1 + b2*Tbar

B = b3 * EXP(-b4*Tbar)

Vt = 0.0 or b7*EXP(b8*Tbar-b9*p)

Tbar = T - b5

b5 = 4.2815E+002 K

b6 = 8.4500E-008 K/Pa

Liquid phase

Solid phase

b1 = 1.0760E-003

b1 = 9.9083E-004 m³/kg

b2 = 7.7500E-007

b2 = 4.4500E-007 m³/kg-K

b3 = 9.4300E+007

b3 = 1.7600E+008 Pa

b4 = 5.2439E-003

b4 = 5.0739E-003 1/K

b7 = 8.5100E-005 m³/kg

b8 = 1.6332E-001 1/K

b9 = 1.6900E-008 1/Pa

Tabulated polymer specific heat

Temperature

Specific Heat

T (K)

Cp (J/kg-K)

 3.3315E+002

1.6700E+003

3.4315E+002

1.7500E+003

3.5315E+002

1.8400E+003

3.6315E+002

1.9300E+003

3.7315E+002

2.0600E+003

3.8315E+002

2.9600E+003

3.9015E+002

1.3000E+004

3.9315E+002

6.6900E+003

4.0315E+002

2.0600E+003

4.1315E+002

2.0900E+003

4.2315E+002

2.1200E+003

4.3315E+002

2.1500E+003

4.4315E+002

2.1800E+003

4.5315E+002

2.2100E+003

4.6315E+002

2.2400E+003

4.7315E+002

2.2600E+003

4.8315E+002

2.2900E+003

4.9315E+002

2.3100E+003

5.0315E+002	2.3300E+003
5.1315E+002	2.3400E+003
5.2315E+002	2.3400E+003

Tabulated polymer thermal conductivity

Temperature T (K)	Thermal Conductivity K (W/m-K)
3.0115E+002	3.0100E-001
3.1015E+002	2.9000E-001
3.3115E+002	2.9000E-001
3.5215E+002	2.9200E-001
3.7215E+002	2.9400E-001
3.9215E+002	2.9100E-001
4.1215E+002	2.7800E-001
4.3115E+002	1.9600E-001
4.5115E+002	1.8900E-001
4.7015E+002	1.8800E-001
4.8915E+002	1.8400E-001
5.0915E+002	1.9100E-001
5.2815E+002	1.8900E-001

Cross-WLF polymer viscosity

ETAo = -----
 $1 + (ETAo * GAMMA / TAUS)^{(1-n)}$
 $A1 * (T - TS)$

where ETAo = D1 * EXP(- -----)
 $A2 + (T - TS)$

TS = D2 + D3 * p
A2 = A2T + D3 * p
n = 3.0232E-001
TAUS = 2.2278E+004 Pa
D1 = 1.1200E+015 Pa-s
D2 = 2.6315E+002 K
D3 = 0.0000E+000 K/Pa
A1 = 3.2933E+001
A2T = 5.1600E+001 K

Transition temperature
Ttrans = 4.0315E+002 K

Transversely-isotropic elastic tensor

E1 = 1.7000E+009 Pa
E2 = 1.7000E+009 Pa
v12 = 3.8000E-001
v23 = 3.8000E-001
G = 6.1600E+008 Pa

Transversely-iso thermal expansion coef.

a1 = 9.4400E-005 1/K
a2 = 1.0400E-004 1/K

(3) Process conditions : Description of TCODE

Machine parameters :

Max machine clamp force (4.905E+07) = 1.6211E+006
 N
 Max machine injection volume (0.02) = 3.3993E-004
 m³
 Max machine injection pressure (1.800E+08) = 1.3303E+008
 Pa
 Max machine injection rate (6.667E-03) = 2.8981E-004
 m³/s
 Machine hydraulic response time (0.2) = 2.0000E-001
 s

Process parameters :

 Fill time = 8.9084E-001
 s
 Post-fill time = 1.7754E+001
 s
 F/P switch over by % volume = 9.9000E+001
 %
 Timer for hold pressure = 1.7754E+001
 s

Ram speed profile (rel):

% stroke	% speed
-----	-----
0.0000E+000	5.0000E+001
2.0000E+001	5.0000E+001
4.0000E+001	5.0000E+001
6.0000E+001	5.0000E+001
8.0000E+001	5.0000E+001
1.0000E+002	5.0000E+001

Pack/hold pressure profile (rel):

% time	% fill pres
-----	-----
0.0000E+000	1.0000E+002
1.0000E+002	0.0000E+000

Ambient temperature = 2.9800E+002
 K
 Inlet melt temperature = 5.1313E+002
 K

Coolant circuit control:

ID	Temperature	Flow rate	Pres drop	CID
---	-----	-----	-----	---
1	2.8815E+002 K	1.6667E-004 m ³ /sec	0.0000E+000 Pa	1
2	2.8815E+002 K	1.6667E-004 m ³ /sec	0.0000E+000 Pa	1

Average coolant temperature = 2.8815E+002
 K

C-MOLD Cooling mold wall temp data was not used.

(4) Finite-element mesh : .FEM file for model: sample_4

 Total number of nodes = 596
 Total number of polymer entrance nodes = 1

Polymer entrance nodal numbers are:

```

                                                    128
Total number of elements                        =      1100
Total number of part elements                  =      1100
Total number of sprue/runner/gate elements    =          0
Total number of channel elements              =          0
Total number of connector elements            =          0

Parting plane normal                           (dx) = 0.0000E+000
                                                (dy) = 0.0000E+000
                                                (dz) = 1.0000E+000

Average aspect ratio of 2D elements            = 1.0227E+000
Maximum aspect ratio of 2D elements           = 1.6033E+000
2D element number w/ max. aspect ratio        =          202
Minimum aspect ratio of 2D element           = 1.0000E+000
2D element number w/ min. aspect ratio        =          635
Total volume                                  = 1.1520E-004
m^3
Total volume filled initially                  = 0.0000E+000
m^3
Total volume to be filled                     = 1.1520E-004
m^3
Part volume to be filled                      = 1.1520E-004
m^3
Sprue/runner/gate volume to be filled        = 0.0000E+000
m^3
Total projected area                          = 2.8800E-002
m^2

```

```

-----
-----
C-MOLD Filling 99.7
C-MOLD Post-filling 99.7
C-MOLD Residual Stress 99.7
analysis is beginning ....

```

```

At time = 8.0062E-002 s, 8.8204E+000 % of volume filled,
entrance pressure = 1.2753E+006 Pa,
total clamp force = 8.3885E+002 N,
filling under ram speed control.

```

```

At time = 1.5557E-001 s, 1.7094E+001 % of volume filled,
entrance pressure = 1.7031E+006 Pa,
total clamp force = 2.2635E+003 N,
filling under ram speed control.

```

```

At time = 2.2342E-001 s, 2.4516E+001 % of volume filled,
entrance pressure = 1.9687E+006 Pa,
total clamp force = 3.6995E+003 N,
filling under ram speed control.

```

```

At time = 2.9744E-001 s, 3.2591E+001 % of volume filled,
entrance pressure = 2.2122E+006 Pa,
total clamp force = 5.4978E+003 N,
filling under ram speed control.

```

```

At time = 3.7821E-001 s, 4.1356E+001 % of volume filled,
entrance pressure = 2.4629E+006 Pa,
total clamp force = 7.9342E+003 N,
filling under ram speed control.

```

At time = 4.4769E-001 s, 4.8843E+001 % of volume filled,
entrance pressure = 2.7871E+006 Pa,
total clamp force = 1.1981E+004 N,
filling under ram speed control.

At time = 5.2049E-001 s, 5.6621E+001 % of volume filled,
entrance pressure = 3.1681E+006 Pa,
total clamp force = 1.7568E+004 N,
filling under ram speed control.

At time = 5.9811E-001 s, 6.4863E+001 % of volume filled,
entrance pressure = 3.5315E+006 Pa,
total clamp force = 2.3670E+004 N,
filling under ram speed control.

At time = 6.6979E-001 s, 7.2437E+001 % of volume filled,
entrance pressure = 3.8604E+006 Pa,
total clamp force = 2.9764E+004 N,
filling under ram speed control.

At time = 7.4373E-001 s, 8.0204E+001 % of volume filled,
entrance pressure = 4.2399E+006 Pa,
total clamp force = 3.7552E+004 N,
filling under ram speed control.

At time = 8.1772E-001 s, 8.7967E+001 % of volume filled,
entrance pressure = 4.5810E+006 Pa,
total clamp force = 4.5088E+004 N,
filling under ram speed control.

At time = 8.9093E-001 s, 9.5637E+001 % of volume filled,
entrance pressure = 4.9496E+006 Pa,
total clamp force = 5.4004E+004 N,
filling under ram speed control.

At time = 9.3204E-001 s, cavity is completely filled.
entrance pressure = 5.1253E+006 Pa,
total clamp force = 5.9675E+004 N,

At time = 1.5915E+000 s, 3.7147E+000 % of post-filling time,
entrance pressure = 5.1253E+006 Pa,
total clamp force = 1.2755E+005 N,

At time = 3.0915E+000 s, 1.2164E+001 % of post-filling time,
entrance pressure = 5.1253E+006 Pa,
total clamp force = 1.2584E+005 N,

At time = 4.5915E+000 s, 2.0612E+001 % of post-filling time,
entrance pressure = 5.1253E+006 Pa,
total clamp force = 1.1993E+005 N,

At time = 6.0915E+000 s, 2.9061E+001 % of post-filling time,
entrance pressure = 5.1253E+006 Pa,
total clamp force = 1.1089E+005 N,

At time = 7.5915E+000 s, 3.7510E+001 % of post-filling time,
entrance pressure = 5.1253E+006 Pa,
total clamp force = 1.0940E+005 N,

At time = 9.0915E+000 s, 4.5959E+001 % of post-filling time,

entrance pressure = 5.1253E+006 Pa,
total clamp force = 9.5495E+004 N,

At time = 1.0592E+001 s, 5.4408E+001 % of post-filling time,
entrance pressure = 5.1253E+006 Pa,
total clamp force = 7.7600E+004 N,

At time = 1.1842E+001 s, 6.1449E+001 % of post-filling time,
entrance pressure = 5.1253E+006 Pa,
total clamp force = 5.9517E+004 N,

At time = 1.3342E+001 s, 6.9898E+001 % of post-filling time,
entrance pressure = 5.1253E+006 Pa,
total clamp force = 2.7335E+004 N,

At time = 1.4842E+001 s, 7.8347E+001 % of post-filling time,
entrance pressure = 5.1253E+006 Pa,
total clamp force = 2.9145E+004 N,

At time = 1.6342E+001 s, 8.6796E+001 % of post-filling time,
entrance pressure = 5.1253E+006 Pa,
total clamp force = 2.4774E+004 N,

At time = 1.7842E+001 s, 9.5244E+001 % of post-filling time,
entrance pressure = 5.1253E+006 Pa,
total clamp force = 2.5727E+002 N,

At time = 1.8675E+001 s, holding pressure is released.

At time = 1.8687E+001 s, 1.0000E+002 % of post-filling time,
entrance pressure = 4.8023E+006 Pa,
total clamp force = 2.4106E+002 N,

Beginning of preparing the interface data

 Preparing PPC file for C-MOLD Cooling

 Preparing LSP file for C-MOLD Residual Stress/Shrinkage & Warpage

End of preparing the interface data.

C-MOLD Filling 99.7
C-MOLD Post-filling 99.7
C-MOLD Residual Stress 99.7
is successfully completed.

ENDF

F.2 Shrinkage and Warpage Report

```
=====
C-MOLD Shrinkage and Warpage 99.7 summary report.
Name : sample_3
Date : JUL31-02
Time : 11:13:52
-----
```

Maximum process-induced shrinkage

```
=====
Maximum shrinkage is between node 13 and 310
```

```
Initial      distance = 2.6833E+002 mm
```

```
Displaced   distance = 2.6664E+002 mm
```

```
Change of distance = -1.6834E+000 mm
```

```
Percentage of change = -0.63%
```

Appendix G

Melt Front Advancement

The following are output data from the case study conducted in Chapter 4. These Figures illustrate the position of the flowing polymer inside the mould cavity at certain intervals.

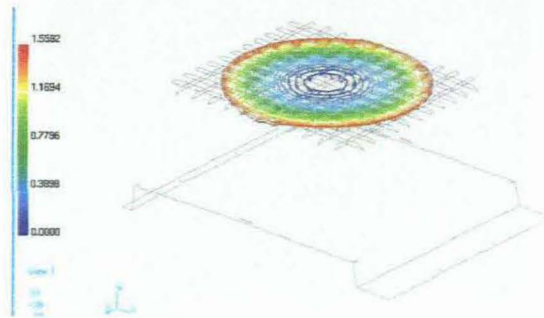


Figure G.1 Melt Front at 25% fill.

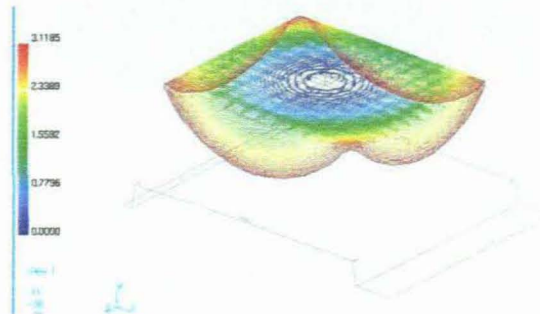


Figure G.2 Melt Front at 50% fill.

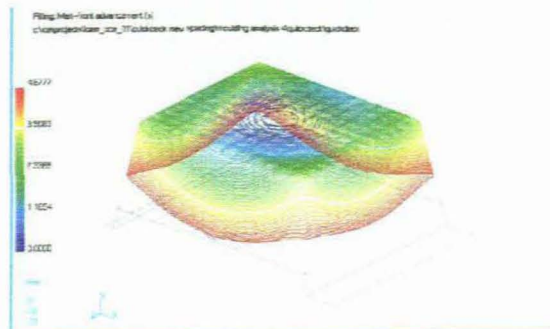


Figure G.3 Melt Front at 75% fill.

Appendix H

Part Performance

The Figures illustrated in this appendix are data relating to the case study conducted in Chapter 4. It shows the part successfully performing its intended task.

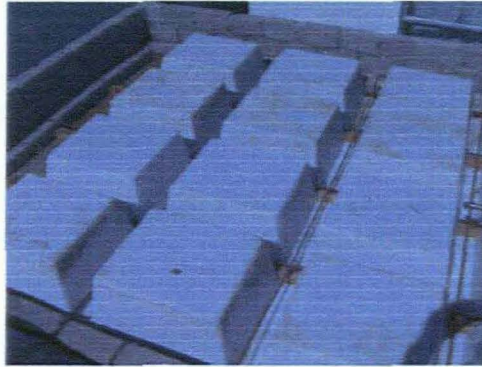


Figure H.1 Top view of installed component on rooftop.
(Photo courtesy of Overberg Consulting Engineers)



Figure H.2 Bottom view of installed component.
(Photo courtesy of Overberg Consulting Engineers)



Figure H.3 Reinforcement and installation of cabling.
(Photo courtesy of Overberg Consulting Engineers)



Figure H.4 Pouring of cement.
(Photo courtesy of Overberg Consulting Engineers)

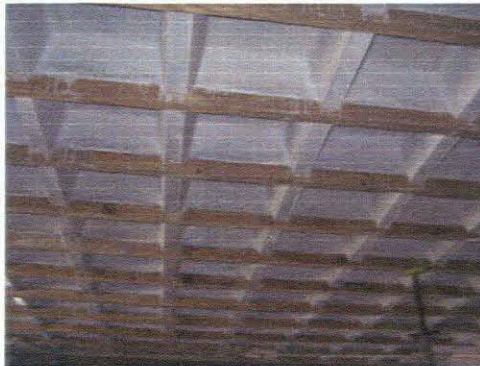


Figure H.5 Bottom view of ceiling with part removed.
(Photo courtesy of Overberg Consulting Engineers)

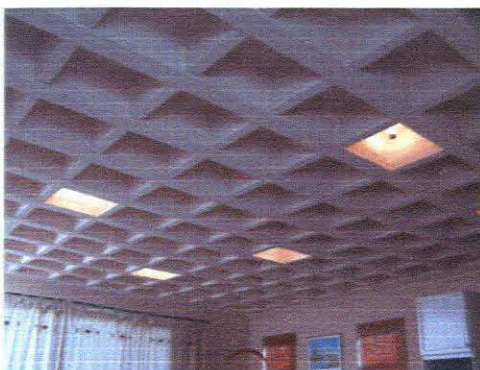


Figure H.6 Finished ceiling.
(Photo courtesy of Overberg Consulting Engineers)